Tissue Engineering Strategies to Improve Post-MI Engraftment of

hESC-Derived Cardiomyocytes

Kaytlyn A. Gerbin

A dissertation

submitted in partial fulfillment of the

requirements for the degree of

Doctor of Philosophy

University of Washington

2016

Reading Committee:

Dr. Charles Murry, Chair

Dr. Michael Regnier

Dr. Cole DeForest

Program Authorized to Offer Degree:

Department of Bioengineering

University of Washington

Abstract

Tissue Engineering Strategies to Improve Post-MI Engraftment of hESC-Derived Cardiomyocytes

Kaytlyn Anne Gerbin

Chair of the Supervisory Committee:

Charles Murry, M.D., Ph.D.

Departments of Pathology and Bioengineering

Transplantation of stem cell-derived cardiomyocytes is a promising strategy for repairing damaged cardiac muscle following a myocardial infarction. Our group and others have demonstrated both long-term engraftment and increased cardiac function after implantation in preclinical models using rodents and large animals. Despite this progress, there are still significant limitations to address in order to facilitate successful clinical translation of this therapy. Firstly, multiple delivery methods have been used to transplant stem cell-derived cardiomyocytes (hESC-cardiomyocytes) in rodents, including injecting cell suspensions and implanting engineered tissues. However, the ability of human cardiomyocytes to electrically and mechanically integrate with rodent myocardium using these delivery methods is not well

understood. Secondly, current transplantation methods only retain a small fraction of implanted cells, leading to small graft size and an excess of cells needed for transplant. Here, we first conducted a comparative study to assess the engraftment and electromechanical integration of hESC-cardiomyocytes in the infarcted rat myocardium. This research demonstrated for the first time that human cardiomyocytes electrically integrate with the rat myocardium and beat in synchrony to rates over 6 Hz. We demonstrated that intramyocardially delivered cells (injected as a cell suspension or as cardiac micro-tissues) were electrically coupled to the host tissue, compared to no observed coupling when delivered as epicardial patches. All implant methods resulted in human myocardial grafts, however there was no improvement in graft area using these scaffold-free tissue engineering approaches compared to cell suspensions. To address this limitation, we designed an approach to improve engraftment and limit the number of cells required for implantation by promoting cardiomyocyte proliferation after transplantation. We developed a collagen-based hydrogel with the immobilized Notch ligand Delta-1, which was used *in vitro* to promote Notch signaling and increase cardiomyocyte proliferation by over 2-fold in engineered cardiac tissues. The optimized Notch-signaling hydrogel was then translated *in vivo* and used as a delivery vehicle for hESC-cardiomyocytes in the infarcted rat myocardium. This resulted in a 3-fold increase in cardiomyocyte proliferation and a 3-fold increase in graft size compared to controls. Taken collectively, the research in this dissertation highlights the potential of tissue engineering strategies to improve implantation of stem cell-derived cardiomyocytes, by promoting electromechanical integration and cell proliferation in preclinical models of myocardial infarction.

Table of Contents

List of Figures

List of Tables

Acknowledgements

Getting a PhD takes the support of an entire lab, and I am grateful for having the Murry Lab to grow with and learn from during my years in graduate school. First and foremost, I would like to thank my advisor, Chuck Murry, for his support and mentorship throughout my years of research and training in his lab. His passion for science and his vision for translating research into the clinic are unmatched, and it has been a privilege to train in his laboratory.

It has been a pleasure working with everyone in the Murry Lab. I would like to thank Kareen Coulombe, who took me under her wings as a new graduate student and trained me on everything from cell culture to animal surgeries and career development. I would like to specifically acknowledge Hans Reinecke and Lil Pabon for their scientific insight and advice, Amy Martinson for her surgical expertise and company during long surgery days, Veronica Muskheli for help with histology and Russian tutoring, Mark Saiget and James Fugate for years of being my go-to scientists for any lab-related question, and Martha Lee and Kristen Meredith for their advice and scheduling help at any hour of the day. I would like to thank all members of the Murry Lab for their constant support and mentorship, as I truly think these are the best people I could have imagined working with: Xiulan Yang, Florian Weinberger, James Chong, Nathan Palpant, Shin Kadota, Jia-Ling Ruan, Sarah Dupras, Melissa Walzer, Billy Cheng, Yen-Wen Liu, Astrid Breitbart, Sarah Fernandes, Becky Zaunbrecher, Peter Hofsteen, Hiroshi and Akiko Tsuchida, Scott Thies, Eric Nuber, Mardi Nenni, Paul Fields, Shiv Bhandari, Andrea Leonard, Christine Yoo, Katie Mitzelfelt, and Alessandro Bertero. I would also like to thank the undergraduates that have helped me over the years, including Daniel Burnham, Alexander Moon,

Chapter 1. Introduction

1.1 Ischemic Heart Disease

Ischemic Heart Disease: A Global Problem

Cardiovascular disease is the leading cause of death worldwide, accounting for 3 in every 10 deaths annually [8]. Ischemic heart disease is the leading contributor to this cardiovascular disease burden, resulting in 7.4 million fatalities each year [8]. Cardiac ischemia occurs when there is reduced blood flow in the coronary arteries, which can be caused by the gradual buildup of atherosclerotic plaques or by plaque rupture resulting in a myocardial infarction (MI) [9]. In the case of MI, healthy and contractile myocardium is transformed into an akinetic and fibrotic tissue within a few weeks after injury. The adult human heart has an extremely limited regenerative capacity, and as such many patients develop chronic heart failure and are subsequently faced with a 50% survival rate over 5 years [10]. Current treatment options are limited to palliative drugs such as ACE inhibitors and Beta Blockers, heart transplant (available to 1 in 1000 patients), or ventricular assist devices (complicated by risk of infection, thrombosis, and power supply). With these available treatments patients are living longer than ever before, but ischemic heart disease still remains the number one cause of death and disability worldwide [11].

Response of the Heart to Myocardial Infarction

In the human heart, up to 1 billion cardiomyocytes are lost during an MI [12]. Unlike most

organs in the human body that have some level of endogenous repair and proliferative cellular response after injury [13], adult cardiomyocytes have an extremely low proliferation capacity. Although there is increasing evidence of cardiomyocyte turnover after MI [14], this innate generation of *de novo* cardiomyocytes is orders of magnitude behind what is needed to replace those lost during injury. Instead, the natural wound healing response after MI is the development of fibrotic scar, which is necessary to maintain wall strength and prevent left ventricular (LV) rupture. This process is overviewed in Figure 1.1.
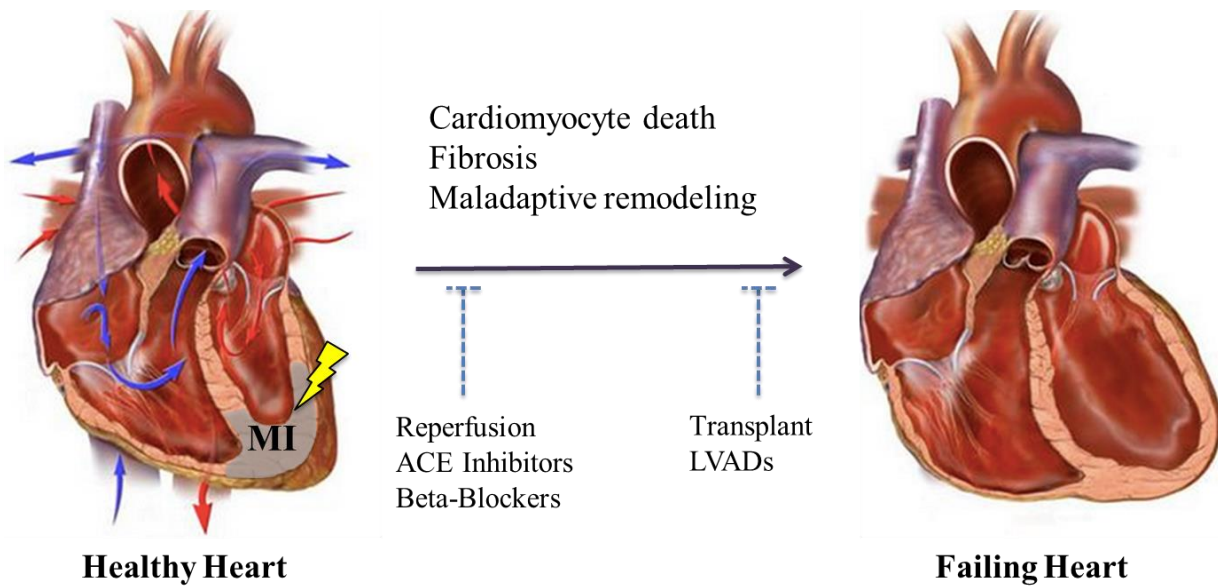
Figure 1.1. The response of the heart to myocardial infarction (MI). An MI induces a cascade of events including cardiomyocyte death, fibrosis, and maladaptive remodeling. This process leads to an enlarged heart chamber and a thin myocardial wall. Currently, early clinical intervention includes reperfusion therapy or drugs such as ACE inhibitors or Beta Blockers, however these do not prevent the transition towards heart failure. At end stage heart failure, organ transplants or left ventricular assist devices (LVADs) are current clinical treatment options, but are not in adequate supply to meet the demands of heart failure worldwide. Figure adapted from [6].

This wound healing process occurs more rapidly in rodents than in humans, beginning with the influx of inflammatory cells including macrophages and neutrophils peaking between days 2 and

2

4 [15], the formation of granulation tissue and the increase in myofibroblasts peaking in the first week [16], and collagen accumulation peaking within the first week after injury but reaching a plateau by two weeks in the rat heart [17]. In order to maintain force production in the weeks following injury, the heart adapts and reshapes from a conical structure to a more globular shape with thinner myocardial walls. There are multiple contributing factors to this adaptation, including cell death, cell stretching, and cardiomyocyte 'slippage' [18]. While initially beneficial, this compensation becomes maladaptive over time and causes extensive fibrosis and wall stiffening, leading to chronically diminished contractility [19].

Heart Regeneration in Lower Vertebrates and Mammals

In contrast to the human heart's response to MI, complete heart regeneration has been well documented in lower vertebrates. The impressive regenerative capacity of zebrafish makes them one of the most robust models for heart regeneration [20]. After surgical resection of the apex [21], as well as after cardiomyocyte ablation [22], the adult zebrafish heart is capable of full regeneration with minimal scarring after only a few months. Both of these examples have highlighted the importance of cardiomyocyte proliferation in this regenerative process, and studies have shown that the majority of new cardiomyocytes arise from the de-differentiation and proliferation of pre-existing cardiomyocytes [23, 24] (Figure 1.2). Until recently, this regenerative capacity had only been observed in lower vertebrates. However, mammalian heart regeneration has been demonstrated in neonatal mice when injury occurs within a short timeframe after birth [25]. This study found that the mouse myocardium fully regenerates by 3 weeks after apical resection, when the injury is induced in 1-day old mice. However, this regenerative response was lost when the injury occurred in 7-day old mice, and resected tissue

was replaced with dense scar tissue. Lineage tracing studies indicated that the renewed cardiomyocytes were again arising from pre-existing cardiomyocytes that have dedifferentiated and re-entered the cell cycle, as was shown previously in regenerated zebrafish hearts [26]. Collectively, these studies highlight the potential for complete heart regeneration in specific contexts which is in contrast with our knowledge of the adult human heart.
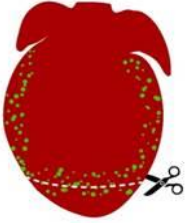
Figure 1.2. Cardiomyocyte proliferation by pre-existing cardiomyocytes is an important part of heart regeneration across various injury models in both zebrafish and neonatal mice. Adapted from [5].

1.2 Cell and Tissue Engineering Therapies for Heart Regeneration

Cell Therapy for Heart Repair

Although multiple strategies to regenerate the heart after injury have been explored, the most established strategy to date has been the delivery of exogenous cells. This approach aims to repair damaged myocardial tissue by one of two mechanisms: 1) paracrine-mediated effects, or 2) direct contribution to force production from *de novo* cardiomyocytes. There has been a wave of clinical trials for cell-based heart repair conducted in the past decade, using cell types including skeletal myoblasts, bone marrow-derived hematopoietic and mesenchymal stem cells, adipose-derived cells, endothelial progenitor cells, and cardiac-derived cells (reviewed in [27-30]). However, results from these trials have been modest at best, suggesting that there is a more effective cell type for transplant [3]. The cell therapy clinical trials for myocardial repair are discussed in detail in Chapter 2.

Tissue Engineering Strategies for Heart Repair

While the transplantation of single cell suspensions is the most established method for heart repair, tissue engineering strategies for regenerative medicine are improving rapidly and have the potential to overcome the some of the limitations of current cell transplantation techniques. Firstly, multiple studies have described improved cellular engraftment and cell retention using tissue engineering approaches, such as implantation of cell sheets, epicardial patches, or by delivering cardiomyocytes in biomaterials [31, 32]. Transplanting engineered tissues allows for control over macro- and microscopic geometry [33-37], which is particularly useful for developing vasculature within the engineered tissues [38, 39]. Most of these implantation

approaches require a thoracotomy to expose the heart prior to suturing tissues onto the epicardium, which is an invasive procedure that may be difficult to implement in the clinic. Thus, the development of minimally-invasive tissue delivery methods is an important consideration in order to facilitate the clinical translation of cell-based therapies. For this reason there has been great interest in micro-scale cardiac tissues or injectable hydrogels that gel *in situ,* both allowing for minimally-invasive delivery. Injectable hydrogels have been shown to increase LV wall thickness and prevent adverse remodeling after MI (reviewed in [40]), although few studies have advanced this approach to combine injectable biomaterials with cardiomyocyte cell therapy [40, 41].

Stem Cell-Derived Cardiomyocytes for Cardiac Repair

Many different cell types have been tested for use in cardiac repair methods, however stem cell-derived cardiomyocytes have been the focus of many preclinical research studies. In considering cell types, we expect that the ideal cell type for replacing damaged myocardial tissue should have contractile and electrophysiological properties, the ability to survive and integrate into an ischemic area, proliferation potential, and the ability to elicit a paracrine effect to stimulate endogenous regeneration (e.g. vascularization; discussed in detail in [30, 42]). Despite the plethora of cell types tested in clinical trials to date, none have met all of these expectations. Human pluripotent stem cell (hPSC)-derived cardiomyocytes have been brought to the forefront of cell therapy research as a next-generation cell source. Numerous groups have demonstrated robust engraftment in the infarcted heart and shown an increase in global cardiac function (reviewed in [43]). Our group has also shown that injected human embryonic stem cell (hESC)-cardiomyocytes electrically integrate with the host myocardium in guinea pigs [44], athymic rats

6

([45], Chapter 3), and in non-human primates [1]. Unlike previously transplanted cells that are thought to function via paracrine signaling, this electrical integration provides evidence that engrafted cardiomyocytes are directly contributing to force generation with the host myocardium.

1.3 Cardiomyocyte Proliferation

Cardiomyocyte Proliferation in the Adult Mammalian Heart

During normal organ growth and development, cardiomyocytes turn over at a very low yet detectable rate in adult rodents (reviewed in [46]), which is increased slightly following myocardial injury [14]. After injury, up to 3% of pre-existing cardiomyocytes adjacent to the injury region in mice undergo cell division. However most DNA replication occurs without cytokinesis as a hypertrophic response, and there is only a minimal contribution from progenitor cells [14]. Cardiomyocyte proliferation under homeostatic and injury conditions is even further reduced in the human heart compared to rodents, although studies suggest that the most proliferative state occurs early in life. Cardiomyocytes in the human heart undergo a 3.4-fold increase between birth and 20 years of life [47], however this rate falls dramatically during aging. Human adult cardiomyocytes have a turnover rate of less than 1% after age 25, which further diminishes to less than 0.5% by age 75 [48]. Although this turnover is clearly not sufficient for regeneration after an injury, mammalian cardiomyocyte proliferation in neonates and in adults suggests that enhancing proliferation may be a reasonable therapeutic target in the adult human heart, possibly by engaging developmental programs or repair pathways that have

been 'evolutionarily-turned off'. Strategies to target these pathways are discussed below.

Strategies to Promote Cardiomyocyte Proliferation

Promoting cardiomyocyte proliferation is of great interest to the field of heart regeneration, both *in vitro* and in the context of cardiac repair *in vivo*. Multiple molecular targets have been identified as regulators of cardiomyocyte proliferation, which include primarily mitotic signaling pathways such as the overexpression of cyclins [49-51], signaling pathways induced by FGF and NRG [52, 53], Notch signaling [54, 55], and microRNAs [26]. Neuregulin (NRG) has also been described for its role in mediating cardiomyocyte proliferation and heart regeneration in uninjured zebrafish [56] and in infant myocardial explants [57].

Many of the approaches to promote cardiomyocyte proliferation used to date *in vivo* have relied on the forced genetic overexpression of proliferative cues with minimal temporal or tunable dose control of the proliferative signal. We expect that there are two important aspects to consider while promoting cardiomyocyte proliferation in the context of heart repair, (1) dedifferentiation and proliferation, and (2) exit from the cell cycle and subsequent maturation. Thus, we believe that having the ability to turn off the proliferative cues is of critical importance and is a major limitation to many of the approaches described above. This limitation has been described in the context of Hippo signaling, where animal models show enhanced cardiomyocyte proliferation with increased Hippo signaling, but hearts have decreased global function with long-term overexpression [58]. Thus, there is a need for therapeutic strategies that allow for localized and spatiotemporal control of a transient signal.

Of particular interest to this research is the role of Notch signaling in mediating cardiomyocyte proliferation. Mice lacking the downstream Notch target RBPJk showed inhibited proliferation in ventricular cardiomyocytes [59], and experiments using genetically-forced Notch expression demonstrated that cardiomyocytes showed increased proliferation in response to Notch [60, 61]. Our group has previously demonstrated that hESC-cardiomyocytes in 2D monolayers proliferate in response to the Notch ligand Jagged-1, which was more potent than IGF1 delivery and was partially inhibited by blocking Notch signaling with a gamma secretase inhibitor [62].

1.4 Notch Signaling

The Notch Pathway

The Notch signaling pathway is a highly-evolutionarily conserved pathway that plays a major role in cell fate decisions during development and disease, in species from *C. elegans* to humans [55, 63, 64]. Unlike many signaling families which rely on the secretion of soluble proteins, Notch signaling relies on direct cell-cell contact, in which one cell presents the signaling ligand and the other cell presents the receptor (Figure 1.3) [7]. The Notch pathway consists of four Notch receptors [65] (Notch1, Notch2, Notch3, and Notch4) and five Notch ligands (Delta1, Delta3, and Delta4, and Jagged1 and Jagged2 in mammals). Notch signaling is initiated upon biding of a Notch ligand (presented by the signaling cell) to a Notch receptor (on the receiving cell). After binding of a Notch ligand (e.g. Delta1) to a receptor (e.g. Notch1), it is hypothesized that the tension produced upon binding exposes an extracellular cleavage site, which is cleaved by ADAM metalloproteases (S2 cleavage). On the intracellular surface of the receptor-presenting

cell, S3 cleavage by gamma secretase follows and releases the Notch intracellular domain (NICD) from the membrane, allowing its nuclear translocation and activation of downstream target genes. CSL (CBF1, Su(H), and Lag-1) is one of the major binding partners for NICD in the nucleus, which normally represses transcription through its interaction with histone deacetylases (HDACs) [66] and corepressor (Co-R) proteins [65]. Binding with NICD displaces this repressive interaction and allows for binding with the transcriptional coactivator Mastermind (MAM), and together this complex activates transcription of various gene pathways including the HES and HEY families [67].
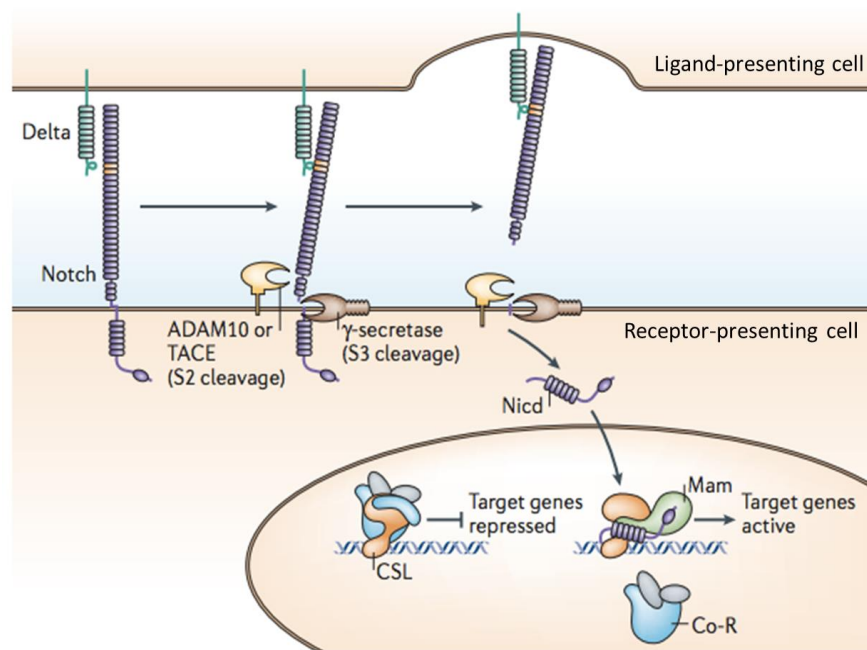
Figure 1.3. The Notch signaling pathway. Adapted from [7].

Notch Signaling in Response to Injury

Notch signaling has been previously explored in the context of myocardial injury, and most studies have reported the same general trend: enhanced Notch signaling limits the extent of

fibrosis, prevents global remodeling, and improves heart function after injury. Deletion of Notch1 expression in the heart exacerbates maladaptive remodeling and fibrosis in models of cardiac hypertrophy [59, 68] and leads to larger infarcts and worsened heart function after MI [69]. In contrast, enhancing Notch signaling in cardiomyocytes by genetic overexpression [59, 70], by the delivery of a Notch1 antibody [70], or by adenoviral-induced NICD overexpression [71] improves heart function and limits fibrosis compared to control animals. Notch is expressed at low levels under homeostatic conditions in the heart, but is upregulated following injury [71, 72]. In fact, increased Notch signaling has been found to precede the regenerative process in the zebrafish heart after injury, playing a key role in regulating cardiomyocyte proliferation during the repair process [73, 74]. In addition to these effects on the myocytes, enhanced Notch signaling has been shown to modulate myofibroblast activity, limit cellular apoptosis, and promote neovascularization after injury, suggesting a role for Notch on the non-myocyte cell populations in the heart [75, 76]. Collectively, these studies support the modulation of Notch signaling as an attractive approach for cardiac repair, which could have broad implications across cell types, potentially to promote wound healing on an organ-wide scale.

1.5. Thesis Motivation and Overview

Stem cell-derived cardiomyocyte therapy has been established as a promising strategy moving forward for cardiac regeneration, and tremendous progress has been made in the past few years to develop this therapy in preclinical models of myocardial infarction. However, there are still significant hurdles that must be addressed to facilitate more successful translation of these preclinical strategies into larger animals and into the clinics. To address some of these hurdles, the work described in this dissertation takes lessons from tissue engineering and applies them to hESC-cardiomyocyte cell-based therapy.

The first limitation addressed in this dissertation is that the ability of human stem cell-derived cardiomyocytes to electrically and mechanically integrate with host myocardium in preclinical rodent models is not well established (Figure 1.4). Multiple delivery strategies have been used for cardiomyocyte transplantation including cell suspensions and engineered tissues, however the outcome of these methods to integrate and engraft has not been directly compared in a controlled study. There is a discrepancy in the heart rate of rodents and the human cells that are being implanted, and the validity of these rodent models for modeling and predicting the behavior of cells in large animals and humans relies on the electromechanical integration between engrafted cells and host myocardium. Thus, there is a need for comparative studies in small animal models designed to assess the performance of these diverse delivery methods in terms of engraftment and electromechanical integration.

Secondly, current transplantation techniques of hESC-cardiomyocytes are hindered by small graft size and limited cell retention, with only a small fraction of transplanted cells remaining in the surviving graft (Figure 1.4). To facilitate the clinical translation and scalability of hESC-cardiomyocyte cell therapy, there is a need for methods to enhance graft size and to maximize the number of transplanted cardiomyocytes. Gaining control over cardiomyocyte proliferation is one strategy to achieve this, and previous studies suggest that manipulating the Notch signaling pathway promotes cell cycle activity in cardiomyocytes. However, no small molecule agonists for Notch signaling currently exist, and the presentation of Notch ligands must be immobilized to elicit robust signaling. This is a constraint that has limited applications primarily to transgenic animal models and has hindered its use in tissue engineering and its potential for clinical translation. This motivated our work to present immobilized Notch signaling ligands in a biomaterial platform that would be compatible with tissue engineering applications and therapeutic delivery *in vivo,* to promote cardiomyocyte proliferation and improve engraftment.

The research described in this thesis dissertation addressed the challenges described above by investigating the electromechanical integration of hESC-cardiomyocytes in intramyocardially-delivered engineered tissues (Chapter 3), designing a hydrogel platform to regulate Notch signaling to control cardiomyocyte proliferation in 3D engineered tissues (Chapter 4), and investigating the intramyocardially-delivered Notch hydrogel as a therapeutic strategy for cardiac repair (Chapter 5).
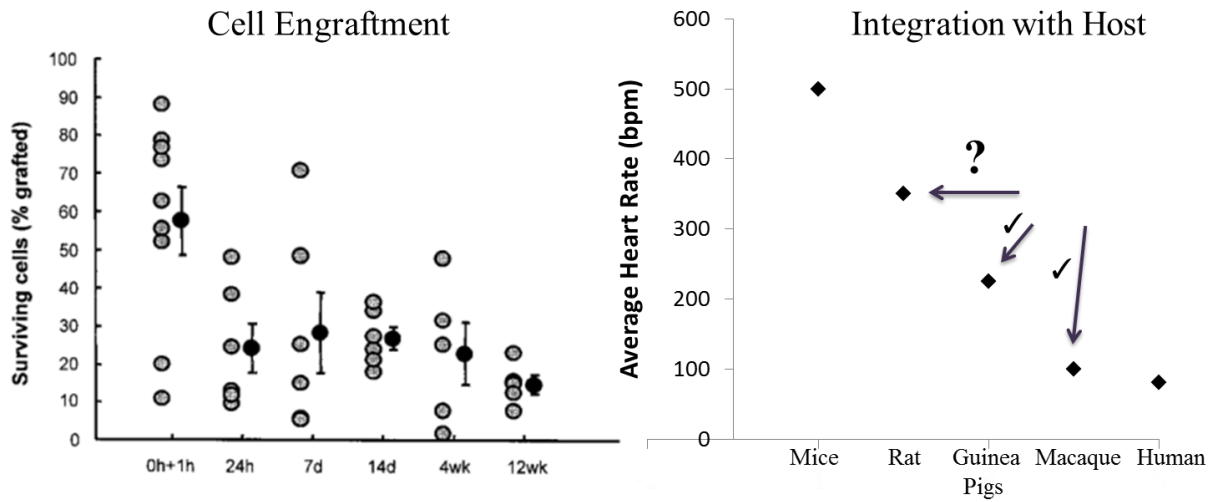
Figure 1.4. Current challenges with hESC-cardiomyocyte cell therapy approaches. The graph on the left demonstrates that the majority of implanted cells are lost after engraftment. Roughly 60% of implanted cells are remaining after 1 hour, which further decreases to only a quarter of the cells surviving after 24 hours. Figure from [2]. The graph on the right summarizes electrical coupling ability of hESC-cardiomyocytes across various animal species. Rodents such as mice and rats have high heart rates, and previously it was not known if human cardiomyocytes were capable of electrically coupling with these host tissues. The work in Chapter 3 demonstrated electrical coupling in the rat heart. Our group had previously demonstrated electrical coupling of hESC-cardiomyocytes with guinea pigs [4] and macaques [1].

Chapter 2: Clinical progression of cell therapy for heart regeneration

This chapter has been published in [2].

2.1 Overview

Regenerating the human heart is a challenge that has engaged researchers and clinicians around the globe for nearly a century. From the repair of the first septal defect in 1953, followed by the first successful heart transplant in 1967, and later to the first infusion of bone marrow-derived cells to the human myocardium in 2002, significant progress has been made in heart repair. Yet, chronic heart failure remains a leading pathological burden worldwide. Why has regenerating the human heart been such a challenge, and how close are we to achieving clinically relevant regeneration? Exciting progress has been made to establish cell transplantation techniques in recent years, and new pre-clinical studies in large animal models have shed light on the promises and challenges that lie ahead. In this chapter, the history of cell therapy approaches is discussed, and an overview is given of clinical trials using cell transplantation for heart regeneration. Focusing on the delivery of human stem cell-derived cardiomyocytes, current experimental strategies in the field will be discussed as well as their clinical translation potential. Although the human heart has not been regenerated yet, decades of experimental progress have guided us onto a promising pathway.

2.2 Introduction

A myocardial infarction transforms healthy and contractile myocardium into an akinetic, fibrotic tissue, resulting in a heart that cannot pump blood at full capacity. As the heart is one of the least regenerative organs in the body, this often leads to the development of chronic heart failure – a disease with a 50% survival rate over 5 years [10]. Current treatment options are limited and consist primarily of palliative drugs, organ replacement by heart transplant (available to <0.1% of heart failure patients), or mechanical assist devices (with complications related to infection, thrombosis, and power supply). While these available treatments have greatly impacted the trajectory of patient health after a myocardial infarction, ischemic heart disease remains the number one cause of death and disability worldwide [11].

In recent years, the field of heart regeneration has emerged from a far-fetched notion to the forefront of cardiac research. Heart regeneration is an interdisciplinary field with the goal of restoring functional myocardium after cardiac injury [12]. Approaches to repair the injured heart have been widespread and include cell transplantation, gene therapy, stimulating innate repair pathways, direct cellular reprogramming, cardiac tissue engineering, and biomaterial delivery. The most established strategy for heart repair has been the delivery of exogenous cells. Nearly every cell type imaginable has been transplanted into the damaged myocardium, from skeletal myoblasts to pluripotent stem cells and their derivatives. It is an exciting but challenging time for physicians, scientists, and engineers in the field – we now have over a decade of experience in clinical trials contributing to heart regeneration research, and there are several promising pre-clinical strategies emerging as contenders to our current clinical approaches.

2.3 Cell Therapy Clinical Trials for Heart Repair

Approximately 1 billion cardiomyocytes are lost during a myocardial infarction (MI) [12]. As the adult human heart has an extremely limited regenerative capacity, this damaged myocardial tissue is replaced by fibrotic scar. There is increasing evidence of the slow cardiomyocyte turnover rate during normal organ growth and development (reviewed in [46]), and following myocardial injury [14], however this turnover accounts for a low percentage of cells. Up to 3% of pre-existing cardiomyocytes near the injury region undergo cell division while most DNA replication occurs without cytokinesis as a hypertrophic response, and there is minimal contribution from progenitor cells [14]. As a result, the innate generation of *de novo* cardiomyocytes post-infarction falls orders of magnitude short of meaningful regeneration.

Exogenous cell transplantation aims to repair damaged myocardial tissue by delivering cells that either act via paracrine-mediated effects or by providing *de novo* cardiomyocytes that directly contribute to force production. Towards this goal, numerous clinical trials have been conducted using cell types including skeletal myoblasts, bone marrow-derived hematopoietic cells, mesenchymal stem cells (aka marrow stromal cells), adipose-derived cells, endothelial progenitor cells, and cardiac-derived cells (reviewed in [27-30]). A schematic overview of the derivation, delivery mode, and proposed mechanism of action for the major groups of cell therapies is provided in Figure 2.1. An ideal cell type for replacing damaged myocardial tissue would have contractile and electrophysiological properties, the ability to survive and integrate into an ischemic area, proliferation potential, and the ability to elicit a paracrine effect to

17

stimulate endogenous regeneration (e.g. vascularization; discussed in detail in [30, 42]). Despite

the plethora of cell types tested in clinical trials to date, none have met all of these expectations.
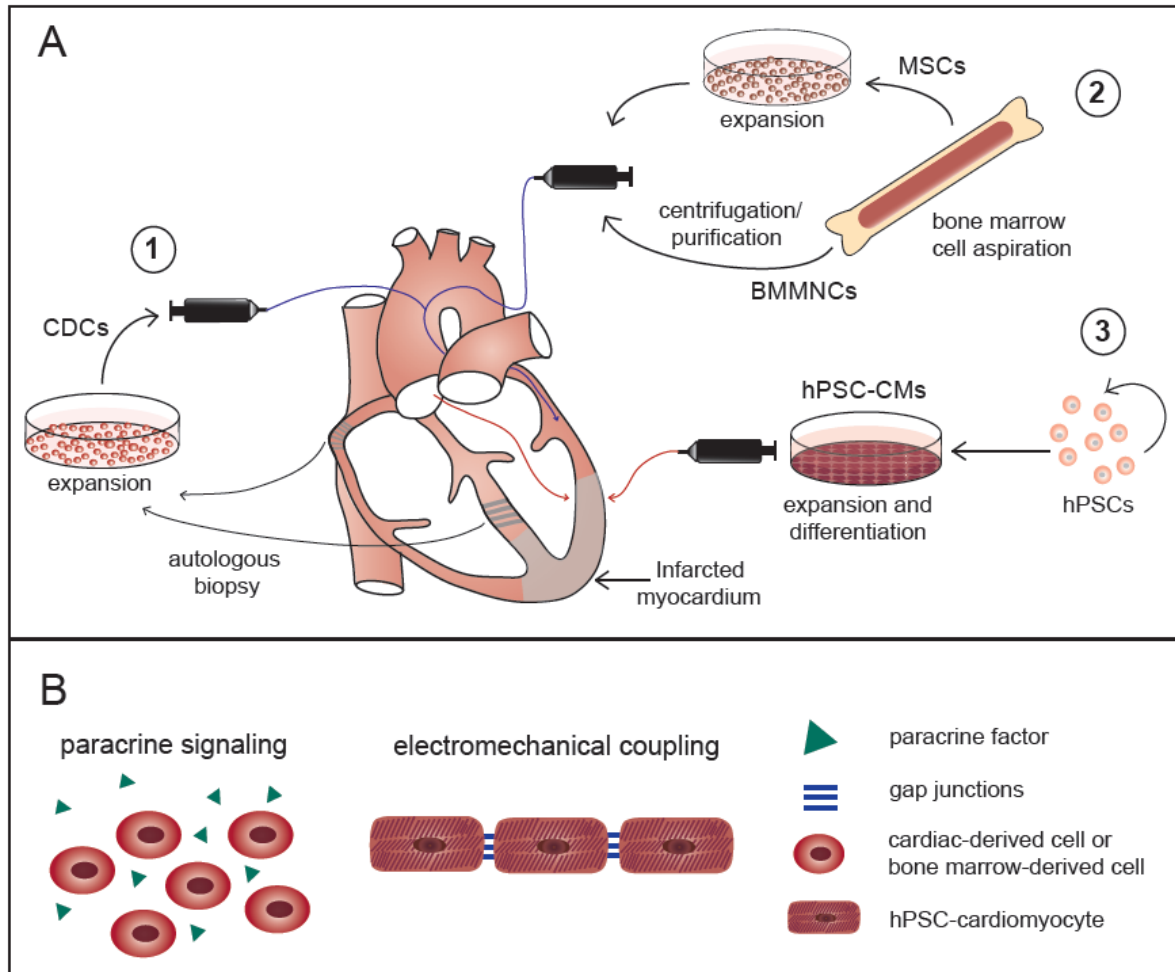
 Figure 2.1. Cell therapy for heart repair. (A) Post-MI, cardiac-derived cells (CDCs, 1) are isolated by autologous biopsy, expanded, and transplanted. Bone marrow mononuclear cells (BMMNCs, 2) and mesenchymal stem cells (MSCs, 2) are harvested from the bone marrow, purified, and BMMNCs are transplanted while MSCs require expansion prior to transplantation. HPSC-cardiomyocytes (hPSC-CMs, 3) undergo differentiation, and the proposed clinical delivery method is via transepicardial or transendocardial catheter. (B) Proposed mechanism of action after cell transplantation. BMMNCs and CDCs primarily work through paracrine signaling, while hPSC-CMs act primarily though the direct electromechanical integration with host cardiomyocytes. Figure adapted from [3].

The type of cell used for transplantation inherently places restrictions on important variables that may affect the success of cell therapy, making it difficult to directly compare results across trials. These include the delivery mode (intracoronary catheter, transendocardial catheter, or epicardial catheter delivery compared to epicardial delivery in tissue patches or hydrogels), the availability of autologous or allogeneic cells, and the timing of cell delivery dependent on the need for *in vitro* cell expansion (i.e. mesenchymal stem cells require extensive *in vitro* expansion, while unfractionated bone marrow cells may be delivered the same day of isolation).

The field has made tremendous progress in terms of establishing clinical trial design, delivery techniques, and demonstrating safety, however the clinical benefits have been modest at best. This indicates that there is room for improvement on our cell source. The two major cell sources used in the clinics thus far have been bone marrow-derived cells and cardiac explant-derived cells, which are discussed below.

Bone Marrow-Derived Cells

Following closely behind the first major wave of clinical trials in the field using skeletal myoblasts [77], bone marrow-derived cells paved the way for intracoronary cell therapy in the heart, transitioning quickly into the clinic despite the scarcity of published evidence supporting their role in heart regeneration at the time [78, 79].

Bone Marrow-Derived Mononuclear Cell Derivatives

Most bone marrow-derived cell transplantation trials in the heart have used an unfractionated subpopulation called bone marrow mononuclear cells (BMMNCs) (reviewed in [80]). Referring to BMMNCs as a stem cell preparation is a misnomer, because true stem cells comprise well below 0.1% of the total mononuclear cell population. Unfractionated BMMNCs principally consist of a heterogeneous population of hematopoietic cells including monocytes, committed myeloid progenitor cells and lymphocytes, and a small population of hematopoietic and mesenchymal stem cells [30, 81].

Intracoronary transplantation of BMMNCs into patients with acute MI was first reported in 2002 [79], and while this trial has been discredited for ethics violations, it was followed by a flurry of more rigorously performed studies. Most of these early BMMNC studies enrolled acute-MI patients with ST-segment elevation and a baseline ejection fraction of 40-50%, and reported functional improvement after treatment. One such study was the BOOST trial [82], in which autologous BMMNCs (characterized as <1% CD34$^+$) were isolated from patients and delivered by intracoronary infusion to the infarct-related artery the same day. No serious adverse events were reported in either group, and cardiac MRI at 6 months indicated a significant increase in left ventricular (LV) ejection fraction after cell treatment (compared to placebo control), providing evidence that intracoronary infusion of BMMNCs improves systolic function in acute MI patients. In longer term follow up studies, however, the control group showed a "catch-up" period of recovery, such that benefits of BMMNCs could no longer be demonstrated [83].

Results from the REPAIR-AMI trial [84] further supported efficacy for BMMNCs, reporting a 5.5% increase in LV ejection fraction at 4 months after intracoronary infusion of BMMNCs compared to a 3.0% improvement in controls. While the results of this study were hindered by the use of quantitative LV angiography to assess function as opposed to cardiac MRI, the enrollment of over 200 patients made this the largest BMMNC trial at the time and set the standard for expected systolic improvement, albeit a modest increase, after cell therapy. The same group reported that functional improvement persists up to 5 years post-treatment in a subset of patients who were enrolled in the TOP-CARE-AMI trial [85-87], which compared the benefits of BMMNCs to those of autologous circulating progenitor cells isolated from venous blood.

Despite these and other studies reporting functional improvement after BMMNC treatment (reviewed in [88]), larger trials employing greater degrees of randomization, placebo controls, and blinding conducted in the years following have not replicated these results. The Cardiovascular Cell Therapy Research Network (CCTRN) was designed to facilitate cell-based therapies in the United States [89] and sponsored the FOCUS-CCTRN trial [90], which was one of the first trials to target patients with chronic LV dysfunction who had not qualified for revascularization therapy post-MI. Enrolled patients had a mean baseline ejection fraction of 30-32% and New York Heart Association (NYHA) class of 2 or 3, and while there was no improvement in the primary endpoints of LV end systolic volume (LVSEV) or maximal oxygen consumption, there was a small yet statistically significant 1.4% improvement in LV ejection fraction over baseline at 6 months. The CCTRN also sponsored the TIME and LateTIME trials to assess the influence of BMMNC delivery timing on LV function [91-93]. Each of these double-blinded and placebo-controlled trials enrolled successfully reperfused MI patients and delivered

150 x 10^6 autologous BMMNCs by intracoronary perfusion either at day 3 or 7 (TIME) or at 2-3 weeks (LateTIME) after MI. Neither study detected any functional benefit by cardiac MRI at 6 months after cell treatment, regardless of delivery timing. Similar in cell dose and design, the SWISS-AMI study [94] compared BMMNC delivery at days 5-7 to delivery at weeks 3-4 after post-MI reperfusion, and again detected no improvement in LV ejection fraction at 4 months.

Collectively, these studies challenge the earlier reports of functional improvement, but they differ in using a double-blinded study design and in targeting patients with significantly worse baseline cardiac function (for example, the median ejection fraction of SWISS-AMI patients was 37%). It seems unlikely to us that this difference in baseline cardiac function underlies the difference, however, because the REPAIR-AMI trial found that the patients with the worst ejection fractions showed the greatest improvement with treatment. Results are eagerly awaited from the 3,000 patient enrollment, multicenter phase 3 trial (the BAMI trial), which is currently underway in Europe, as results will help clear up some of the conflicting results in the field (clinical trial identifier NCT01569178 [95]).

Mesenchymal Stem Cells

Numerous trials have been conducted using mesenchymal stem cells (MSCs) purified from bone marrow, which are adult cells characterized for their osteogenic, chondrogenic, and adiopogenic differentiation potential [96, 97]. Less than 0.01% of the cells isolated from bone marrow are considered MSCs [98, 99], therefore obtaining clinically-relevant cell numbers requires *ex vivo* expansion.

The first clinical trial investigating the intracoronary injection of MSCs reported an improvement in LV ejection fraction and increased myocardial perfusion 3 months after treatment [99], echoing the results reported using BMMNCs at the time. A few studies have directly compared the safety profile and efficacy of BMMNCs to MSCs, including the TAC-HFT trial [100]. In this study, chronic MI patients received a transendocardial injection of BMMNCs (harvested the day of implant) or MSCs (expanded 4-6 weeks *in vitro* prior to implantation). While there was no difference between groups in the 1-year serious adverse event rate or LV ejection fraction, patients receiving MSCs showed increased regional function by strain analysis and an improvement in exercise capacity. These studies used autologous MSCs; however a limitation of this approach is that autologous MSCs require a significant expansion period between the time of bone marrow aspiration and implantation. The POSEIDON trial was designed to address this and to directly compare the safety and efficacy of autologous MSCs to allogeneic MSCs [101]. Chronic MI patients received a dose of 20, 100, or 200 million autologous or allogeneic MSCs, injected into the myocardium via a transendocardial catheter, and the study concluded that neither cell source stimulated a significant adverse immune response. Curiously, there was an inverse dose response in terms of improved ejection fraction and reversed LV remodeling, with more improvement with the 20 million cell dose than the 200 million cell dose.

Up until this point, studies focused their efforts on testing cells in their native MSC state, but the C-CURE trial took a unique approach by treating autologous MSCs with a cytokine cocktail prior to transplantation [102]. Guided by NOGA electromechanical mapping, these cytokine-stimulated MSCs were transplanted transendocardially into chronic heart failure patients an average of 1540 days post-MI. Cell-treated patients showed an absolute improvement of 7% in

their ejection fraction and enhanced exercise capacity, compared to no improvement in controls. This is a surprisingly large treatment effect, given the long duration post-infarction in these patients. As previously reviewed [103], most MSC studies have demonstrated that the cells die off within a week or two post-transplantation with little direct cardiac differentiation. Mechanisms of benefit in this trial could not be determined, but animal studies suggest it is likely a paracrine action.

Comments on Bone Marrow-Derived Cell Therapy

Through the successful completion of numerous Phase I clinical trials, bone marrow-derived cell therapies have established an important feasibility and safety baseline for delivering cells into the myocardium [80, 104]. While there have been a few reports of significant functional improvement, for the most part these therapies have resulted in a modest reduction in scar size after infarction with little (at best) improvement in systolic function. Because the majority of transplanted cells die off within a few weeks [105] and there is no solid evidence of cardiogenic potential, all benefits are believed to be paracrine-mediated (Fig. 2.1B) [12]. Therapies using BMMNCs and MSCs suggest that intervention by cell therapy can change the trajectory of wound healing and the inflammatory response after an infarction, but with no long-term improvement in global heart function or long-term engraftment, these therapies are not truly regenerating the heart.

Cardiac-Derived Cells

The most recent addition to the clinical trials has been cardiac-derived cells (CDCs), which are derived from myocardial biopsies and grown as explants in culture to obtain an autologous,

cardiac-derived cell population. Studies in rodents have supported their potential to be a more effective cell source than BMMNCs and MSCs [106], and CDCs were originally postulated to be progenitor cells capable of forming new cardiomyocytes. However, most investigators now think that these cells, like bone marrow cells, show minimal long term engraftment or cardiac differentiation and instead work principally through paracrine signaling pathways. The three leading trials using cardiac-derived cells to date are described below.

The SCIPO Trial

The first trial using cardiac-derived cells focused on cells expressing the surface antigen c-kit, which were first isolated and characterized in the rat [107]. Similar to bone marrow-derived cells, initial animal studies suggested that c-kit$^+$ cells gave rise to cardiomyocytes, however lineage tracing studies have determined these cells show minimal long-term engraftment and only extremely low rates of cardiac differentiation in the adult heart [108-110]. The SCIPIO (cardiac Stem Cell Infusion in Patients with Ischemic CardiOmyopathy) trial enrolled 33 heart failure patients with chronic MI (mean ejection fraction of 27.5% at baseline), who underwent a right atrial appendage biopsy during coronary bypass surgery. This atrial tissue was used to isolate a putative cardiac progenitor cell that expressed the surface antigen c-kit and was negative for hematopoietic lineage markers. After four months of *in vitro* expansion, 0.5-1 million cells were injected via the coronary arteries perfusing the ischemic myocardium of 20 patients, while 13 patients remained as controls. Analysis of heart function by 3D echocardiography or cardiac MRI showed an 8.2% and a 12.3% improvement in LV ejection fraction at 4 and 12 months respectively, and, somewhat surprisingly, a reduction in infarct size in a subset of patients [111]. Readers should know, however, that as of this writing, results from this study have been flagged

with an "expression of concern" by the editors of the Lancet relating to an ongoing investigation pertaining to data integrity [112].

The CADUCEUS Trial

The next trial of cardiac-derived cells involved "cardiosphere-derived cells", a mesenchymal cell population obtained by explant culture of endomyocardial biopsies, followed by transient growth as cellular spheroids [113]. Cardiosphere-derived cells are heterogeneous by surface markers, but are primarily $CD105^+/CD45^-$. In the Phase I CADUCEUS trial (CArdiosphere-Derived aUtologous stem CElls to reverse ventricUlar dySfunction) [114, 115], patients with a mean LV ejection fraction of 39% undergoing primary angioplasty 2-4 weeks after MI had a right ventricular biopsy removed to expand autologous cells. After a 1-3 month expansion period, 25 million cardiosphere-derived cells were delivered as an intracoronary infusion into the infarct-related artery. Although the primary endpoint was safety, cardiac MRI at 6 and 12 months after cell delivery revealed a reduction in infarct size (identified as a reduced region of delayed gadolinium enhancement) and an increase in viable myocardium. Although there was no significant change in global ejection fraction, cell-treated patients showed improved regional systolic wall thickening that was maintained from 4 months to 1 year after treatment. The authors interpreted the increase in viable myocardium seen by MRI as regeneration, but pathological hypertrophy of pre-existing cardiomyocytes cannot be ruled out as an alternate explanation. Although not statistically significant, cell-treated patients experienced higher levels of non-sustained ventricular tachycardia and serious adverse events at the 1-year follow-up, which will require closer evaluation in future trials.

The ALCADIA Trial

The ALCADIA (AutoLogous human CArdiac-Derived stem cell to treat Ischemic cArdiomyopathy) trial is ongoing at the time of this review (clinical trial identifier NCT00981006), and takes a combined cell therapy and controlled growth factor-release approach that was first established in a porcine model of chronic MI [116]. The trial enrolled advanced heart failure patients with LV ejection fraction of 15-45% and NYHA class of 3 or 4, with primary endpoints of 1-year safety and secondary endpoints of assessing functional improvement by echocardiography and MRI, NYHA class, and exercise capacity at 6 months. At the time of coronary artery bypass grafting, patients received a transepicardial injection of autologous $CD105^+CD90^+$ cardiac-derived cells grown from an endocardial biopsy (0.5 million cells/kg patient body weight). Injection sites were subsequently covered with a biodegradable gelatin sheet that was loaded with basic fibroblast growth factor (bFGF) by incubation with bFGF prior to implantation. Although there were only six patients enrolled and no controls at the time, preliminary reports suggest an increase in ejection fraction, a decrease in infarct size, and an increase in patient aerobic exercise capacity [117]. If successful in larger-enrollment trials, this dual cell delivery and biomaterials method may promote a shift in clinical approaches in the future towards the combined use of cell and drug delivery, and is a progressive approach that deserves more attention in the pre-clinical and clinical setting. Of course, sorting the effects of the cells from the growth factor delivery will require additional control groups where one of the combined factors is omitted.

Comments on Cardiac-Derived Cell Therapy

Taken together, the achievements made with cardiac-derived cells support some advantages over previous bone marrow-derived cell therapies. The need for *ex vivo* cell expansion of CDCs has provided insight to a later post-MI delivery timeline, and it is promising that cell delivery into mature infarct scars 1-4 months post-MI has resulted in detectable improvements in clinical endpoints (primarily a reduction in infarct size). How such a reduction in scar volume is achieved remains mysterious, because scar size is typically quite stable by 3 months post-MI. We speculate that the cells may reactivate innate immune mechanisms, particularly related to the macrophage. It is important to note that long-term cell retention is almost nil with both CDCs and BMMNCs, so any benefits must require only the transient presence of the cell. Although double-blinded studies with cardiac-derived cells have been precluded by the need for myocardial biopsy, such trials in bone marrow-derived cell therapy have demonstrated the importance of using proper controls, and this will be necessary in moving forward with larger-scale trials. Since some groups are now moving toward allogeneic CDCs, it should be feasible to have placebo-controlled trials and to test these cells in acute MI patients [118].

2.4 Pluripotent Stem Cell-Derived Cardiomyocyte Delivery

Preclinical Development

Considering the modest benefits from heart regeneration clinical trials to date, there has been some debate over cell source – is there a more potent cell type to use for transplantation into the heart? D*e novo* cardiomyocytes meet many of the desired characteristics outlined earlier, but

28

finding a reliable cell source for cardiomyocytes was precluded until the last decade. Methods to derive cardiomyocytes from human pluripotent stem cells (hPSCs) have progressed tremendously since the first report of mouse embryonic stem cell (ESC)-cardiomyocyte derivation [119], and there are now several efficient protocols to achieve cardiac differentiation that mimic developmental pathways (reviewed in [120]). These differentiation advancements have brought hPSC-cardiomyocytes to the forefront as a promising next-generation cell source, and their transplantation into the heart has been studied extensively in pre-clinical experiments. The leading strategy for cell delivery has been the intramyocardial injection of dispersed cardiomyocytes, which mirrors the delivery methods established in many cardiac- and bone marrow-derived cell transplantation clinical trials. Using this approach, various groups have demonstrated that hPSC-cardiomyocytes engraft in the infarct region of numerous animal models and result in an increase in cardiac function (reviewed in [43]).

In contrast to bone marrow derivatives and cardiac-derived cells, human cardiomyocytes give stable, long-term grafts in infarcted hearts [121]. Inherent cell properties give transplanted cardiomyocytes the capability to electrically integrate with the host tissue, which is a prerequisite for synchronous contraction with the host myocardium. The fluorescent calcium reporter protein GCaMP3 [122] has been a useful tool to study the gap junction coupling between graft and host tissue, and genetically modified human embryonic stem cell (hESC)-cardiomyocytes expressing GCaMP have been found to electrically integrate with ischemia/reperfusion injured rat hearts [45] as well as in cryoinjured guinea pig hearts [4, 44] and even non-human primates [1, 123]. Unlike previous cell transplantation studies that are paracrine-driven, this electrical coupling indicates that the engrafted cardiomyocytes are electrically integrating with the host myocardium

and are directly contributing to force generation (Fig. 2.1B). Indeed, improvements in systolic function have been reported in various injury models after hPSC-cardiomyocyte transplantation ([124-126]).

Successful studies demonstrating long-term cardiomyocyte engraftment and functional integration in rodents have motivated the translation of this approach into a non-human primate injury model [1]. Pig-tailed macaques (*Macaca nemestrina*) received an ischemia/reperfusion injury by inflating a balloon catheter into the distal left anterior descending coronary artery for 90 min followed by reperfusion. Two weeks later, after initiating immunosuppression, 1 billion hESC-derived cardiomyocytes were transplanted through transepicardial injections into the infarcted myocardial wall. This study was the first to demonstrate large-scale myocardial remuscularization (Fig. 2.2A), and large cardiomyocyte grafts were found in the infarct region 3 months after transplantation. Engrafted human cardiomyocytes demonstrated *in vivo* maturation from 14 days to 84 days, as indicated by an increase in cell diameter, sarcomere alignment, and myofibril content (Fig. 2B). Grafts were perfused by the host vasculature, which was shown by the presence of $CD31^+$ endothelial cells in the GFP^+ graft and further supported by 3D rendered microcomputed tomography to visualize vessels within the graft region (Fig. 2.2C-D). Furthermore, GCaMP3 fluorescence imaging showed that engrafted cardiomyocytes were electromechanically coupled to the host (Fig. 2.2E), as had been previously demonstrated in rodents. A notable concern from these studies, however, was the detection of non-fatal ventricular arrhythmias in the cardiomyocyte-engrafted hearts. These arrhythmias were not observed in mice, rats or guinea pigs [4], demonstrating the importance of using relevant large animal models. The ventricular arrhythmias will need to be managed for safe translation of

human cardiomyocytes to the clinic. This research in non-human primates was recently replicated using iPSC-derived cardiomyocytes, which further validates the approach [123].

Translating hPSC-Cardiomyocyte Delivery to the Clinic

While pre-clinical therapies with hPSC-derived cardiomyocytes have shown promise and are progressing quickly, questions regarding cardiomyocyte engraftment, phenotype, and large-scale production must be addressed in order to promote successful translation from bench to bedside. Firstly, cell survival after transplantation is low regardless of the cell type and injury model used. Despite the improved engraftment after adopting 'pro-survival' cell treatments prior to implantation [124], current methods are not sufficient to achieve high cell retention long-term. The use of tissue engineering approaches such as the implantation of cell sheets, epicardial patches, or cardiomyocytes delivered in biomaterials may help increase the engraftment rate (reviewed in [32, 38, 127], Chapter 5), although the development of minimally-invasive delivery techniques will be important for clinical translation.
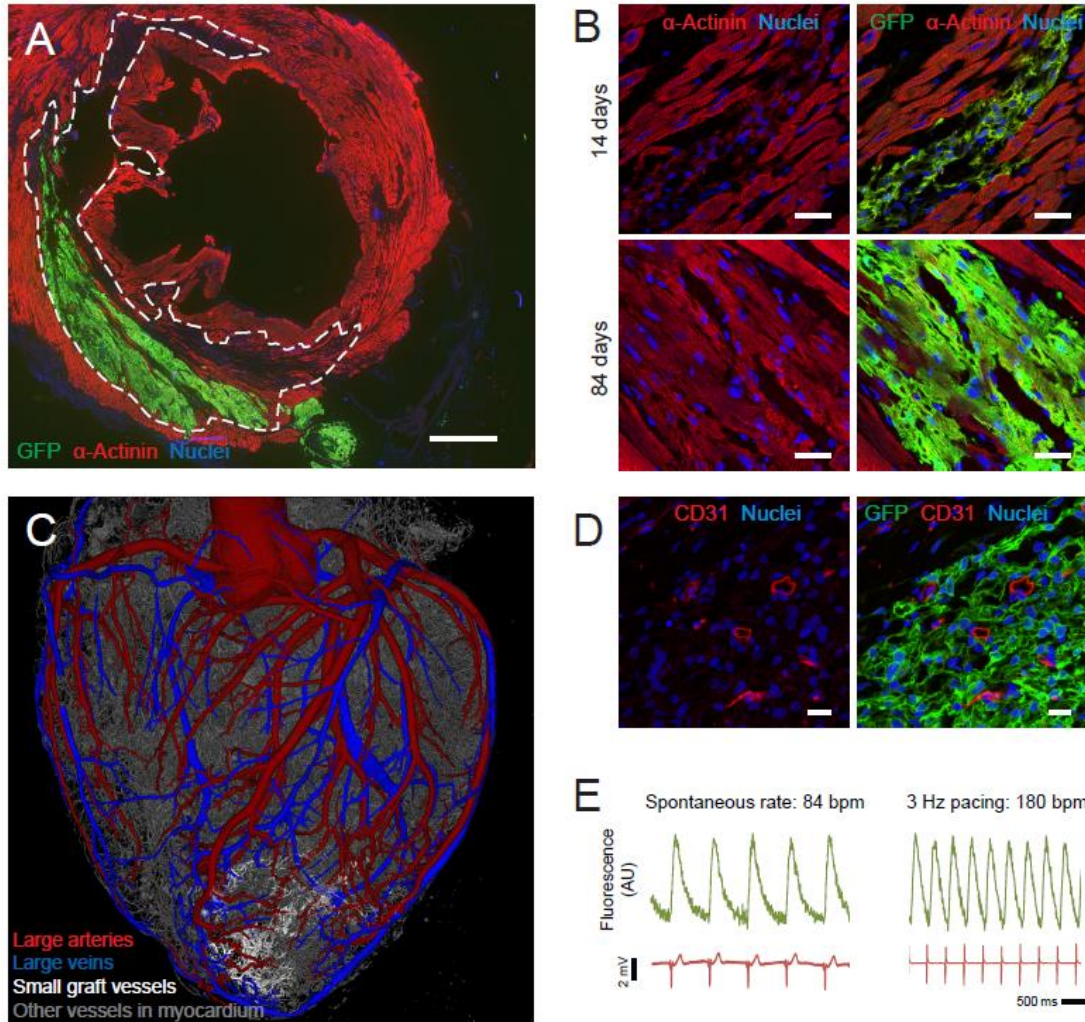
Figure 2.2. Human pluripotent stem cell-derived cardiomyocytes remuscularize the infarcted heart [1]. (A) HESC-cardiomyocytes engraft in the infarcted myocardium (dashed line) at day 14 post-transplantation. Engrafted cardiomyocytes express GFP (human, green) and both hESC-cardiomyocytes and host cardiomyocytes express alpha-actinin (human and monkey, red) with nuclear DAPI counterstain (blue). Scale bar = 2 mm. (B) The *in vivo* maturation of engrafted hESC-cardiomyocytes is evident from 14 days to 84 days post engraftment by co-staining for alpha-actinin (human and monkey, red) and GFP (human, green). Scale bar = 20 μm. (C) Host vasculature perfuses the hESC-cardiomyocyte graft at 84 days post engraftment, as visualized by 3D rendered microcomputed tomography. Large host arteries and veins are shown in red and blue, respectively, and small vessels perfusing the graft are shown in white. Other vessels in the myocardium are shown in gray. (D) Host-derived blood vessels are found within the hESC-cardiomyocyte grafts at 84 days post engraftment. Host endothelial cells express CD31 (human and monkey, red) and infiltrate the GFP-positive graft area (human, green). Scale bar = 20 μm. (E) *Ex vivo* fluorescent GCaMP3 imaging indicates that engrafted human cardiomyocytes are electrically coupled to the infarcted macaque heart at 14 days post engraftment. GCaMP3 fluorescence intensity (green) and host ECG (red) are plotted versus time and demonstrate 1:1 coupling at spontaneous rate as well as during atrial pacing at 3 Hz.

Secondly, the optimal maturation state of cardiomyocytes for transplantation is not fully understood. Previous studies suggest that an intermediary maturation state may be ideal: mature adult cardiomyocytes do not survive transplantation [128], immature hESC-cardiomyocytes have automaticity, slow conduction and may be pro-arrhythmic [1], and mesodermal cardiac progenitor cells do not outperform definitive cardiomyocytes in terms of engraftment or efficacy [129]. Current *in vitro* approaches may mature cardiomyocytes from the 'early fetal' state typically achieved after differentiation into a late-fetal or neonatal stage. While *in vitro* maturation to an adult phenotype will be difficult, as indicated above it also is undesirable for transplantation purposes (reviewed in [130]). Experiments that directly compare the engraftment of aged hPSC-cardiomyocytes to the current standard are needed, as well as studies designed to track implanted cells and characterize their maturation *in vivo*.

Lastly, one of the major hurdles for successful translation of hPSC-cardiomyocytes into the clinic is developing an "off-the-shelf" cardiomyocyte cell product: will these come from hESCs or from human induced pluripotent stem cells (hiPSCs)? The biggest advantage of using hiPSCs is their ability to provide an autologous cell source, but unfortunately this is also one the major limitations when it comes to clinical and financial feasibility. The process of obtaining patient-specific somatic cells, reprogramming to iPSCs, differentiating into cardiomyocytes (perhaps requiring individual protocol optimization), and performing quality control would take over four months [30]. This precludes their use in an acute or subacute MI setting, and conversely, we have shown that hPSC-derived cardiomyocytes have no beneficial effect on cardiac function when delivered into chronic myocardial infarcts in rodents [44, 121]. An additional limitation of the autologous hiPSC approach is the cost. At present there are very expensive quality control

experiments that are required before the release of a product derived from pluripotent stem cells, and doing this for each patient is cost-prohibitive unless the regulatory path is changed. There is also an inherent risk of residual undifferentiated stem cells giving rise to teratoma formation, and proper quality control measures must be taken to minimize this risk [131].

Most pre-clinical models thus far have used hESC-cardiomyocytes, although immunosuppression after an allogeneic hESC-cardiomyocyte implantation is a potential downfall of the therapy and requires more research to elucidate proper immunosuppression strategies that address the differential immunogenicity and rejection of autologous vs allogenic cells (reviewed in [132]). Research strategies to engineer HLA-homozygous hESC subclones or "universal donor cells" that are HLA class 1-negative will be useful in addressing this problem, and exciting progress has been made on this front in recent pre-clinical work [133]. Regardless of cell source, it remains unclear if this number of cells can be mass-produced for clinical use in a way that is financially manageable and biologically controlled. Cardiomyocyte production will need to be scaled up significantly to meet the current demand, although the development of methods to increase cardiomyocyte proliferation for *in vitro* scale-up may help alleviate this concern.

2.5 Summary and Concluding Thoughts

As the field of cell-based cardiac repair has matured there has been a natural shift from basic studies towards more clinical and translational goals. Nevertheless, it is important to continue with studies focusing on the underlying biology of heart regeneration; understanding the biological mechanisms of cardiac repair will be critical in the field's success regardless of therapeutic approach used. Simply put, unless we understand the mechanisms through which cell therapies work, there is no way to rationally improve upon them. A promising alternative approach to heart regeneration is stimulating endogenous repair after injury, which takes advantage of cues learned from regeneration experiments in lower vertebrates and the discovery of the mammalian regenerative window after birth (reviewed in [5]). Although this approach is far from the clinic, exciting progress has been made to identify factors that promote cardiomyocyte dedifferentiation and proliferation after injury, including the overexpression of cyclins [49-51], FGF and NRG signaling pathways [52, 53], Notch signaling [54, 55], and microRNAs [26]. Lessons learned here will provide important insight to the cell therapy field and may guide the development of dual gene and cell delivery therapies.

There are multiple parameters to consider when working towards clinically meaningful regeneration including functional recovery, attenuation of fibrosis, preventing adverse remodeling, cardiomyocyte proliferation (and subsequent increase in viable myocardium), and the maturation of regenerated cardiomyocytes. Because an ideal therapy would be suitable for patients with recent cardiac injury or with established heart failure, pre-clinical studies will require careful evaluation of how to translate benefits to a more chronically affected patient

population. The approaches discussed in this review were limited to ischemic heart disease; however the advancements in the field will have broad implications for other heart failure patients, such as those suffering from dilated cardiomyopathy, hypertrophic cardiomyopathy, or congenital heart disease. Better understanding the biology governing the heart's response to injury and to regenerative cues will provide insight to better direct gene therapy, drug delivery, and tissue engineering approaches that target non-ischemic heart disease.

In conclusion, the past few decades of heart regeneration research have been exciting and informative. Considerable progress has been made to establish cell transplantation techniques with bone marrow-derived cells and cardiac-derived cells, and hPSC-derived cardiomyocytes have been well established in pre-clinical studies as a promising cell type moving forward. While many challenges lie ahead before successfully regenerating the human heart, we are optimistic that the field is moving forward on a promising path.

Chapter 3. Intramyocardial delivery to enhance electrical integration of hESC-cardiomyocytes

This chapter has been published in [45] .

3.1 Abstract

Human embryonic stem cell-derived cardiomyocytes delivered as suspended cells or engineered cardiac tissues are a promising approach to regenerate the heart after ischemic injury, however, integration with the host myocardium is required to achieve electromechanical benefit. We conducted a comparative study to assess the engraftment and the ability to electrically integrate with the host of three distinct cell delivery methods. HESC-derived cardiomyocytes were used to form either scaffold-free epicardial tissue patches or micro-tissue particles delivered by intramyocardial injection, and compared to intramyocardial injection of dispersed cells into the left ventricular wall of the ischemia/reperfusion injured athymic rat heart. All three implantation methods resulted in consistent engraftment after 4 weeks, and showed a negative correlation with scar size. Based on the graft-autonomous GCaMP3 Ca2$^+$ reporter and *ex vivo* fluorescent imaging, 100% of the detected intramyocardially-delivered grafts (suspended cardiomyocytes and micro-tissue particles) were electrically coupled to the host heart at spontaneous rate and could follow host pacing up to a maximum of 300 - 390 beats per minute (5 - 6.5 Hz). Evidence of gap junction formation between intramyocardial grafts and host tissue were identified histologically. In contrast, epicardial tissue patches were electromechanically active but beat slowly and were not electrically coupled to the host, separated from the host myocardium by a

layer of scar tissue. Thus, we demonstrated for the first time the electrical coupling of hESC-cardiomyocytes to the rat heart, supporting the use of the rat ischemia/reperfusion model for further assessment of remuscularization and electromechanical integration of human cardiomyocytes, and highlighting the benefits of intramyocardial versus epicardial delivery approaches.

3.2 Rationale

This chapter focuses on investigating the effect of delivery strategy on hESC-cardiomyocyte graft size and electromechanical integration. The two hypotheses tested are (1) engineered cardiac tissue will produce larger grafts than single cell transplantation, and (2) intramyocardial delivery methods will promote electrical integration of the graft with host tissue compared to epicardially-delivered tissues. To address this, we chose a rat model of ischemia/reperfusion with cell delivery 4 days after injury.

Cell-based regenerative medicine methods for cardiac repair have been well-described in rodent models [4, 124, 125], and involves the transplantation of hESC-cardiomyocytes either as dispersed cells or as tissue engineered patches, sheets, or in biomaterials. Engineered cardiac tissues are typically attached to the epicardial surface with sutures or adhesives [127, 134-136], however in our experience they are often separated from the host myocardium by scar tissue. This observation raised concerns about their ability to form gap junctions with host myocardium, which are necessary for electromechanical integration. Transplanted hPSC-cardiomyocytes have been shown to electrically couple to the host myocardium in the guinea pig (with a heart rate of 200–250 bpm [4, 44]) and the macaque monkey (with a heart rate of 80–120 bpm [1]). However

38

many groups have transitioned to larger animal models or discredited the potential to achieve electrical coupling of human cardiomyocytes in rodent models, due to the fast heart rate of rats and mice of over 300 beats per minute. In this chapter, we demonstrate for the first time the direct electrical coupling of hESC-cardiomyocytes to the rat heart when delivered intramyocardially, supporting the use of the rat ischemia/reperfusion model and highlighting limitations of current cardiac tissue engineering implantation strategies.

3.3 Methods and Scientific Strategy

HESC-Derived Cardiomyocyte Culture and Differentiation

RUES2 cells were genetically engineered to express GCaMP3 as described elsewhere [1, 4]. Undifferentiated GCaMP3 hESCs were maintained in culture on Matrigel™ in mouse embryonic fibroblast (MEF)-conditioned media supplemented with 5 ng/ml basic fibroblast growth factor (bFGF). Cardiomyocyte differentiation was induced using a previously-described protocol with minor modifications [124] (Figure 3.1). Briefly, cells were seeded in a high-density cell monolayer with 1 μM CHIR99021 followed by the addition of 100 ng/ml Activin A and 1x Matrigel in RPMI-1640 basal medium with B27 Supplement minus insulin the following day. After 18 hours media was changed to the same basal media supplemented with 1 μM CHIR99021 and 5 ng/ml BMP4. Two days later media was changed and supplemented with XAV939 for an additional 48 hours. Following day 7 of differentiation cells were maintained in RPMI-1640 supplemented with B27 supplement containing insulin. Beating was typically observed between days 7 and 10, and media was changed every 2-3 days thereafter. For the *in*

vitro electrical stimulation experiments, hESC-cardiomyocytes at 21-24 days of differentiation were replated in triplicate into Matrigel-coated 6-well plates coated with Matrigel™ and field-stimulated at 1 or 6 Hz (5 V/cm, 4 ms pulse width) using the C-Pace Culture Stimulator. Cells were analyzed at 2, 4, and 6 weeks for measurement of spontaneous rate, excitation threshold (V), and maximum capture rate (Hz).
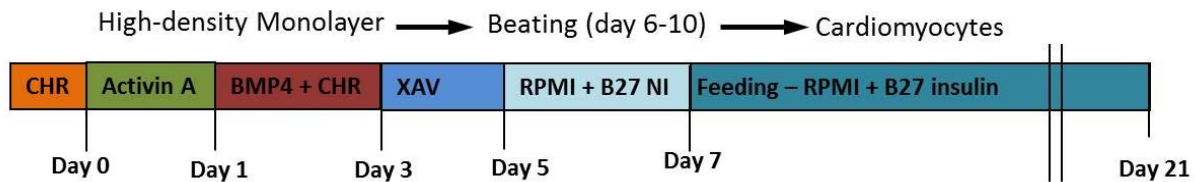
Figure 3.1. High-density monolayer directed cardiac differentiation protocol. Human pluripotent stem cells are plated in a monolayer on Matrigel and pre-treated with CHR (CHIR99021). At induction (Day 0), media is changed to RMPI-1640 containing Activin A and Matrigel. Media is changed to include BMP4 and CHR the next day, followed by another media change at Day 3 with XAV treatment.

Flow Cytometry to Assess Cardiac Purity

Fluorescence activated cell sorting (FACS) was used to characterize the differentiated cell population. Briefly, cells were fixed with 4% paraformaldehyde and incubated with a cardiac troponin T (cTnT) antibody, followed by incubation with a PE-conjugated secondary antibody. Fluorescence characterization was performed on a BD FACS Canto II and subsequently analyzed using FloJo software. The input cardiomyocyte purity showed $50 - 94\%$ pure populations (average $70.2 \pm 14.2\%$; Figure 3.2).
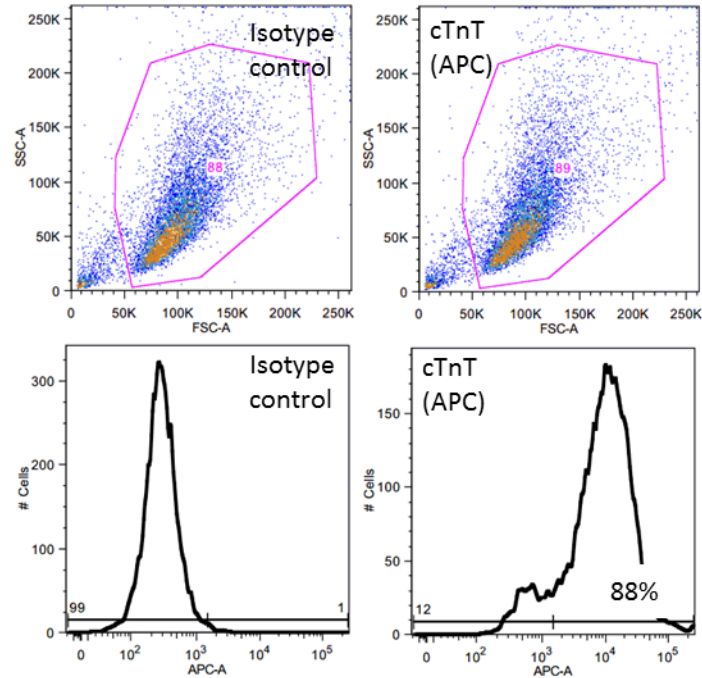
Figure 3.2. Flow cytometry for cTnT is used to assess cardiomyocyte purity. Isotype control sample is shown in the left column, and cTnT-stained sample is shown in the right column. The top panel shows forward scatter (FSC) and side scatter (SSC) used to identify single cells (outlined in pink). An APC-labeled secondary antibody labels cTnT$^+$ cells, shown here as a histogram identifying 88% of cells express cTnT-APC.

Cryopreservation of hESC-Cardiomyocytes

Cardiomyocytes were cryopreserved on day 21-24 of differentiation and thawed immediately prior to engineered tissue formation or cell injection, following a previously described protocol [137]. Briefly, cells were heat shocked for 1 hour at 42°C the day prior to cryopreservation. 10 µM ROCK inhibitor Y-27632 was added to the culture medium for 1 hour, and cells were washed with PBS, briefly incubated with EDTA, dispersed to single cells with 0.25% trypsin in EDTA, and resuspended in CryoStor and frozen in cryovials in a controlled rate freezer to -80°C before storage in liquid nitrogen. For thawing, cryovials were incubated briefly at 37°C followed by addition of basal media supplemented with 200 U/ml DNAse. Cells were washed and resuspended in either basal media with 10 µM Y-27632 for micro-tissue particle or patch

formation, or in an RPMI-based pro-survival cocktail [124] for cell implantation containing 50% (vol/vol) growth factor-reduced Matrigel™, 100 μM ZVAD (benzyloxycarbonyl-Val-Ala-Asp(O-methyl)-fluoromethyl ketone), 50 nM Bcl-X_L BH4 (cell-permeant TAT peptide), 200 nM cyclosporine A, 100 ng/mL IGF-1, and 50 μM pinacidil.

Engineered Tissue Formation

Immediately after cell thawing, cardiac micro-tissue particles were formed in polydimethylsiloxane (PDMS) microwells using AggreWell™ 400 plates. 10 million hESC-cardiomyocytes were distributed by centrifugation into 8 wells containing approximately 1,200 microwells each, yielding approximately 1000 cells/micro-tissue particle (Figure 3.3A). Micro-tissue particles formed overnight and were easily washed out of wells to be used for implantation the following day (Figure 3.3B). Epicardial patches were formed by seeding 10 million cardiomyocytes into custom made round-bottom PDMS molds and allowed to settle for 1 hour at 37°C before additional media was added, incubated overnight, and then maintained in rotating suspension culture for 4-6 days prior to implantation (Figure 3.3C, D). Media was changed every other day. Micro-tissue particles and cardiac patches were heat shocked for 1 hour at 42°C the day before implantation and incubated in 200 nM cyclosporine A and 100 ng/ml IGF-1 overnight. For implantation, engineered tissues were harvested by gently pipetting media to wash particles and patches out of the PDMS molds as necessary, suspended in pro-survival cocktail as described above, and maintained on ice until implantation.
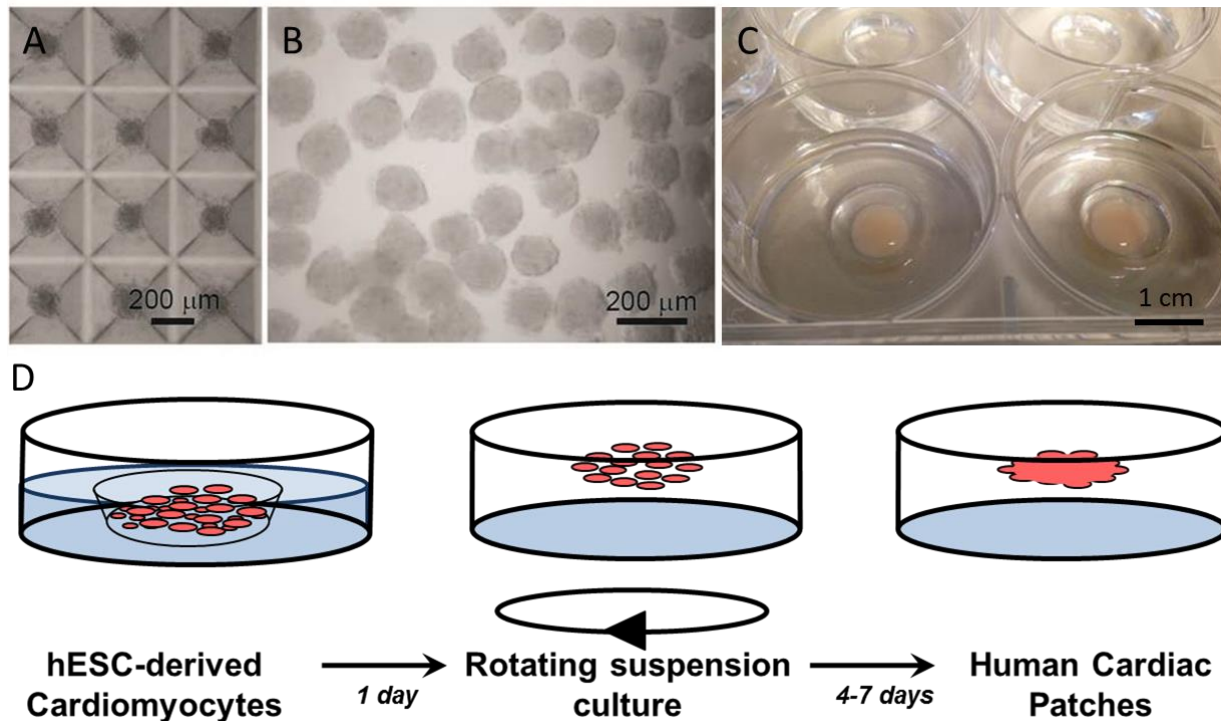
Figure 3.3. Engineered cardiac tissue formation. (A) Micro-tissue particles are formed overnight in PDMS molds and (B) can be easily washed out of wells prior to implantation. (C) Engineered cardiac patches are formed in custom-made PDMS molds overnight. (D) After overnight incubation, tissues are moved to suspension culture for up to 1 week. *Image (D) courtesy of Kareen Coulombe.*

Ischemia/Reperfusion Injury and Cardiomyocyte Implantation

All animal procedures were conducted in accordance with the US NIH Policy on Humane Care and Use of Laboratory Animals and the UW Institutional Animal Care and Use Committee (IACUC). Eight-week old (250g) male athymic Sprague-Dawley rats were anesthetized with intraperitoneal injection of 90 mg/kg ketamine and 6 mg/kg xylazine, intubated, and mechanically ventilated. The rat was placed on a warming pad with a water circulation system to maintain core body temperature at 37°C. A thoracotomy exposed the heart, and the left anterior descending (LAD) coronary artery was occluded for 60 minutes, reperfused, and the chest was

43

aseptically closed. Four days after ischemia/reperfusion injury, rats were anesthetized with up to 5% isoflurane supplemented with oxygen, intubated, and mechanically ventilated. A second thoracotomy was used to open the chest and dispersed single cells or micro-tissue particles suspended in 90 µl of pro-survival cocktail were injected into the center of the infarcted left ventricle wall and each lateral infarct border zone ($10x10^6$ cells total input cells, 3 injections, 30 µl each, purse-string suture with 8-0 suture). Sham control rats received injection of vehicle only. A 29-gauge needle was used for dispersed-cell and sham injections, and a 24-gauge needle was used for micro-tissue particle injections. For epicardial patch implantation, the patch was bathed in pro-survival cocktail for 1 hour prior to being placed over the infarct. One to three 8-0 sutures were used to attach the epicardial patch. The chest was closed and animal recovery was monitored. Rats received buprenorphine for 2 days post-surgery. Animals received a 0.75 mg cyclosporine A by subcutaneous injection for 7 days beginning the day before implantation, as per the established pro-survival cocktail protocol [124].

Ex Vivo Fluorescent Imaging of GCaMP3 Micro-Tissue Particle Grafts

4 weeks after implantation animals were sacrificed by beauthasol overdose, and the hearts were collected and mounted on a Langendorff apparatus perfused with modified Tyrode solution at 37°C as described previously [1, 4]. 2,3-butanedione monoxime (BDM, 12-20 mM) was used to mechanically arrest the heart, and the GCaMP3 fluorescent signal was imaged using an EXFO X-Cite illumination system mounted on an epifluorescent stereomicroscope. The fluorescent signal was captured and recorded by an Andor iXon 860 CCD camera along with the heart ECG (recorded in LabChart). Identified grafts were electrically paced through the host myocardium via insertion of electrodes, and data analysis was performed using Andor software and LabChart

44

as described elsewhere [4]. At the end of the imaging experiment, permanent medical dye that survives histological processing was used to mark the location of imaged grafts (Figure 3.4).
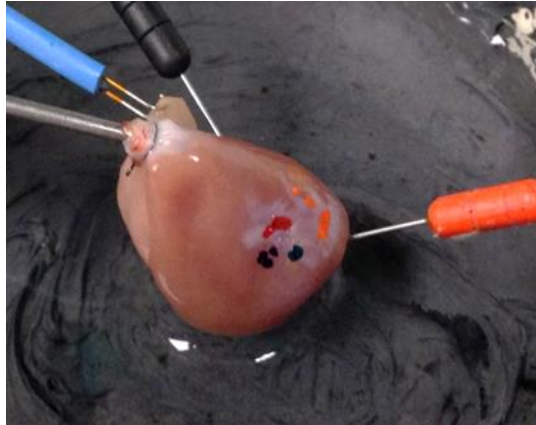
Figure 3.4. Epicardial dye is painted onto the graft regions identified via *ex vivo* fluorescent GCaMP3 imaging. The scar is identified by the white region on the heart. Equipment of interest are the blunted aortic perfusion needle (gray), the stimulating electrode (blue), and the ECG leads (black, red).

Immunohistochemical Analysis

Immunohistochemistry and analysis were performed as described previously by our group [1, 124]. Briefly, following *ex vivo* imaging, hearts were perfused with 150 mM KCl solution, fixed overnight in 4% paraformaldehyde, and then processed, sectioned, and stained histologically. Infarct area was quantified by measuring the area of collagenous scar labeled by picrosirius red within each section, normalized to left ventricular area. To quantify graft size, sections were incubated overnight with rabbit anti-GFP antibody followed by a one-hour incubation with either Alexa Fluor-488 goat anti-rabbit or with an avidin-biotin goat anti-rabbit antibody and developed with diaminobenzadene (DAB). Cardiac purity and analysis of engrafted cells was assessed on sections double-stained for GFP and alpha-actinin (mouse monoclonal) or connexin 43 (rabbit polyclonal) with corresponding Alexa Fluor secondary antibodies.

45

Statistical Measurements

All histological measurements were made using ImageJ. All 8 animals in each treatment group were included in the analysis, including one animal per group that showed zero graft regions in an "intent-to-treat" analysis. Statistical significance ($p < 0.05$) was determined using correlation analysis or by two-way ANOVA where significant differences followed by a two-tailed Student's t test assuming unequal variance in Graphpad Prisim software. All values are reported as means, and error bars represent SEM.

3.4 Results

In Vitro Characterization of Engineered Cardiac Tissues

Engineered cardiac tissues were highly-cardiac, demonstrated by histological staining for beta myosin heavy chain for the micro-tissue particles (Figure 3.5 A) and epicardial patches (Figure 3.5B). Micro-tissue particles consolidated overnight and showed reproducible diameters based on input number of cells per particle (Figure 3.5C). For this study we chose to use 1000 cells per particle, corresponding to a diameter of <200 μm to be compatible with 24 gauge needle delivery (inner diameter of 311 μm). When MTPs are formed using less pure cTnT$^+$ cell populations (not used for animal studies), culturing micro-tissue particles *in vitro* in standard culture media (RPMI-1640 with B27 containing insulin) results in an increase in cardiac purity over time (Figure 3.6).
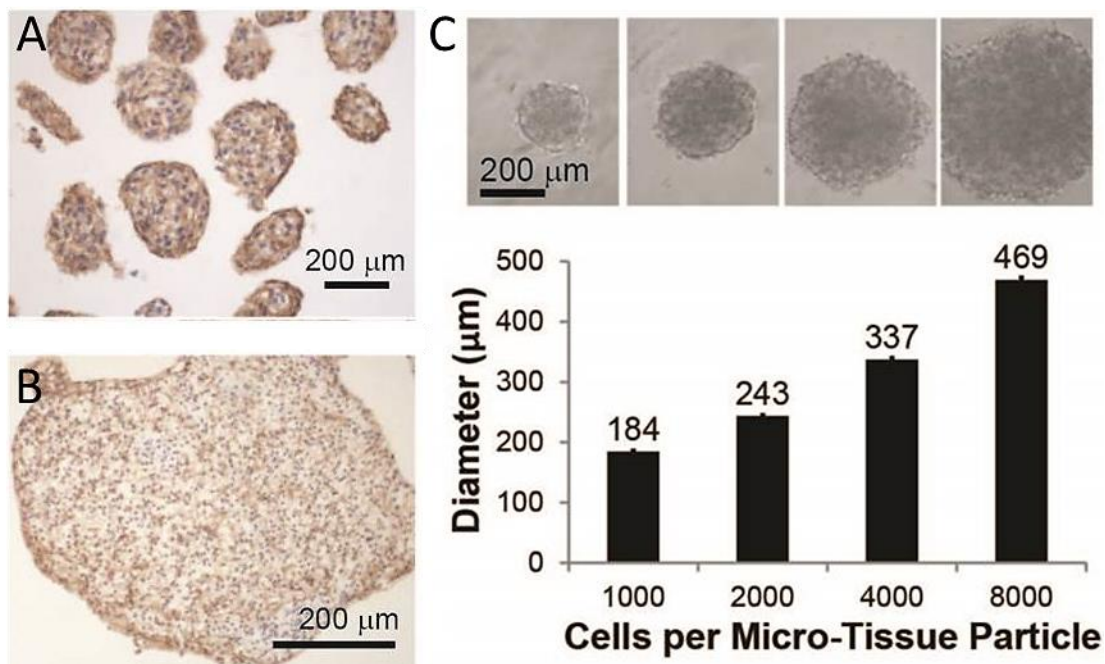
Figure 3.5. Histological assessment of engineered cardiac tissues prior to implant. Cardiac engineered tissues have high cardiac purity as indicated by beta myosin heavy chain (brown) in MTPs (A) and cardiac patches (B). Scale = 200 μm. (C) MTPs have defined particle diameter based on cell input number.
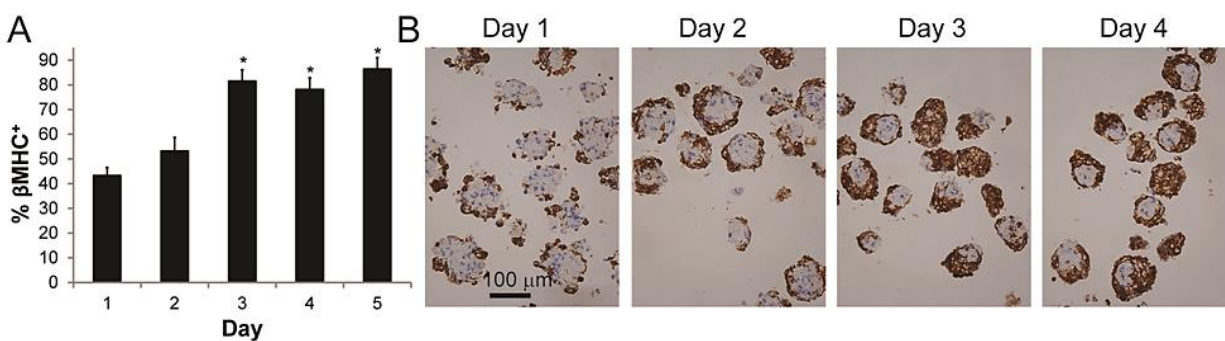
Figure 3.6. Cardiac purity increases in MTPs over days in culture. (A) Percent of βMHC$^+$ area in tissues increases significantly between days 1 and 3 in culture. (B) Representative histological images of MTPs are stained for βMHC and visualized with DAB (brown) after being cultured for one to four days. Scale bar = 100 μm.

Histological analysis for GFP was used to detect the GCaMP3 transduced hESC-cardiomyocytes four weeks after transplantation. In each of the three implantation groups, hESC-cardiomyocytes were identified in 7 of 8 hearts (87.5%) within the ventricular wall for dispersed cells and micro-tissue particles and on the epicardial surface for cardiac patches (Figure 3.7). Co-localization of GFP and α-actinin demonstrated a high percentage of cardiomyocytes within the grafts with visible sarcomere striations, with few surviving non-cardiac cells for all three implantation groups (i.e. only rare GFP^{+}/ α-actinin^{-} cells).
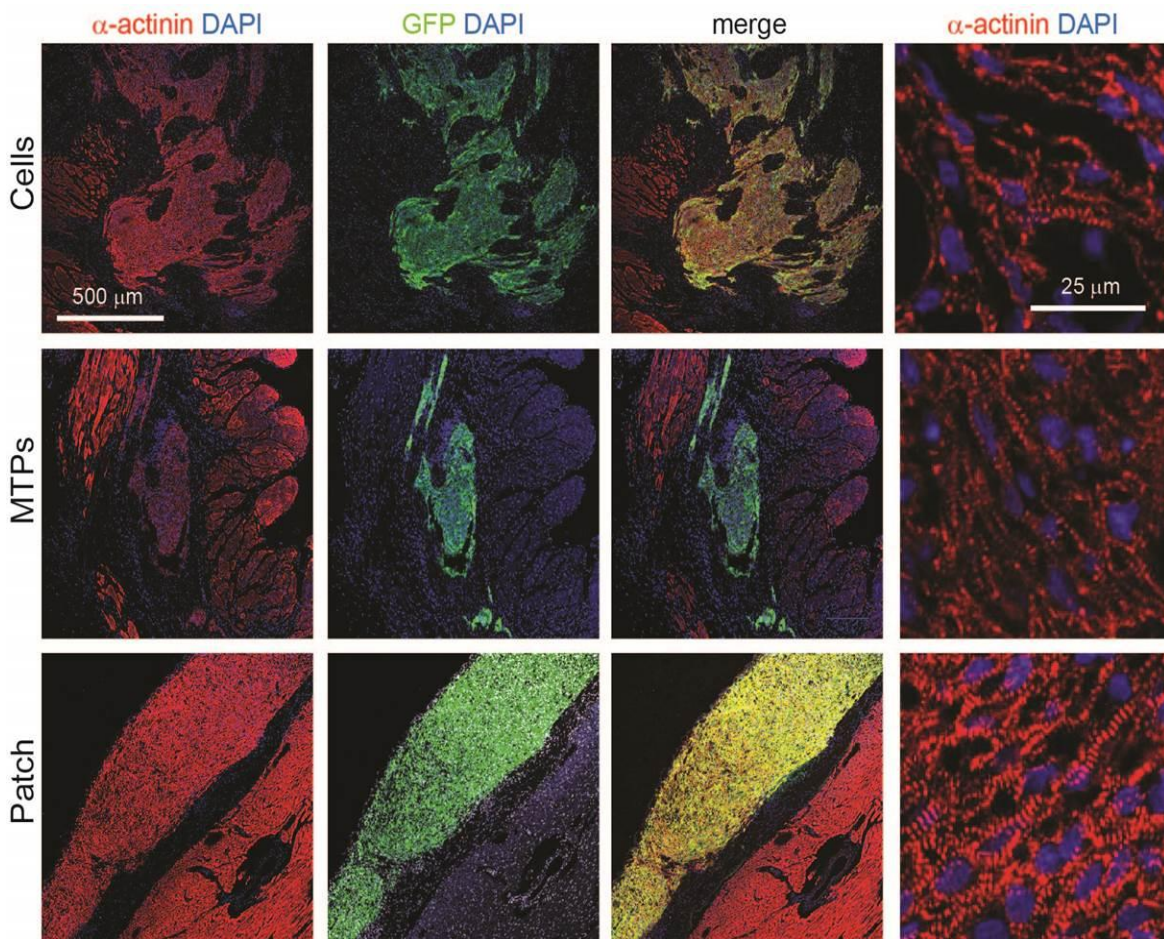
Figure 3.7. All three engraftment methods produce grafts with high cardiac purity at 4 weeks, indicated by a double-positive stain for α-actinin (red) and GFP (green) with nuclear DAPI (blue). All grafts demonstrate sarcomere striations at higher magnification (far right). In the patch graft, scar tissue appears as the dark band separating the patch graft and host myocardium. Scale bar = 500 μm and 25 μm (far right column).

Dispersed cell and micro-tissue particle injections were found spread within the myocardial wall (Figure 3.8), while cardiac patches maintained most of their initial shape to produce a uniform, thick mass of transplanted hESC-cardiomyocytes that was consistently found on the epicardial surface (100% of grafts). Histological analysis of the intramyocardial grafts showed similar distribution between groups with 20% found in the scar, 31% in the border zone, and 49% in the healthy tissue for the dispersed cardiomyocytes, and 34% were found in the scar, 28% in the border zone, and 38% in the healthy tissue for the micro-tissue particle group (Figure 3.9).
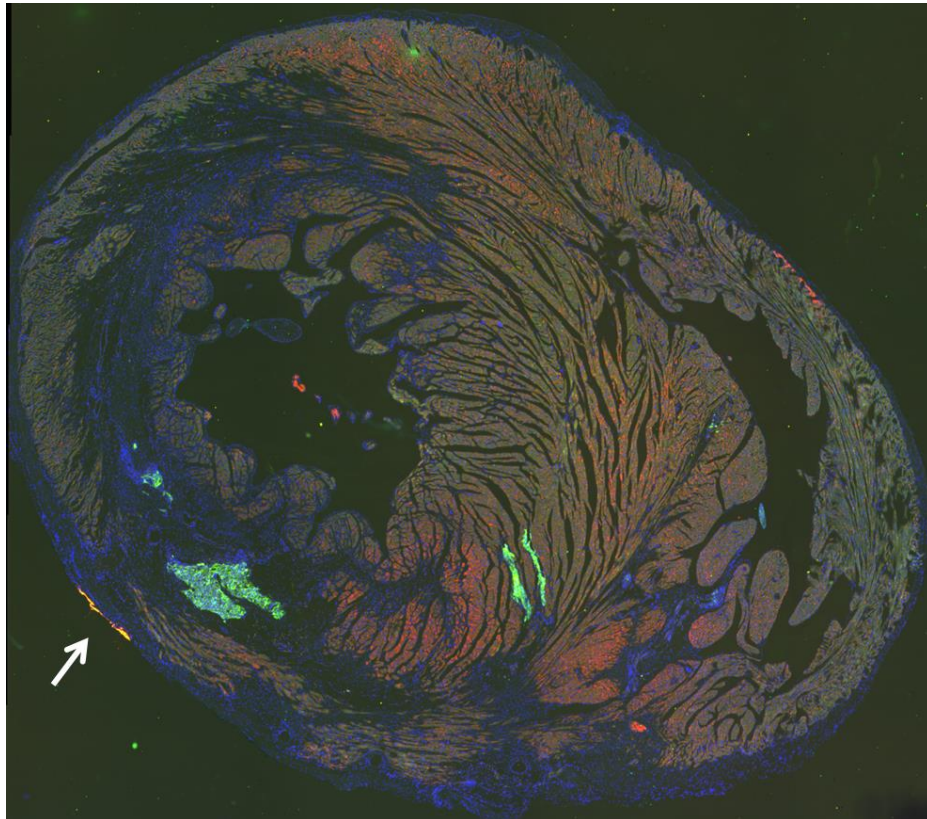
Figure 3.8. Micro-tissue particles engraft within the myocardial wall. A full profile view is shown after histological staining at 4 weeks after implantation of micro-tissue particles. The tissue section is stained for GFP (green) to identify the human cells, connexin 43 (red) to label gap junctions, and nuclei are labeled with DAPI (blue). Scar region here can be identified by the dark regions within the myocardium that lack connexin 43 staining. Epicardial dye applied during *ex vivo* imaging labels a fluorescent graft region that was recorded for electrical coupling analysis (white arrow).
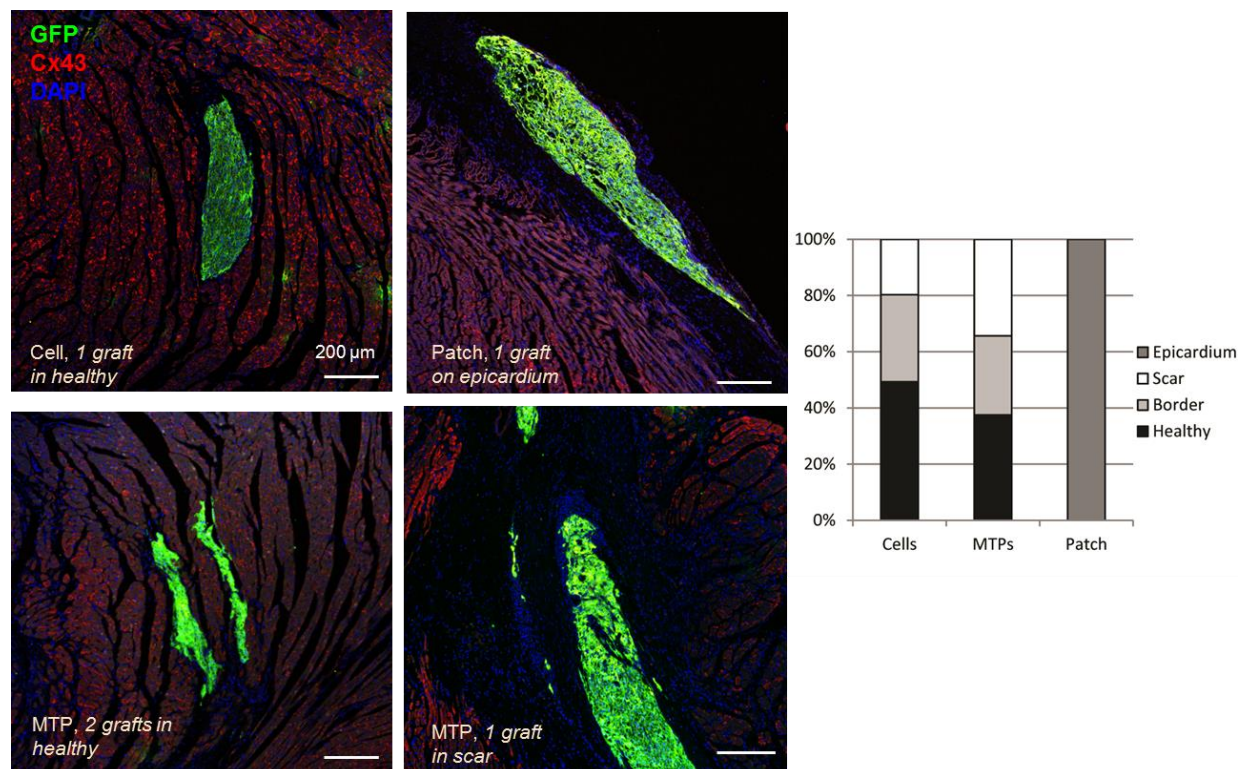
Figure 3.9. Distribution of graft area between groups. Human myocardial grafts are identified within the myocardium after histological staining for GFP (green), with a nuclear DAPI stain (blue) and gap junctions are visualized by Cx43 (red). Images show sample graft regions and criteria used for graft distribution analysis as labeled. At right, distribution of graft localization in the heart is graphed for grafts identified on the epicardium, within the scar region, in the healthy myocardium, and in the border zone region between the infarct and healthy tissue.

Graft Size is Equivalent between Groups and is Inversely Correlated with Infarct Size

Although infarct size was not measured at baseline prior to treatment, infarct size was equivalent between the three groups by histology at four weeks after implantation (Figure 3.10, Table 3.1). Contrary to our hypothesis, there was no statistical difference in graft size between the three implantation groups (Figure 3.10, Table 3.1). In looking more closely at the data, we noticed an apparent inverse correlation between graft size and scar size. Considering all engraftment groups

collectively, correlation analysis showed that engraftment declined significantly with increasing infarct size (r= -0.36, P<0.05, R^2=0.13). This trend remained significant for cell grafts (r= -0.76, P=0.03, R^2=0.58) but not for MTP or patch grafts. This finding requires further follow-up, because an ideal therapy would result in robust engraftment regardless of infarct size. Thus, if the engineered cardiac tissue is able to overcome the inverse correlation observed here, it represents a potential advantage over dispersed cardiomyocytes. Anterior wall thickness of the left ventricle was measured by histology and increased in all implantation groups compared to sham, which is consistent with previous reports (2.2 ± 0.1 mm for the cell group, 2.4 ± 0.1 mm for the MTP group, 2.0 ± 0.1 mm for the patch group, and 1.4 ± 0.1 mm for sham controls, Figure 3.11).
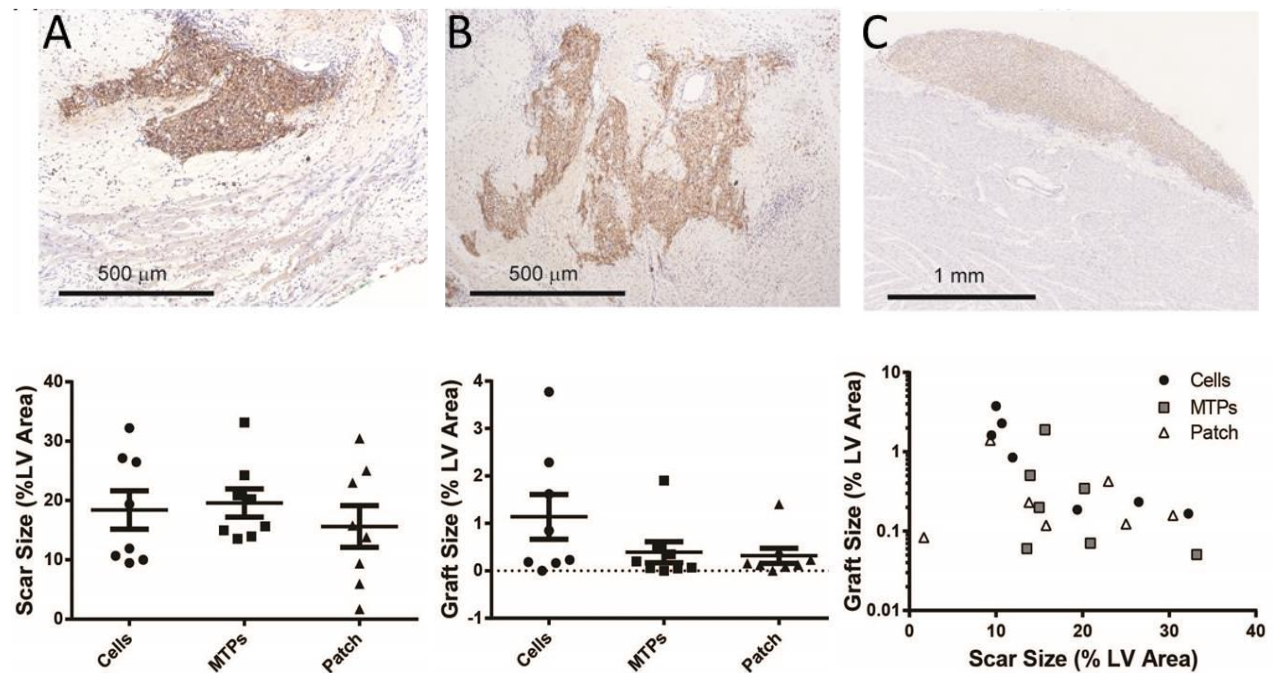
Figure 3.10. Infarct and graft area at 4 weeks between cells, MTPs, and Patches. Graft regions are analyzed by quantifying βMHC$^+$ area within the myocardium as shown here in (A) cells, (B) MTPs, and (C) patches. Infarct area shows no difference at 4 weeks between groups, normalized to LV area. Graft area normalized to LV area is equivalent between groups, but graft area declines with larger scar area for the cell grafts (not significant in the engineered tissue groups).

Group	Scar Size (%LV area)	Graft Size (% LV Area)	Graft Size (% Scar Area)	Grafts Detected by Ex Vivo Imaging	Detected Grafts Coupled to Host	MCR Range (Hz)
Dispersed Cells	18.4 ± 3.2	1.1 ± 0.5	9.7 ± 4.5	4/8 hearts	4/4 grafts	5.5 - 6.5
Micro-Tissue Particles	19.6 ± 2.4	0.4 ± 0.2	2.5 ± 1.2	6/8 hearts	6/6 grafts	5.0 - 6.0
Patches	15.6 ± 3.5	0.3 ± 0.2	10.8 ± 9.5	6/8 hearts	0/6 grafts	NA

Table 3.1. Summary of hESC-cardiomyocyte engraftment by histology and *ex vivo* fluorescent imaging. MCR, maximum capture rate; NA, not applicable.
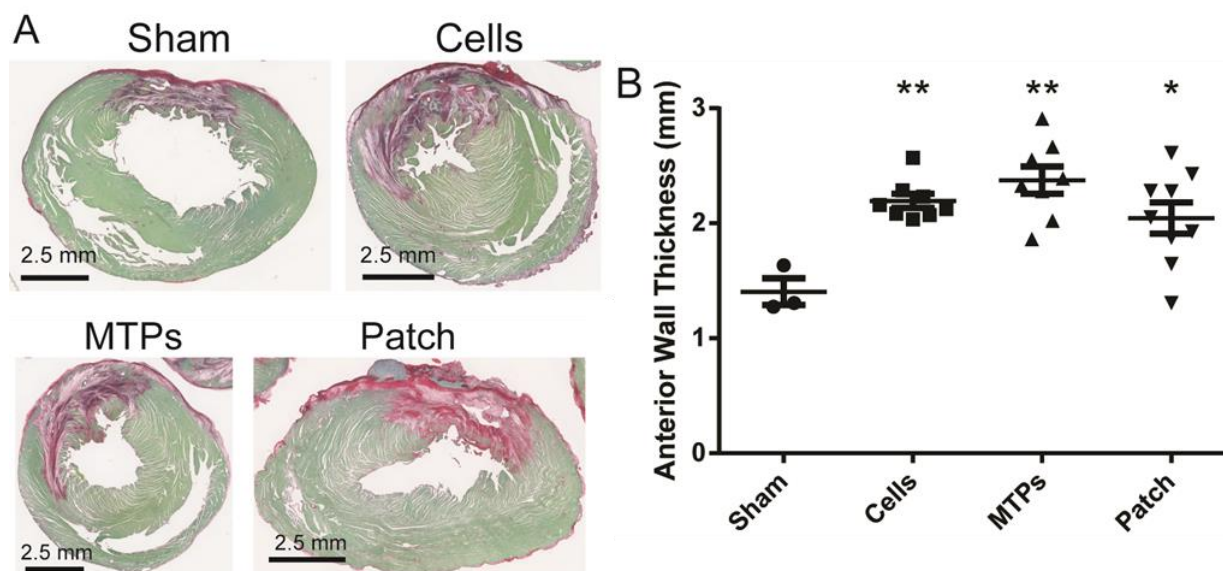
Figure 3.11. Picrosirius red infarct area and anterior wall thickness. (A) Infarct area is identified by staining for picrosirius red to label collagenous scar (red) with a fast green counterstain (green) to label healthy myocardium. Representative images are shown for Sham, Cells, MTPs, and Patch implants. Scale = 2.5 mm. (B) Anterior wall thickness is quantified by histology in mm.

Intramyocardial Delivery Improves Electrical Coupling of Graft to Host vs Epicardial Delivery

Electrical coupling between engrafted cells and host tissue is required in order for engrafted cardiomyocytes to directly contribute to force production. To evaluate the possibility of hESC-cardiomyocytes electrically coupling with the rat heart in the three implantation groups, we used *ex vivo* imaging of the GCaMP3 fluorescent signal in Langendorff-perfused hearts. Grafts were identified by GCaMP3 imaging in all implantation groups (Table 3.1), although it was most difficult in the dispersed cell injection group where only 4 of 8 hearts had grafts detectable *ex vivo* even though 7 of 8 hearts had grafts detectable by immunohistochemistry (Figure 3.7). For both micro-tissue particles and epicardial patches, 6 of 8 hearts had grafts detectable by GCaMP3 imaging, while 7 of 8 hearts had grafts detectable by immunohistochemistry. In both the dispersed cell and micro-tissue particle groups, 100% of the grafts identified during GCaMP3 imaging produced fluorescent GCaMP3 signals that were coupled 1:1 with the heart's ECG recording under spontaneous rhythm, indicating electrical coupling of the cardiomyocyte grafts to the host heart (Figure 3.12). Some of these rats exhibited up to 4 detectable graft regions, all of which were coupled with the ECG under spontaneous rhythm. To challenge these grafts, we electrically stimulated them through the host ventricle at increasing frequencies to determine the maximum pacing capture rate of the graft, some up to a maximum of 6.5 Hz. Maximum capture rate was 6.1 ± 0.2 and 5.4 ± 0.2 for cell and MTP groups, respectively (Table 3.1). In stark contrast, cardiac patches were easily detected on the epicardial surface but were not coupled to the host in any of the 6 detected patches, showing spontaneous excitation rates of 68.4 ± 11.5 beats per minute (Figure 3.12). In one implanted patch, we identified multiple sub-regions with distinct GCaMP3 fluorescence activation (likely due to fragmentation during or after implantation), but none of these were coupled to the host myocardium.
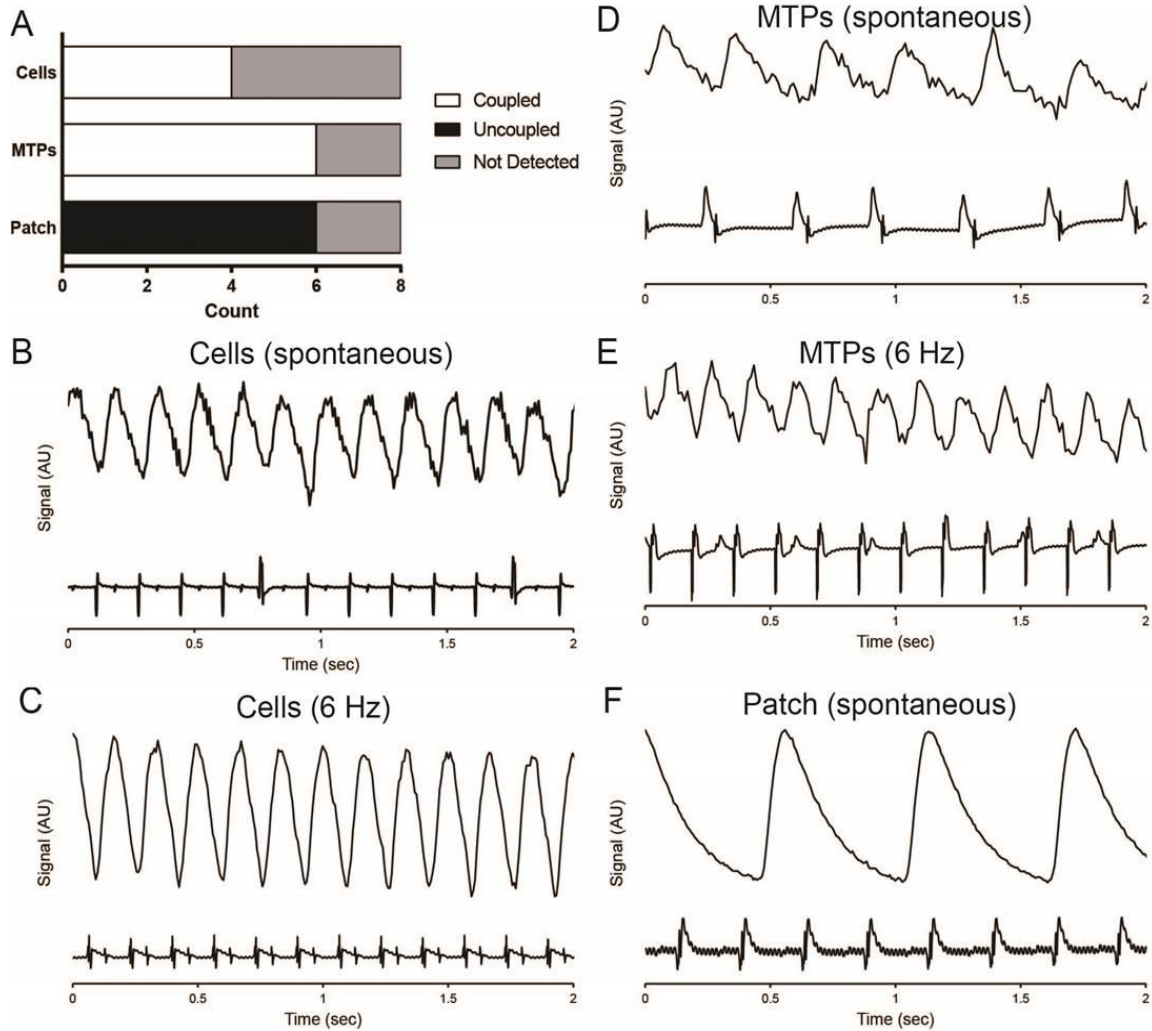
Figure 3.12. Electrical coupling of graft to host myocardium. All micro-tissue particle and cell injection graft regions detected by *ex vivo* imaging are electrically coupled to the host, while all patch grafts were uncoupled (A). Fluorescence signal of a GCaMP3 graft region (top line) vs. time is synchronized with the host ECG (bottom line) for cell grafts at spontaneous rate (B) and with 6 Hz stimulation (C) and for micro-tissue particle grafts at spontaneous rate (D) and 6 Hz stimulation (E). Epicardial patch grafts are uncoupled with a slower spontaneous rate (F).

The electrical coupling of intramyocardially-delivered hESC-cardiomyocytes is the first report of human stem cell-derived cardiomyocytes electrically integrating with the rat heart, and supports the use of the rat as a valuable small animal model in this context. It also demonstrates that

hESC-cardiomyocytes are highly plastic and can adapt to their local excitation environment *in vivo*. This finding is in contrast to preliminary studies by our group, which did not detect any coupled grafts at an early timepoint 2 weeks post-implantation, regardless of delivery method (n=12, data not shown), suggesting that the electrical integration doesn't occur until after 2 weeks.

Electrical Stimulation in 2D Culture in vitro does not Recapitulate in vivo Electrical Coupling

After observing the fast beating rate of hESC-cardiomyocytes *in vivo,* we wanted to see if the cells could electrically pace *in vitro* with prolonged electrical stimulation during cell culture. HESC-cardiomyocytes were field stimulated with 1 and 6 Hz, with stimulation starting immediately at those frequencies with no ramp-up period to mimic the implantation situation. Although we found reliable capture at 1 Hz the cells could not be paced at 6 Hz even after 6 weeks (Figure 3.13). The excitation threshold needed to pace the cells was significantly lower in both stimulation conditions relative to unstimulated controls, but these differences were lost after long-term culture and there were no differences in maximum capture rate. The lack of electrical pacing to 6 Hz *in vitro* suggests that there is something unique about the *in vivo* environment that is not captured in 2D culture. Recent studies have shown that hESC-cardiomyocytes can be paced up to 6 Hz *in vitro* in 3D engineered tissue using a paced ramp-up from 1 Hz [138]. Additionally, hiPSC-derived cardiomyocytes have been shown to couple to neonatal rat cardiomyocytes *in vitro*, but spontaneous beating rates were less than 1 Hz [139].
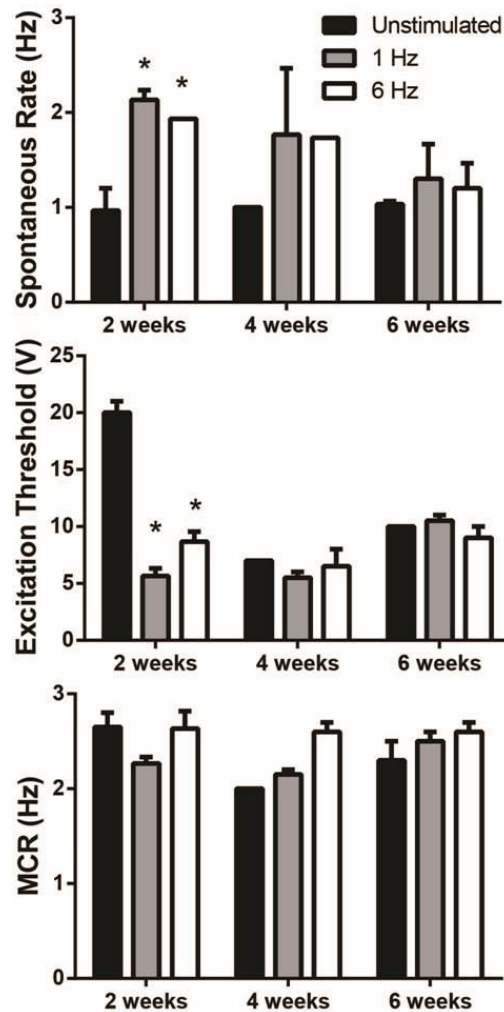
Figure 3.13. Field stimulation of hESC-cardiomyocytes *in vitro* showed that the spontaneous contraction rate and excitation threshold was higher at 2 weeks with pacing at 1 and 6 Hz compared to unstimulated controls (*$p < 0.05$). However, maximum capture rate (MCR) was not different among groups at any time point and all significant differences are lost after 4 weeks in culture.

Evidence of Gap Junction Formation between Graft and Host after Intramyocardial Delivery

Cardiomyocytes regulate synchronous contraction via calcium exchange through gap junctions [140], and electrical coupling between the graft and host tissue would suggest that there is direct physical contact and gap junction formation. The primary gap junction protein in cardiomyocytes, connexin 43, was identified at the border of the GFP-positive grafts between the

graft cells and host cells (Figure 3.14), suggesting that physical contact and the formation of gap junctions are required for coupling to occur.
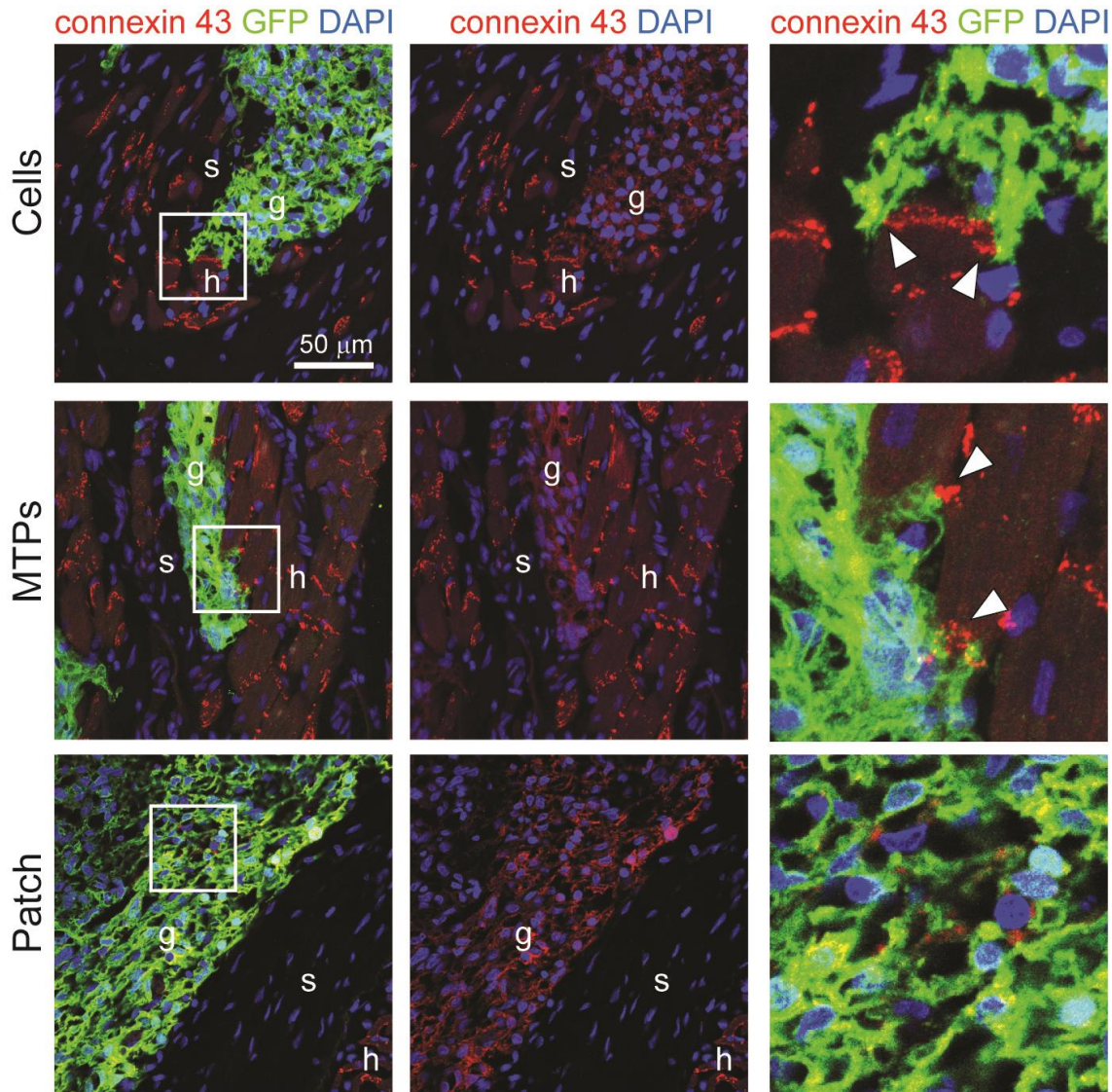
Figure 3.14. Evidence of connexin 43$^+$ gap junction formation between host cardiomyocytes and hESC-cardiomyocyte grafts was found for cell grafts and micro-tissue particle grafts. Patch implants showed no such evidence but instead were physically separated from the host myocardium by scar tissue. The outlined box region in the left panel is shown at high magnification in the right panel. White arrowheads identify regions of graft-host connexin 43 junctions. S = scar, h = host, g = graft. Scale = 50 μm.

Despite the limited sites of connexin 43 between graft and host identified in histology, this appears to be sufficient for electrical integration of the intramyocardially-delivered grafts even within the scar tissue. Lower levels of connexin 43 are apparent in the graft than in the surrounding host myocardium, possibly due to a lack of structural organization or development of anisotropy and intercalated discs, however this also appears sufficient to maintain uniform conduction across the graft. In contrast, there was no evidence of gap junctions between the host myocardium and the epicardial patch implants but instead a band of scar tissue separating the graft from the host myocardium (Figure 3.7).

3.5 Discussion

Improvement of cardiac function after myocardial infarction will require remuscularization by cell-based therapies that electrically and mechanically integrate with damaged host tissue. The experiments presented here are the first to our knowledge to directly demonstrate electromechanical integration of hESC-cardiomyocytes with rat myocardium after an ischemia/reperfusion injury. This finding supports the use of the rat model for studying human cardiomyocytes in the context of remuscularization and electromechanical integration in the injured heart.

Up until this study, it was unknown whether human cardiomyocytes (basal rate $60 - 100$ beats per minute) could electrically couple to the rat heart ($350 - 400$ beats per minute), which is a widely-used small animal pre-clinical model. We demonstrated here that hESC-cardiomyocytes consistently couple with the rat heart under spontaneous rhythm and can be paced through

electrical stimulation of the myocardium as high as 5 - 6.5 Hz (Fig 3.12, Table 3.1). Electrical coupling of hESC-cardiomyocytes was recently demonstrated in acutely and chronically injured guinea pig hearts [4, 44] and in acutely infarcted monkey hearts [1] at lower heart rates. In addition, hiPSC-derived cardiomyocytes have been shown to couple to neonatal rat cardiomyocytes *in vitro*, but spontaneous beating rates were less than 1 Hz [139]. Recent studies have shown the ability to pace hESC-cardiomyocytes up to 6 Hz *in vitro* in 3D engineered tissue using a paced ramp-up from 1 Hz [138], but our attempts to electrically field pace monolayer-plated hESC-cardiomyocytes *in vitro* immediately at 6 Hz (designed to mimic the *in vivo* situation without a ramp-up period) were unsuccessful (Fig 3.13). There are a number of potential explanations as to why our hESC-cardiomyocytes could not capture the 6 Hz pace *in vitro*, including the 2D environment of our cells, the absence of a ramp-up period, the more terminally-differentiated state of our hESC-cardiomyocytes when experiments are started (day 21-24 of differentiation), or the possibility that the *in vivo* environment provides additional cues not recapitulated *in vitro* in our hands. Preliminary studies by our group demonstrated that at 2 weeks post-implantation, no grafts were coupled by GCaMP3 imaging at this early time point regardless of delivery method (n=12, data not shown). This raises the possibility that with additional time *in vivo*, the epicardial patches could electrically couple to the host.

Surprisingly, all intramyocardial grafts that were detected by GCaMP3 imaging at 4 weeks were coupled to the rat host heart at the spontaneous heart rate. This finding differs from hESC-cardiomyocyte grafts in the guinea pig heart where 40% of grafts were not coupled after 4 weeks. This difference in ability for grafts to couple to the host in the rat at 4 weeks may be due to the injury model used, which was a cryoinjury model in the guinea pigs and an ischemia/reperfusion injury model in the rat [4], or the distribution of graft within the injured

59

heart. Analysis of the distribution of the intramyocardial grafts in the rat heart shows that at least 20% are located within the scar region and some of these were detected by *ex vivo* imaging. Electrical stimulation of intramyocardial grafts through the host myocardium up to maximal rates of 6.5 Hz demonstrates that hESC-cardiomyocytes are highly plastic and can adapt to their local excitation environment *in vivo*. How this occurs remains to be fully understood. Fatal arrhythmias did not occur in any rats in this study receiving any of the three transplant groups, likely due to the natural resistance to ventricular arrhythmias found in the rodent heart [141]. However, the physiological consequences of these three delivery modes on myocardial contractility remain to be fully described in a comprehensive functional study.

In the current study, we demonstrate that all three delivery strategies for engrafting hESC-cardiomyocytes produce viable grafts, but that only intramyocardially-delivered cells or micro-tissues can be paced through the host rat heart after four weeks. While detection of micro-tissue particle grafts was higher than cell grafts during GCaMP imaging (75% versus 50% detected, respectively), all detected intramyocardial grafts were coupled to the host (Table 3.1). Epicardial patches were not coupled to the host (Fig 3.12), and histological analysis shows that all patches have a physical barrier between the engrafted patch and the host myocardium (Fig 3.7, Fig 3.9). The absence of coupling with our epicardial patches seems to contrast with the results of Zimmermann et al [134], where engineered heart tissue derived from neonatal rat cardiomyocytes was implanted onto the epicardial surface of infarcted syngeneic rats. They reported that the engineered heart tissues enhanced global systolic function, and they used a multi-electrode array over the epicardial surface to demonstrate that the implanted tissues enhanced cardiac activation patterns and conduction velocities, consistent with electrical integration. However, direct evidence of graft excitation was not used in their study. Our

GCaMP3 system is graft-autonomous, as only the hESC-cardiomyocytes express the GCaMP3 transgene. In contrast, the multi-electrode array measures local tissue electrical properties, irrespective of source. Therefore, additional studies will be required to promote electrical integration of epicardially-implanted engineered tissues, such as through direct contact with healthy myocardium or modulation of gap junction formation [142, 143] or scar remodeling [144], while assessing graft-autonomous excitation. It is important to note that a recently published study by Weinberger et al reported electrical integration of epicardially-implanted cardiac patches in some hearts of a guinea pig injury model, although the method of assessment was optical mapping instead of using a GCaMP reporter [145]. One key difference between the engineered tissues used here is their size, as the patches in Weinberger et al were large enough to span the entire infarct region to form direct contact with healthy regions of myocardium.

Our study is unique in its approach to compare three different implantation techniques for introducing hESC-cardiomyocytes into the injured heart, and the results bring insights to our cell transplantation approaches for cardiac regeneration. First, the most well-studied and well-established technique of delivering dispersed single cells via minimally-invasive needle injection into the ventricular wall is verified as a viable therapeutic approach. Its simplicity is valuable for clinical translation, as this method has been used in larger animal models and will likely be the first mode of delivery used in human clinical trials. Second, the micro-tissue particles, which were designed to be injectable engineered tissues, were more easily detected by *ex vivo* imaging (compared to dispersed cell grafts) and provide the same minimally-invasive delivery route as dispersed cells.

However, we were surprised to find that graft size was not different between micro-tissue particles and dispersed cells by histology, given that cells in micro-tissue particles were not enzymatically dispersed just prior to implantation, which has been suggested to hinder survival upon transplantation [146]. In a study using scaffold-free cardiac cell sheets implanted on infarcted rat hearts, graft size was larger versus injected dispersed cells by *in vivo* bioluminescence imaging [147], suggesting that tissue engineering can produce larger grafts depending on tissue assembly and implant approach. However, electrical integration was not investigated in that study even though whole heart function as measured by echocardiography did not decline with cell sheet implant [147], indicating that paracrine effects on remodeling is possible and that electromechanical integration must be assessed in addition to engraftment size and location. Our graft size results suggest that either anoikis in the dispersed cell group was not a major factor in determining engraftment or that cell death equally affected all implant groups. Further, our graft size data suggests that forming cell aggregates prior to implantation provides no additional benefit over implanting dispersed, single cells when pro-survival factors are included. This contrasts a previous study, where functional benefit was observed via echocardiography of aggregated hESC-cardiomyocytes versus injected cells delivered without pro-survival factors, although graft size was not reported and injected hESC-cardiomyocytes showed minimal engraftment [148]. In our study, there is neither benefit nor detriment to implanting cell aggregates versus a single-cell population in terms of graft size and electrical connectivity achieved. Third, cardiac tissue patches provide the most continuous mass of engrafted cardiomyocytes of all delivery strategies tested and generally maintain their physical architecture as previously demonstrated for cell sheets [147] and scaffold-based engineered heart tissue [134]. However, a lack of difference in graft size versus cells or micro-tissue particles

62

suggests that surgical implantation techniques and detection (by methods other than histology) must be used and developed for epicardial patches.

The correlation of decreased graft size with increased scar size (Fig 3.10) must be overcome, as a desired therapy should result in robust engraftment regardless of infarct size. Future work in cardiac tissue engineering should aim to overcome the negative correlation observed between graft size and scar size. We also emphasize that in this study cell numbers were normalized at the start of tissue engineering procedures, not at the time of implantation into the rat heart, suggesting that the total number of implanted cells could have been reduced in the engineered tissue groups as lower proliferation rates have been previously reported in this context [149]. However, normalizing cell implantation numbers at this time provided more accurate single-cell counts than is possible after tissue formation. Finally, as others have suggested, larger grafts could be obtained if larger cell input numbers were used in any of the groups. In light of this discussion, we believe that cardiac tissue engineering continues to hold promise as the next generation of cell-based therapies. Indeed, macroscopic and microscopic geometry can be controlled in engineered cardiac tissue based on matrix selection and scaffold fabrication [33-37], and multiple groups have demonstrated uniform electrical excitation of engineered human cardiac tissues [136, 150-152]. Implanted engineered tissues are vascularized by the host to some degree as we have previously shown in epicardially implanted patches [153]. Many efforts are underway to develop a more dense and efficiently perfused vasculature within engineered tissues (recently reviewed by Coulombe, Bajpai [38]), and future studies must include analysis of graft perfusion and vascular remodeling, regardless of delivery strategy, to ensure long-term survival and viability of transplanted hPSC-cardiomyocytes.

3.6 Summary

In conclusion, this study brings insight to the value of different delivery strategies for transplanting hPSC-cardiomyocytes into the heart for cardiac regeneration. We developed micro-tissue particles as a novel strategy to deliver engineered tissue via intramyocardial injection and demonstrate electrical coupling of all intramyocardial hESC-cardiomyocyte grafts to the rat host with maximal pacing rates of up to 6.5 Hz. This study supports the use of the rat as a valuable small animal model to study the electromechanical integration and contributions of grafts to global heart function of all grafts including epicardially implanted engineered tissues. Larger animal models will be required for future FDA approval of cell-based cardiac therapeutics and to assess arrhythmic risk of such therapies, as rodents are less sensitive models of arrhythmic risk (demonstrated by the occurrence of arrhythmias detected in non-human primates but not in mice, rats or guinea pigs [1, 123]. Ongoing studies in the field are required to develop remuscularization therapy to restore contractile function of the injured heart, and the pursuit of electromechanical integration of epicardially implanted engineered cardiac tissue continues to be a promising approach. As we demonstrate in this study, the use of the rat ischemia/reperfusion model is sufficient for these types of studies due to the ability of hESC-cardiomyocytes to electrically couple to the host heart.

Chapter 4. Design of a 3D Notch-signaling hydrogel and enhancing Notch-mediated cardiomyocyte proliferation in engineered tissues

4.1 Abstract

Gaining the ability to control cardiomyocyte proliferation would be a powerful tool in the field of cardiac regenerative medicine and hESC-cardiomyocyte cell therapy. Towards this goal, we have developed a Notch-signaling platform to enhance the proliferation of hESC-cardiomyocytes both in 2D cell culture and in 3D engineered cardiac tissue. Culturing hESC-cardiomyocytes on 2D surfaces with the immobilized Notch ligand Delta-1 resulted in a significant increase in cardiomyocyte proliferation relative to IgG control surfaces, showing a dose-dependent proliferative response with $46.3 \pm 6.1\%$ of cardiomyocytes proliferating on 10 µg/ml Delta-1 compared to $24.2 \pm 3.0\%$ on IgG surfaces (p=0.028). We next designed 3D hydrogels with immobilized Delta-1 by modifying collagen-1 using carbodiimide chemistry and subsequently binding the ligand in an oriented manner. This modified collagen was used to form engineered tissues in cell culture wells or PDMS molds. A Notch-driven luciferase reporter cell line was used to verify the Delta-1-mediated Notch activity, which showed significantly higher normalized luciferase expression in Delta-1 3D gels compared to IgG controls. Importantly, a timecourse analysis over 2.5 weeks indicates that the 3D gel promotes a robust increase in total Notch signal compared to the 2D surfaces, with a strong signal remaining at 2 weeks after gel formation in contrast to 2D culture where Notch activity begins to wane after only 2 days. In 3D engineered cardiac constructs formed with Delta-1 gels, cardiomyocytes demonstrated a significant increase in proliferation with $27.4 \pm 2.7\%$ of hESC-cardiomyocytes proliferating in

Delta-1 gels compared to 17.5 ± 2.7% in cardiac constructs formed with the IgG control gel (p=0.037). Collectively, these studies establish a platform in which Notch signaling can be modulated to enhance cardiomyocyte proliferation *in vitro* in both 2D tissue culture and in 3D engineered cardiac tissue.

4.2 Rationale

Current techniques of transplanting hESC-cardiomyocytes *in vivo* are hindered by small graft size and limited cell retention, with only a small fraction of transplanted cells remaining in the surviving graft (Figure 1.4). Despite reports of increased graft size in engineered tissues [154], our results in Chapter 3 did not support this and instead highlighted the benefit of intramyocardial delivery instead of macroscopic engineered tissues for implantation. One of the limitations of those experiments was that hESC-cardiomyocyte graft size was still relatively small despite using engineered tissues as a delivery strategy. However current cell implantation methods injecting a suspension of single cells into the myocardium are not ideal, because the majority of cells are lost after implant [2]. This work highlighted the need for developing strategies to increase graft size and limit the number of cells required for implantation. One such strategy is to enhance the proliferation of cardiomyocytes *in vivo* after transplantation, which will first require validation and optimization *in vitro*.

Previous studies have suggested that the Notch signaling pathway regulates cardiomyocyte proliferation [41, 60-62, 74]. Notch signaling is an evolutionarily-conserved signaling pathway that mediates cell fate decisions in vertebrates such as primates as well as invertebrates including C. elegans ([64], Figure 1.3). Notch signaling relies on the binding of one of the four Notch

66

receptors on a receiving cell (Notch 1, Notch2, Notch3, and Notch4) to one of five Notch ligands on a signaling cell (Delta1, Delta3, Delta4, Jagged1, and Jagged2 in mammals). After receptor-ligand binding, a series of cleavage events releases the Notch intracellular domain (NICD) from the intracellular membrane, which then translocates to the nucleus to activate downstream target genes. It is hypothesized that tension is required between the receptor and ligand to expose an extracellular cleavage site prior to releasing the NICD, and thus direct cell-cell contact is required for Notch activation. Due to this requirement, a major hurdle in designing Notch-signaling therapies is that ligands must oriented and immobilized to elicit a robust signaling response in many contexts [155, 156].

Our group has previously described the use of immobilized Notch ligands in 2D culture to mediate cell fate decisions in hESC-cardiomyocytes [62]. However these surfaces remained active for only 24-48 hours, which was overcome by repeated dosing with fibrin micro-beads containing immobilized Jagged-1 administered in 2D culture. Another group has developed a self-assembling peptide approach to stimulate Notch signaling, which regulated gene expression of cardiac progenitor cells *in vitro* [41]. However, the use of natural, biomimetic scaffolding is appealing for engineered cardiac tissue formation as well as for *in vivo* translational studies. Considering previous studies using full-length Notch proteins in 2D, we hypothesized that the 3D orientation of Notch ligands in a hydrogel platform would prolong the Notch-mediated response and promote Notch signaling in long-term culture compared to 2D systems. We also hypothesized that orientation of Notch ligands would enhance hESC-cardiomyocyte proliferation in both 2D and 3D cell culture systems. However, we suspect that promoting cardiomyocyte proliferation must be balanced with the maturation of *de novo* cardiomyocytes, which will

require the proliferative cue to be turned off over time. In fact, proliferative cardiomyocytes are reported to contribute to decreased global function when proliferative cues are overexpressed long-term [58].

The experiments described in this chapter investigate the use of Notch signaling to promote the proliferation of hESC-derived cardiomyocytes. We first tested a Notch-signaling platform for 2D cell culture using the immobilized, oriented Notch ligand Delta-1. We next designed a biomaterial-based cell culture platform to regulate Notch signaling to control cell behavior in 3D, which was validated *in vitro* using engineered tissues.

4.3 Methods and Scientific Strategy

2D Tissue Culture Platforms with Immobilized Notch Ligands

To achieve oriented immobilization of recombinant human Delta-1-Fc, tissue culture polystyrene culture plates are first pre-coated with 20 mg/ml anti-IgG (human, Fc-specific, Sigma) for 1 hr at 37°C. Wells are washed with PBS, blocked with 20% FBS in PBS for 1 hr at room temperature, and subsequently incubated overnight with the Notch ligand Delta-1 (courtesy of the Bernstein Lab) or IgG (Sigma) to achieve oriented immobilization, and subsequently washed with PBS. A similar method has been previously described [156]. 2D cell culture experiments used Delta-1 or IgG at a 10 µg/ml unless otherwise noted. Prior to cell culture, wells were washed extensively with PBS. In experiments using hESC-cardiomyocytes, 5 µg/ml fibronectin (Invitrogen) was added during overnight ligand incubation to promote cardiomyocyte attachment to the tissue culture surfaces. This method is illustrated in Figure 4.1.
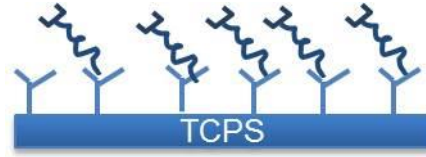
Figure 4.1. Schematic illustrating the 2D indirect, oriented immobilization of Delta-1. Anti-IgG antibody (light blue) is adsorbed onto tissue culture polystyrene (TCPS) followed by incubation with Delta-1 or IgG (dark blue) resulting in ligand orientation.

Collagen Modification and Notch Ligand Immobilization

Carbodiimide chemistry was used to immobilize Delta-1/Fc onto solubilized collagen, by forming covalent bonds between free carboxyl and amine groups similar to previously described methods [157, 158]. This process is outlined in Figure 4.2. Free carboxyl groups on the collagen were reacted to free amine groups on the secondary protein, which was anti-IgG unless otherwise noted (un-oriented ligand immobilization used either IgG or Delta-1 as the secondary protein). Collagen contains both free carboxyls and amines, however carboxyl groups are more abundant than amine groups with 120 compared to 27 per 1000 amino acid residues [159, 160].

A stock concentration of 15 mg/ml rat tail collagen type 1 is dissolved in 0.1% acetic acid, diluted to 2.5 mg/ml using RPMI-1640 cell media, and reacted with 1-ethyl-3-(dimethylaminopropyl)carbodiimide hydrochloride (EDC)/*N*-sulfo-hydroxysuccinimide (sulfo-NHS) on ice for 1 hour, with a 10-fold molar excess of EDC (ThermoFisher) to free carboxyl groups on collagen and 5 mM Sulfo-NHS (ThermoFisher). The solution is gently mixed periodically throughout the incubation period using a 1cc syringe. After 1 hour, 2-mercaptoethanol (2-ME) is added at 20 mM to inactive the EDC, and the pH is adjusted to 7.0 – 7.2 using 1M NaOH. Next, 200 μg/ml of anti-human IgG (Fc specific) is mixed with the

69

collagen and incubated for 48 hrs at 4°C. This provides an excess of primary free amine groups on the anti-IgG relative to that present on the collagen, resulting in carboxyl group activation to amine-reactive sulfo-NHS esters and subsequent amide bond formation to the antibody. Following the 48 hr incubation, 100 µg/ml Delta-1 or IgG (control) is added and the solution is incubated for another 24 hrs at 4°C.

Prior to the addition of cells, the solution is brought to a final concentration of 1.5 mg/ml collagen using media (DMEM for U2OS luciferase characterization studies or RPMI-1640 for cardiomyocyte experiments), 1x HEPES, 30 vol/vol% unmodified rat tail collagen 1 (4 mg/ml stock, ThermoFisher), 1x Matrigel, and the pH is adjusted to 7.4 as needed using 1M NaOH. This entire process occurs with the collagen and syringes kept on ice.
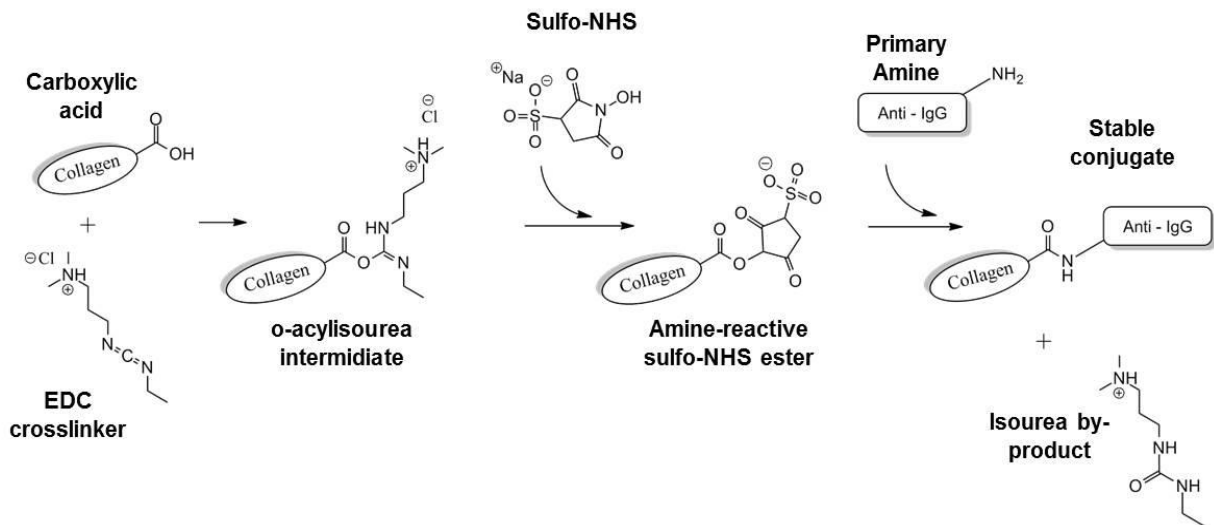
Figure 4.2. 3D immobilization of Delta-1 using EDC:NHS chemical cross-linking. After the stable collagen-anti-IgG conjugate is formed, the solution is incubated with Delta-1 or IgG for ligand immobilization.

Gel lyophilization protocol

Although lyophilized gels were not typically used to make engineered tissues, we developed a gel lyophilization protocol as a method to store the modified Notch-gels long-term and facilitate more reproducible batch-production of the gel. Collagen was lyophilized for long-term storage either after anti-IgG binding (yet prior to incubation with IgG or Delta-1 ligands, where instead ligand incubation occurred after resolubilizing the lyophilized gel) or at the end of the collagen modification protocol with IgG or Delta-1 ligands already bound. Thus, for these experiments, gels were lyophilized at either day 2 or day 3 of the gel modification process as shown below in Figure 4.3.

Day 0   Day 2   Day 3

| Anti-IgG | ligand |

| 1) EDC:NHS reaction (collagen) 2) Add anti-IgG | IgG or Delta | Form constructs |
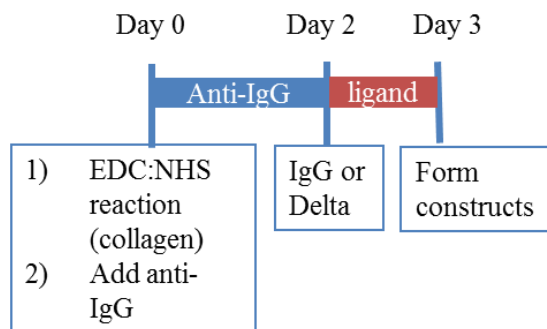
Figure 4.3. Experimental outline for gel lyophilization experiments. Modified collagen was lyophilized either at day 2 or day 3 of the process outlined above, and then resolubulized and continued along the protocol.

Luciferase-based Analysis of Notch Signaling

A CSL-luciferase U20S osteosarcoma cell line (courtesy of the Moon Lab) and the Dual-Luciferase Reporter Assay System (Promega) were used to optimize the developed Notch-gel

and compare its effect to the established 2D immobilization approach. U20S cells were engineered to express constitutively active renilla, as well as firefly luciferase which was under control of CSL (CBF1, Su(H), and Lag-1) expression (referred to here as U20S CSLluc/ren). U20S CSLluc/ren cells were cultured in uncoated 10 cm tissue culture dishes and fed every 2-3 days with DMEM supplemented with 10% FBS, 2 mM l-glutamine, and 100 units/ml penicillin/ 100 µg/ml streptomycin. Cells were passaged at 80% confluence using 0.25% trypsin-EDTA.

For 2D experiments, U20S CSLluc/ren cells were replated onto IgG- or Delta-coated wells in triplicate in a 96-well plate, at a density of 5k cells/well in standard cell culture media. For 3D gel experiments, 25k U20S CSLluc/ren were resuspended in 30 µl of IgG- or Delta-modified collagen, pipetted into a well of a 96-well plate (in triplicate), and allowed to gel at 37°C before adding 200 µl of cell culture media. At the designated experimental endpoint, media was removed and 100 or 200 µl of 1X Passive Lysis Buffer (Promega) was added to 2D and 3D wells, respectively. Cells were lysed during a 10 min incubation followed by pipette trituration and 2-3 repetitive freeze/thaw cycles at -80°C. 3D gels required an additional trituration step to disrupt the gels, which was performed using a handheld tissue homogenizer inserted into each sample tube and triturated for 15 sec. Luminescence was recorded following the Dual-Luciferase Reporter Cells protocol (Promega). Briefly, 20 µl per sample was loaded in triplicate into optical 96-well plates, and background fluorescence was recorded over 3 individual reads on a plate luminometer. 20 µl of Luciferase Assay Reagent II (LARII) was added to each well and firefly luciferase luminescence was recorded as before, followed by addition of 20 µl Stop and Glo Reagent to each well and luminescence recording. Notch-driven luciferase data is shown as firefly luminescence normalized to renilla luminescence for each sample (with background

72

subtraction), expressed as the fold change over the corresponding IgG control (normalized to 1).

HESC-Derived Cardiomyocyte Culture and Differentiation

Undifferentiated RUES2 hESCs were maintained as previously described [45] on Matrigel™ in mouse embryonic fibroblast (MEF)-conditioned media supplemented with 5 ng/ml basic fibroblast growth factor (bFGF). Cardiomyocyte differentiation was performed as described previously [45]. A high-density cell monolayer was pre-treated with 1 μM CHIR99021, and induced with 100 ng/ml Activin A and 1x Matrigel in RPMI1640 with B27 Supplement minus insulin. Medium was changed after 18 hrs to RPMI1640 with B27 Supplement minus insulin supplemented with 1 μM CHIR99021 and 5 ng/ml BMP4. After two days medium was changed and supplemented with XAV939 for an additional 48 hours. After day 7 of differentiation, RPMI 1640 supplemented with B27 supplement containing insulin was used to maintain cells. Beating was typically observed between days 7 and 10, and media was changed every 2-3 days thereafter.

2D platform: Cardiomyocyte Proliferation Experiments

HESC-cardiomyocytes were replated into wells of a 4-well Nunc™ chamber slide (Thermo Scientific) following 2D ligand immobilization (described above) supplemented with 5 μg/ml fibronectin, at a density of 60k cells/well. Culture media was changed the following day along with 10 μM BrdU, and cells were fixed 24 hrs later with 4% paraformaldehyde. This experimental outline is shown in Figure 4.3. For cell count experiments, a 24-well plate format was used and was coated with Delta-1 or IgG as described above. High-purity cardiomyocytes (97.1 ± 0.9% cTnT$^+$ by flow cytometry, Figure 4.4) were replated at a density of 200k cells/well,

media was changed every other day with or without the addition of a gamma secretase inhibitor (5 µM DAPT), and cells were counted on a hemocytometer using Trypan Blue dye at day 7.
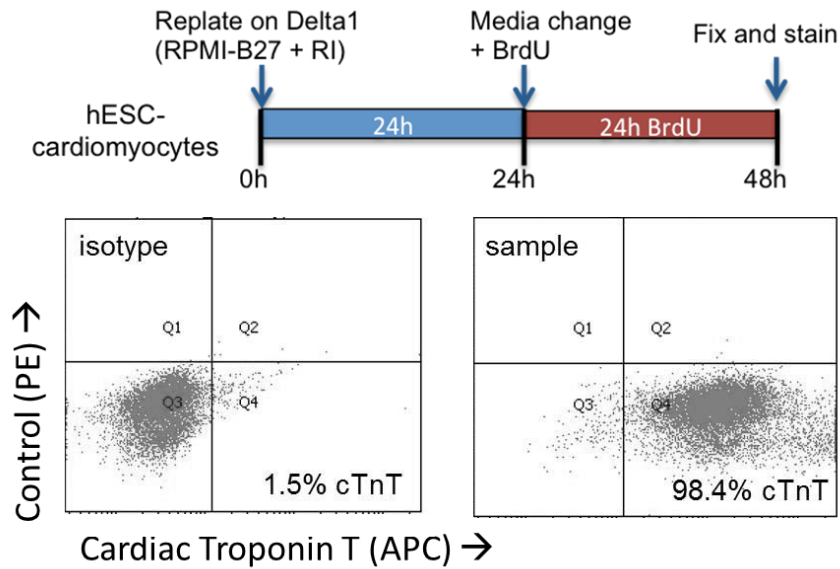
Figure 4.4. 2D cardiomyocyte proliferation experimental timeline. Schematic for histological analysis by BrdU is shown in timeline, and FACs data indicating high cardiac purity for cell count experiments is shown below.

3D platform: Engineered Tissue Formation

Engineered cardiac constructs are formed using methods previously described by our lab [161-163]. HESC-cardiomyocytes are removed from monolayer culture using 0.25% trypsin-EDTA, washed twice with serum-free media, resuspended in the modified collagen with IgG (control) or Delta-1, and added into sterile PDMS molds using a 1cc syringe (Figure 4.5). Two different molds were used over the course of these studies. In the first generation mold, engineered tissues were formed with 30 µl gels and $0.5x10^6$ cells/gel in a PDMS mold following treatment with a handheld corona treater (Figure 4.5A, B). Collagen gels were allowed to polymerize by incubation at 37°C for 1 hour, followed by the addition of RPMI-1640+B27 supplemented with

10 μM Y-27632. A second generation mold was designed to facilitate repeated force measurement readings and increase throughput [163, 164]. PDMS troughs were treated with 5% pluronic acid and the tips of posts were coated in 0.1% polyethylenimine and 0.01% glutaraldehyde (Sigma). In these molds, 100 μl of cell and gel mixture was used containing 1.6×10^6 hESC-cardiomyocytes and when noted, 0.16×10^6 HS-27a stromal cells were added. The cell and gel mixture was added to the troughs, the PDMS strips were gently placed in to submerge the post tips, and the tissues were incubated at 37°C for 90-120 minutes. After this brief incubation, 1 ml of RPMI-1640+B27 supplemented with 10 μM Y-27632 was gently added to each well and the tissues were incubated overnight at 37°C. The following day, each PDMS tissue post strip was carefully transferred into a 24 well-plate, with the posts remaining inverted so that tissues were completely submerged in media. For both generations of molds, media was changed every other day to RPMI-1640+B27, and 10 μM BrdU was added to culture media 24 hrs prior to fixation with 4% paraformaldehyde.
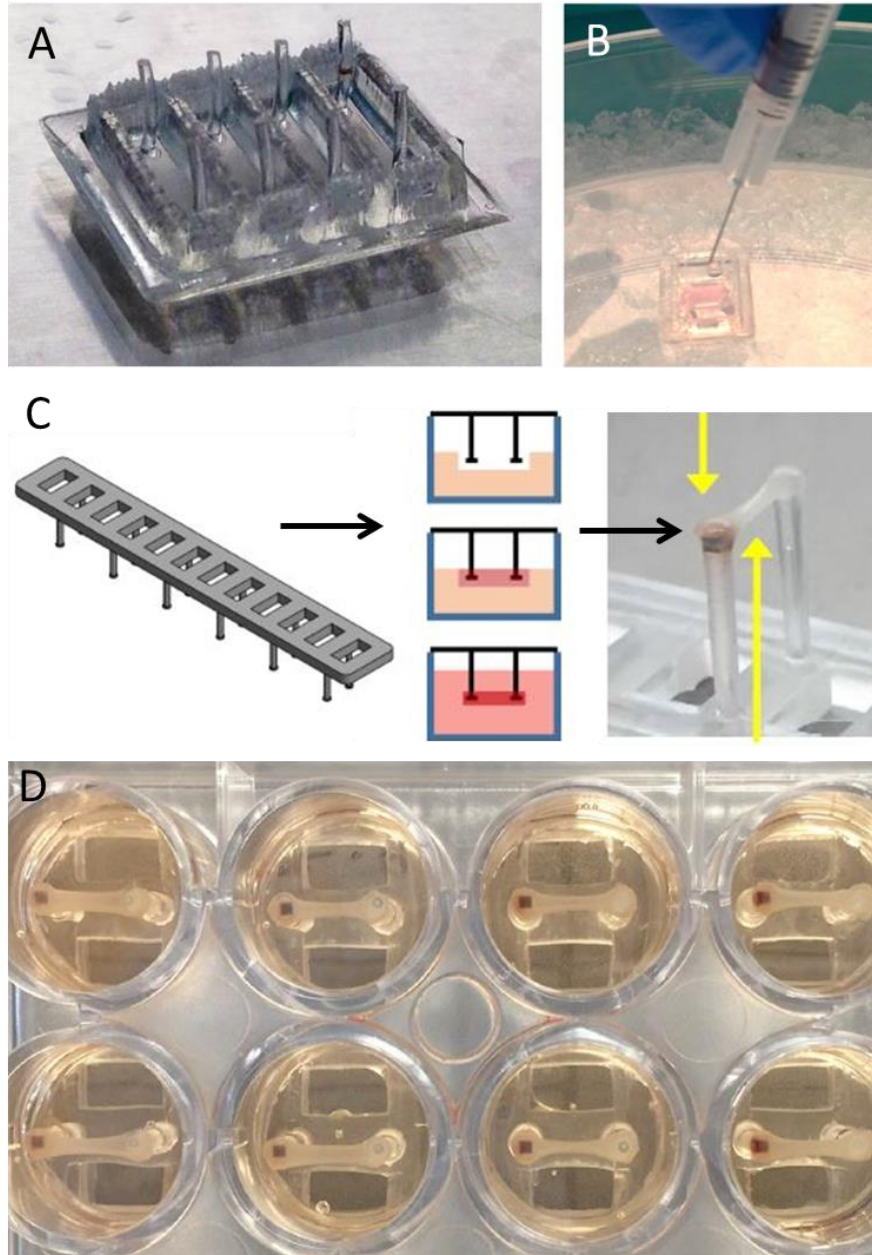
Figure 4.5. PDMS molds used for engineered cardiac tissue formation. First generation molds are shown in (A-B), and second generation molds are shown in (C-D). (A) The first generation molds consisted of 4 troughs with a micropost at each end. (B) The cell and gel preparation was added to the PDMS molds on ice in a 6-well plate. After formation, molds were submerged in cell culture media. (C) The second generation of PDMS molds consisted of a strip with six sets of posts. Cells and gel was pipetted into PDMS troughs, and the PDMS strip was inserted so that the tips of the posts were submerged in the cell and gel mixture. The yellow arrows indicate the magnet at the tip of the flexible post used for optical tracking. (D) After tissue formation, the strips were transferred and inverted in a 24-well plate, with each tissue fully submerged in media. *Images in C-D were provided courtesy of Shiv Bhandari.*

Analysis of Cardiomyocyte Proliferation

There are numerous methods to analyze cell proliferation, as outlined in Table 4.1. The primary analysis technique used in these studies was BrdU incorporation, which labels newly synthesized DNA. Cell number was also counted using a hemocytometer in some studies.

Marker	Method	Identification	Refs.
Cell number	Cell count by histology or in vitro	Cells after division	[47, 56]
BrdU	Histology, FACs	Synthesized DNA (S phase)	[25, 60, 62]
H3P	Histology	Mitotic figures (M phase)	[25, 47, 57]
Ki67	Histology	Cell cycle except G0	[165, 166]
DNA content	FACs	Stages of the cell cycle	[165, 167]

Table 4.1. Analysis techniques for quantifying cell proliferation.

Immunohistochemical analysis

For immunohistochemical analysis, constructs were washed with PBS, fixed with 4% paraformeldehyde for 20 min, washed with PBS + 5% FBS, and paraffin-embedded as described in Chapter 3. For brightfield microscopy, slides were rehydrated, blocked, and underwent heat-induced epitope retrieval (HIER) in a citrate buffer prior to incubation with A.4951 mouse anti-βMHC primary antibody overnight. Slides were then washed, incubated with biotinylated goat anti-mouse secondary antibody for one hour (1:100), and developed with vector red. To visualize BrdU, slides were incubated in 1.5 N HCl, and then incubated with anti-BrdU POD primary antibody (1:40) overnight. Slides were then washed in PBS, developed using diaminobenzadene (DAB), and counterstained with hematoxylin. For confocal imaging, slides underwent proteinase

K antigen retrieval in 10 mM tris-HCl for 15 min at 37°C, were washed in PBS, blocked, and incubated with mouse anti-alpha actinin overnight (1:800). Slides were washed with PBS and incubated for 1 hr with alexaflour 488 goat anti-mouse (1:100). BrdU was subsequently visualized as above but with tyramide amplification using tyramide-alexaflour 594. Cardiomyocyte proliferation was measured following a 24 hr BrdU pulse and histological analysis for double-labeled BrdU$^+$/βMHC$^+$ or BrdU$^+$/alpha-actinin$^+$ cells.

Force Production Analysis of Engineered Cardiac Tissues

To investigate the role of Notch signaling on engineered cardiac tissue structure and function, engineered cardiac tissues were formed using the modified collagen-based Notch-gel and force production analysis was performed. After formation in PDMS micropost molds as described above using either collagen-IgG (control) or collagen-Delta-1, tissues were analyzed at days 4 and 7, and at 3 and 6 weeks for force production, followed by histological analysis of cardiomyocyte proliferation by the methods described above. Force measurements were performed using a customized mold with a rigid post and deflectable post, analyzed on an inverted microscope with optical tracking of post deflection. Tissues were electrically paced at 1.0 − 1.5 Hz at 5 V with a 1.0 ms pulse duration. Videos showing the post deflection were recorded and processed using ImageJ, and a custom MatLab script was used to measure post deflection. Force was normalized to cross-sectional area for each tissue. Tissue cross-sectional area was measured by histology in the fixed tissues and force data is represented as active force normalized to cross-sectional area. This type of analysis has been routinely performed by our group and our collaborators [161, 162, 168].

Statistical Measurements

All histological measurements were performed using ImageJ and statistical analyses were performed using Excel or Prism Graphpad. Statistical significance (p<0.05) was determined using a two-tailed Student's t test assuming unequal variance. All values are reported as means, and error bars represent SEM.

4.4 Results

Oriented Delta-1 Promotes Notch Signaling in 2D

Using the CSLluc/ren luciferase reporter cell line, we found that the 2D immobilized Delta-1 platform promotes Notch signaling compared to controls (Figure 4.6). On 2D culture surfaces with immobilized Delta-1, the peak Notch-driven luciferase expression occurs between 48 and 72 hours with a fold increase in luciferase at 24 hrs of 3.5 ± 0.2-fold, at 48 hrs of 5.8 ± 0.2-fold, at 72 hrs of 6.1 ± 0.4-fold, and at 96 hrs of 4.6 ± 0.2-fold increase over uncoated tissue culture polystyrene surfaces (TCPS) and IgG controls (p<0.005 at all timepoints). These results are consistent with previous reports of immobilized ligand methods [62]. In experiments using hESC-cardiomyocytes, fibronectin (FN) was included during overnight ligand incubation to promote cardiomyocyte attachment to the TCPS. We confirmed that fibronectin addition did not inhibit interaction with the Delta-1 ligand, and instead observed an enhanced Notch response on Delta-1 with a 7.1 ± 0.1 fold increase over IgG, compared to Delta-1 without fibronectin (5.7 ± 0.2, p<0.005) and to IgG controls (Figure 4.6). The observed luciferase response in 2D was dose-dependent, although the dynamic range of the luciferase reporter cells did not exhibit a significant difference in signaling between 1 and 10 µg/ml on 2D surfaces (Figure 4.7).

79
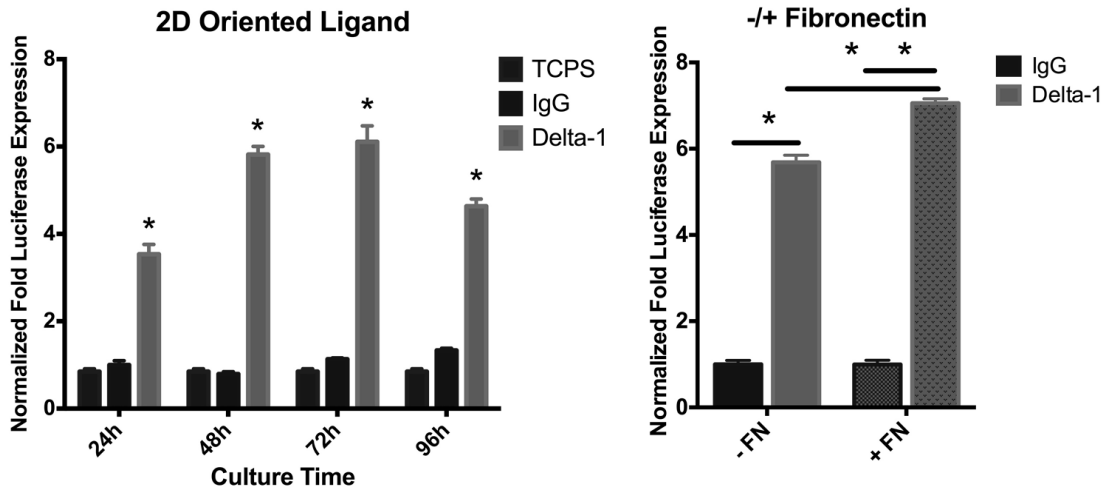
Figure 4.6. Immobilized Delta-1 promotes Notch-mediated luciferase expression in 2D. After U2OS culture on the 2D platform, Notch-driven luciferase expression significantly increases relative to tissue culture polystyrene surfaces (TCPS) and IgG controls, peaking between 48 and 72 hrs. Addition of fibronectin (FN) during ligand immobilization in 2D does not negatively impact Notch response, and in fact results in a slight increase in Notch signaling by CSLluc/ren luciferase analysis.
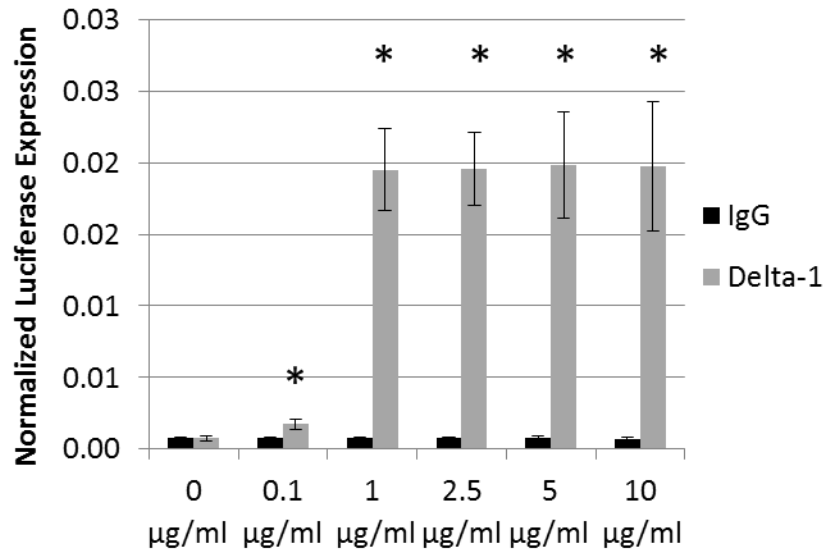
Figure 4.7. Dose-response of immobilized Delta-1 compared to IgG control surfaces at 48 hours. Data is expressed as raw firefly luciferase expression normalized to renilla luciferase expression. * $p < 0.05$

HESC-Cardiomyocyte Proliferation is Enhanced on 2D Notch Platform

After confirming a Notch-mediated luciferase response on the 2D platforms with CSLluc/ren reporter cells, we investigated the effect of culturing cardiomyocytes on immobilized, oriented Delta-1. Culturing hESC-cardiomyocytes on Delta-1 surfaces resulted in a significant increase in proliferation over IgG controls by immunohistochemistry for BrdU and βMHC. This proliferative response is dose-dependent, with the largest increase in proliferation observed at 10 µg/ml coating conditions in 2D. The increase in proliferation on Delta-1 surfaces over IgG control surfaces was $15.1 \pm 3.1\%$, $22.0 \pm 6.7\%$, and $11.5 \pm 2.9\%$ on 5 µg/ml, 10 µg/ml, and 20 µg/ml surfaces, respectively (Figure 4.8). Cell number also significantly increased after week-long culture on 2D Delta-1 compared to cardiomyocytes grown on IgG control surfaces ($p<0.05$, Figure 4.8). This proliferative response is lost after inhibiting Notch by the addition of a gamma secretase inhibitor, suggesting a Notch-dependent increase in proliferation on Delta-1 surfaces.
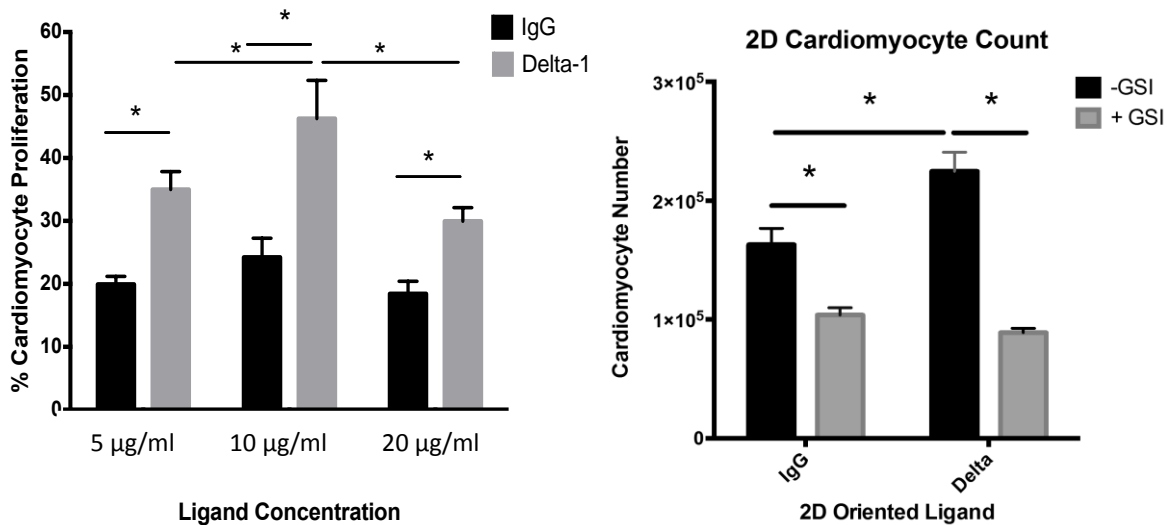
Figure 4.8. HESC-cardiomyocytes proliferate in response to immobilized, oriented Delta-1 in 2D. (Left) Dose-dependent effect on cardiomyocyte proliferation, measured by histology as double-positive βMHC⁺/BrdU⁺ cells. (Right) Cell number increases after culture on 2D Delta-1 surfaces. The Notch inhibitor GSI mitigates these effects. *p<0.05

Optimization of 3D Notch-gels with Immobilized Delta-1

Following characterization of the 2D Delta-1 platform, we designed a 3D scaffold with immobilized Delta-1. Collagen was reacted using EDC:NHS chemistry and covalently bound with either IgG or Delta-1 directly (resulting in un-oriented ligand binding), or with anti-IgG-Fc followed by subsequent binding with IgG or Delta-1 (resulting in oriented, indirect ligand binding). Using the CSLluc/ren Notch reporter cells, we found that immobilized, un-oriented Delta-1 does not significantly increase Notch signaling over IgG controls in 3D collagen gels (Figure 4.9). However, orienting the Delta-1 ligand results in a significant 3.7 ± 0.2-fold increase over oriented IgG gels ($p<0.005$) and a 3.1 ± 0.1-fold increase over un-oriented Delta-1 ($p<0.005$). Given these results, all gel modification protocols moving forward used the indirect binding protocol to achieve ligand orientation via first binding with the anti-IgG antibody. The Notch-gel was further optimized by increasing anti-IgG binding time from 24 to 48 hrs, resulting in a significant increase in luciferase expression (Figure 4.9).
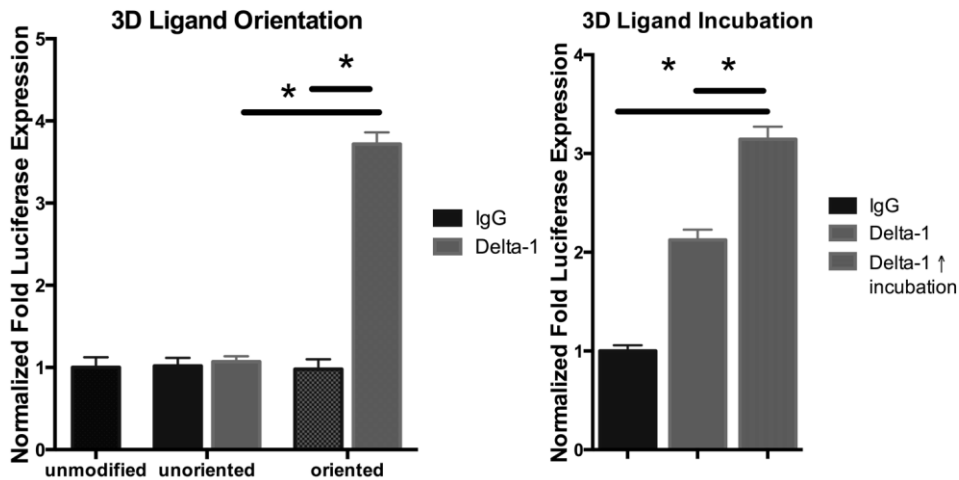
Figure 4.9. Delta-1 ligand orientation via anti-IgG binding is required to achieve detectable Notch-mediated luciferase expression in 3D gels. Luciferase expression is significantly increased with oriented Delta-1 compared to un-oriented Delta-1 and un-oriented IgG control gels. Increasing the duration of anti-IgG binding time facilitates higher Delta-1 immobilization as measured through Notch-driven luciferase expression.

82

Using these optimized protocol modifications, we observed a dose-dependent luciferase signal in the 3D gels similar to what was found on 2D culture platforms although with higher required ligand doses (Figure 4.10). Fold luciferase expression in Delta-1 gels increased by 1.1 ± 0.05-fold in tissues formed 1 µg/ml Delta-1 (p=0.009), by 3.2 ± 0.1-fold using 10 µg/ml Delta-1 (p=2.7E-05), by 5.8 ± 0.4-fold using 50 µg/ml Delta-1 (p=0.0002), by 3.7 ± 0.2-fold using 100 µg/ml Delta-1 (p=6.7E-05), and by 1.9 ± 0.1-fold using 200 µg/ml Delta-1 (p=0.0003, fold increase normalized to 0 µg/ml Delta-1 control). Furthermore, this signal response was retained when collagen was modified and lyophilized after binding with anti-IgG, halting the production at an intermediary step to facilitate batch gel production. Lyophilizing the gel after anti-IgG addition resulted in a 4.3 ± 0.2-fold increase over IgG controls compared to only a 3.2 ± 0.1-fold increase when the gel was lyophilized after binding Delta-1 (Figure 4.10).
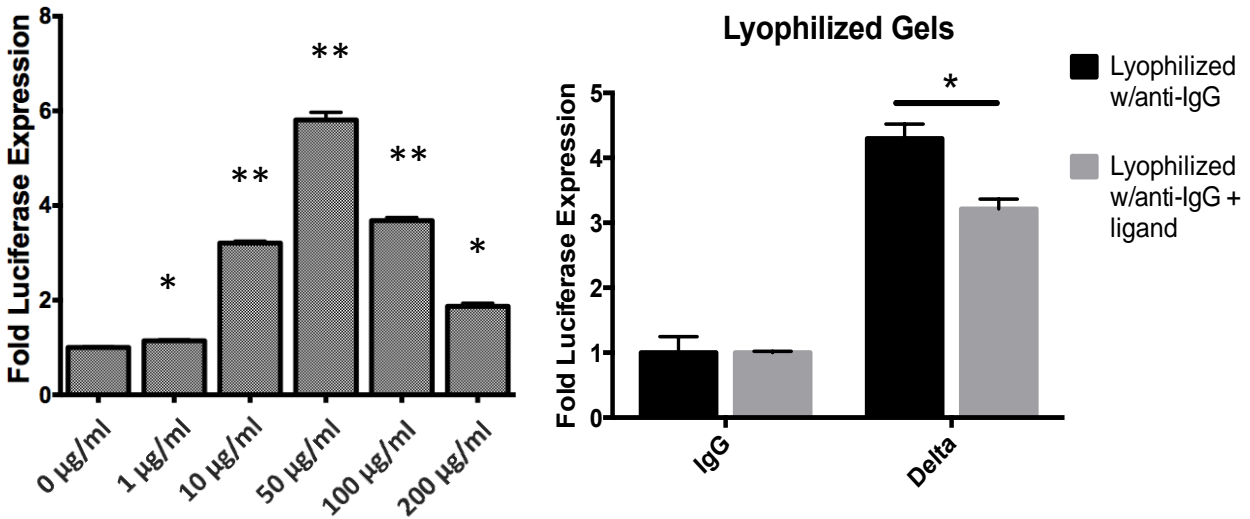
Figure 4.10. Notch activation in 3D gels is dose-dependent and remains after gel lyophilization. (Left) Dose-dependent Notch activation. Culturing U2OS cells in the 3D Notch gel results in a Delta-1 dose-dependent activation of Notch signaling, as indicated by fold luciferase expression compared to IgG control gels. * = p<0.01, ** = p<0.0001. (Right) Lyophilized Notch gels maintain signal response. Collagen was lyophilized for long-term storage either after anti-IgG binding (yet prior to incubation with IgG or Delta-1 ligands) or after collagen modification with IgG or Delta-1 ligands already bound. Both methods resulted in a significant increase in Notch-mediated luciferase expression.* = p<0.05

3D Notch-gel Prolongs Notch Signaling Response Compared to 2D

Due to the 3D environment of the Notch-signaling gel and the ability of cultured cells to infiltrate and remodel the collagen network, we hypothesized that 3D orientation of Notch signaling ligands would prolong the Notch signal response compared to 2D conditions. To test this, we performed a side-by-side time course comparison of the 2D platform and the 3D Notch-gel, again using the CSLluc/ren Notch reporter cells. Consistent with our previous 2D characterization studies, we found that the Notch-driven luciferase signal peaks after day 2 with a 2.8 ± 0.3-fold increase over IgG controls, but this Notch signal wanes quickly back to baseline levels by day 7 (1.1 ± 0.02-fold compared to IgG 2D culture conditions, Figure 4.11). In contrast, Notch-driven luciferase expression in 3D Notch-gels doesn't reach a peak until day 5 with a 4.4 ± 0.2-fold increase over IgG controls, and is still 2.5 ± 0.1-fold higher than IgG 3D control gels at day 10. Detectable luciferase expression is still identified after 2 weeks in 3D Delta-1 gels, although this signal fades back to baseline levels by day 18 (1.1 ± 0.2-fold). The delay in signal onset in 3D is interesting, and may be due to the time needed for cells to remodel the collagen matrix and spread in 3D. We suspect that the prolonged Notch activation in 3D reflects the ability of the cells to move throughout the 3D environment, possibly increasing their exposure to Delta-1 in the process.
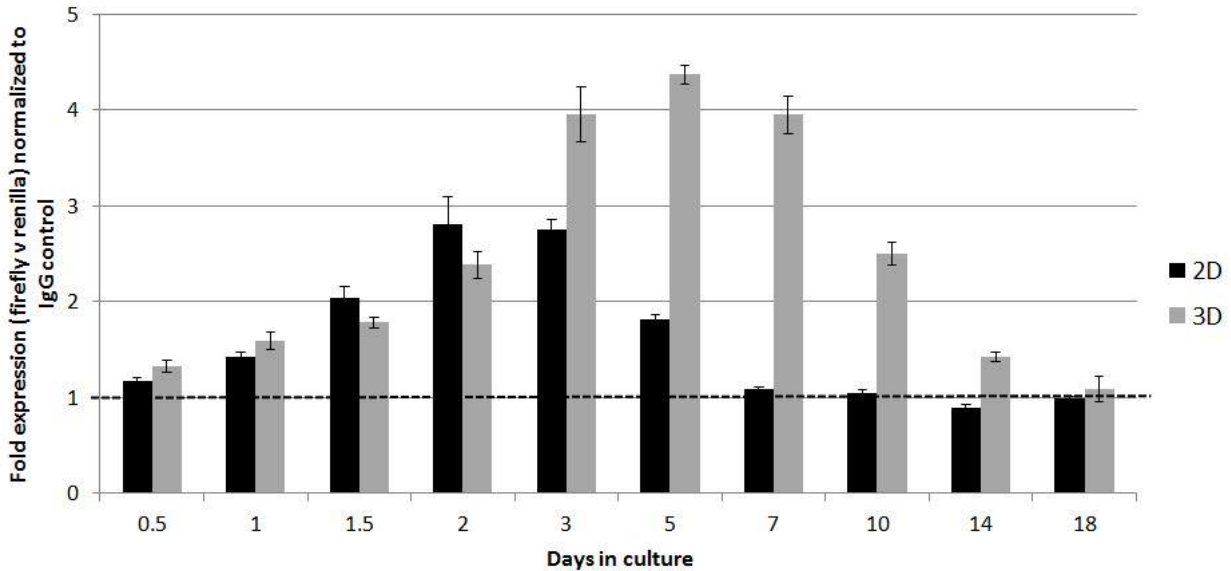
Figure 4.11. Timecourse analysis of Notch-mediated luciferase expression indicates a prolonged Notch signal response in 3D culture conditions compared to the 2D Delta-1 platform. Luciferase signal is expressed normalized to IgG controls (2D or 3D) and plotted against days in culture, ranging from 0.5 (12 hrs) to 18 days (2.5 wks). IgG controls were normalized to one, and a dashed line illustrates the increase in Notch-mediated luciferase expression relative to the control. The 2D samples (black bars) peak in Notch signal around day 2, but decrease back to baseline levels within 7 days. In contrast, the 3D samples (gray bars) don't reach a peak in signal until around day 5, but remain above baseline levels out to 2.5 weeks.

Increased hESC-Cardiomyocyte Proliferation in 3D Engineered Notch-gel Cardiac Tissues

We had previously demonstrated that hESC-cardiomyocytes proliferate in response to 2D immobilized Delta-1, so we next sought to investigate cardiomyocyte proliferation in the 3D Notch environment. Engineered cardiac tissue constructs were formed with modified collagen bound with either immobilized IgG (controls) or Delta-1, labeled with a 24 hr BrdU pulse, and were analyzed histologically for cell cycle activity by BrdU incorporation. Cardiomyocyte proliferation was significantly increased in Delta-1 gels compared to IgG controls (Figure 4.12). When tissues formed with hESC-cardiomyocytes at day 15 after the initiation of directed differentiation, the proliferative rate was $17.5 \pm 2.7\%$ in IgG tissues compared to $27.4 \pm 2.7\%$ in

Delta-1 tissues (p=0.037). As expected, older hESC-cardiomyocytes at day 30 after directed differentiation showed a lower basal rate of proliferation ($10.9 \pm 1.3\%$ on IgG) but also resulted in increased proliferation in response to Delta-1 ($20.0 \pm 1.0\%$, p=0.0002).
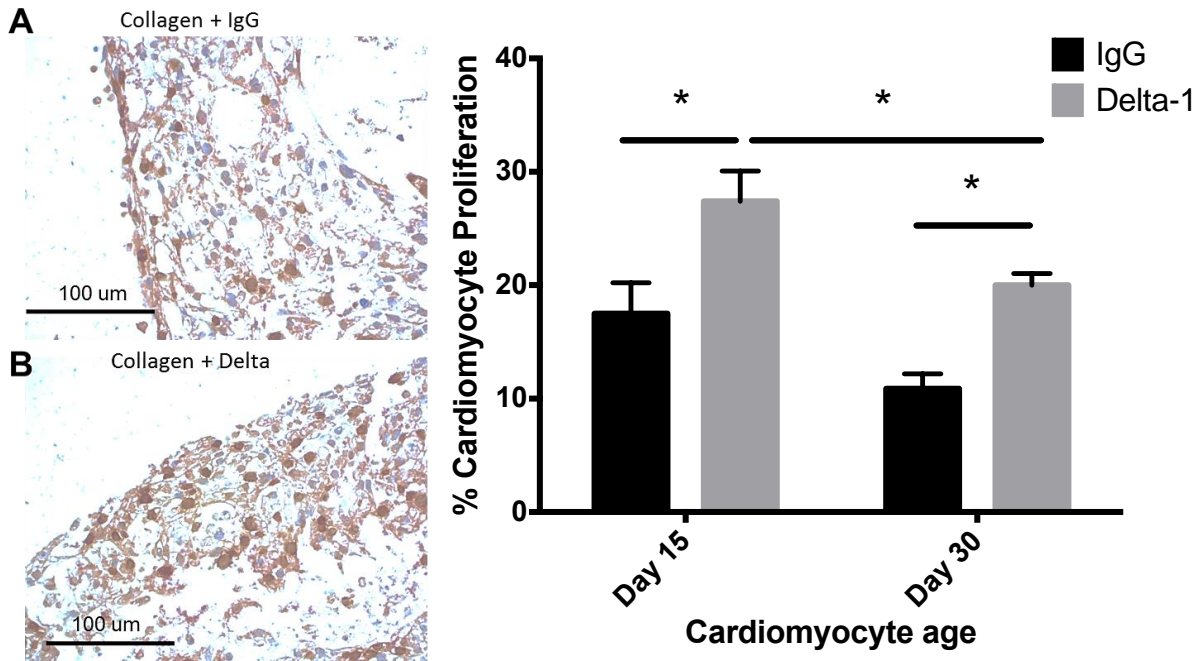
Figure 4.12. HESC-cardiomyocytes in 3D engineered cardiac tissues proliferate in response to Delta-1. Cardiomyocyte proliferation was measured by histology as double-positive $\beta MHC^+/BrdU^+$ cells, shown here in IgG-gels (A) and Delta-1-gels (B). BrdU is visualized using DAB (brown) and βMHC is visualized using vector red (pink). Quantifying cardiomyocyte proliferation results in a significant increase in response to Delta-1 with day 15 cells and day 30 cells over IgG controls. Induced proliferation is highest in day 15 vs day 30 cells in Delta-1 conditions. * indicates p<0.05

Delta-1 Increases Cell Density in Engineered Cardiac Tissues

Motivated by the results described above, we hypothesized that cell density in the engineered cardiac tissues would also increase in response to Delta-1, and may impact force production of the engineered cardiac tissues. Cardiac tissues were formed using the modified collagen (IgG control or Delta-1) incorporating either only cardiomyocytes or cardiomyocytes with the addition

of HS27a mesenchymal stromal cells (MSCs). MSCs are often added to collagen-based engineered cardiac tissues as a supporting cell type to facilitate force production and remodeling [135, 136, 161]. After 4 weeks in culture, tissues were fixed and stained with picrosirius red and fast green counterstain to visualize cellular density within the collagen tissues (Figure 4.13).
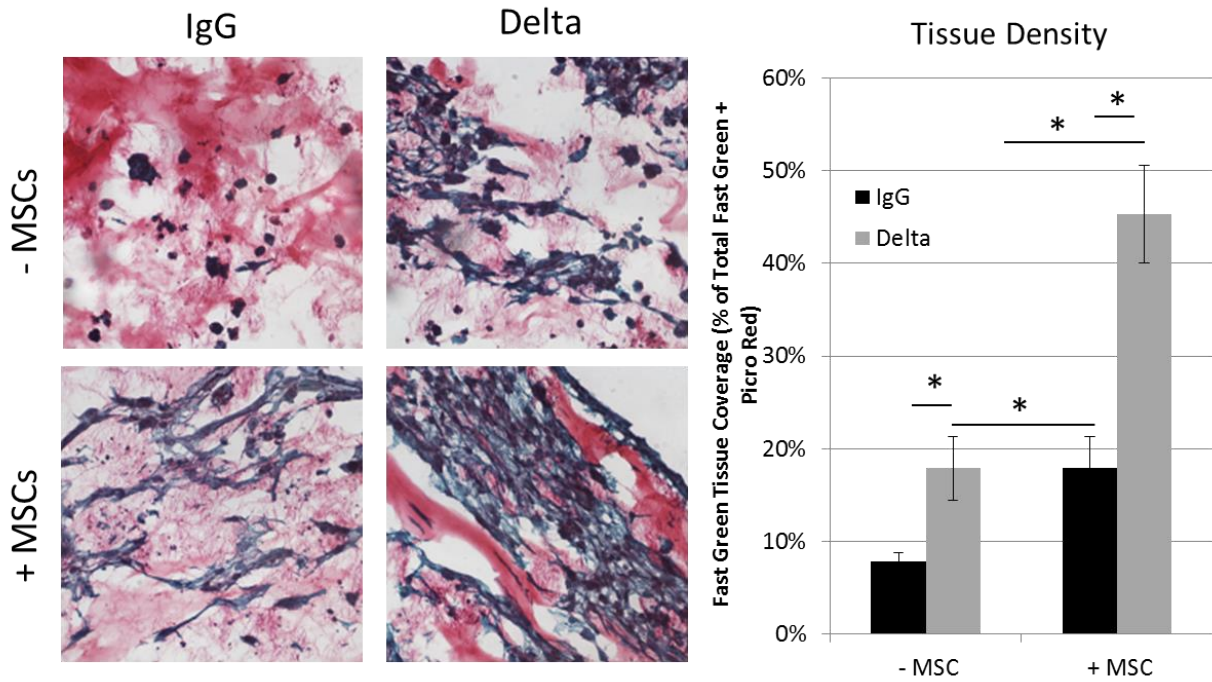
Figure 4.13. Engineered tissues are analyzed histologically following a picrosirius red/fast green stain. (Left) Picrosirius red (red) labels the collagenous gel, and fast green counterstain (blue) labels cellular cytoplasm. Representative images are shown for engineered tissues without stromal cells (MSCs, top panel) and with MSCs (bottom panel) for both IgG (left) and Delta (right) modified gels. (Right) Tissue density was measured in engineered cardiac tissues formed with either IgG (control) collagen or Delta-1 collagen and is reported as fast green tissue coverage normalized as a percent of total fast green to picrosirius red tissue area. Delta-1 significantly increased tissue density compared to IgG controls without MSCs and with MSCs. There was no difference between tissue density between the Delta-1 tissues without MSCs and the IgG tissues with MSCs. * indicates $p<0.05$

Even without the addition of MSCs, tissue density significantly increased from $7.8 \pm 0.9\%$ to $17.9 \pm 3.5\%$ in IgG and Delta-1 gels, respectively (measured following a picrosirius red/fast green stain as % total fast green to fast green + picrosirius red tissue area, $p=0.01$). When stromal cells were included in the engineered tissues, tissue density increased even further from $18.6 \pm$

3.5% to 45.3 ± 5.3% in IgG and Delta-1 gels, respectively (p=0.0005, Figure 4.13). There was no statistical difference between Delta-1 tissues without MSCs and IgG tissues with MSCs (17.9 ± 3.5% in the Delta-1 tissues without MSCs compared to 18.6 ± 3.5% in the IgG tissues with MSCs, p=0.88), suggesting that the addition of Delta-1 may be sufficient to increase tissue density and alignment in the absence of a supporting stromal cell type. Cells also visually showed more alignment with the addition of stromal cells, and tissues lacking stromal cells but containing Delta-1 appear to mimic this effect compared to IgG control gels. This increased tissue density also corresponded to an increase in active twitch force in the tissues formed without stromal cells, with the greatest difference occurring at one and three weeks after tissue formation. Compared to IgG tissues, Delta-1 significantly increased active twitch force by 3.5-fold at 1 week and 3.4-fold at 3 weeks (p=0.007 at 1 week and p=0.02 at 3 weeks). Active twitch force trended higher in the Delta-1 tissues across all timepoints (shown in Figure 4.14).
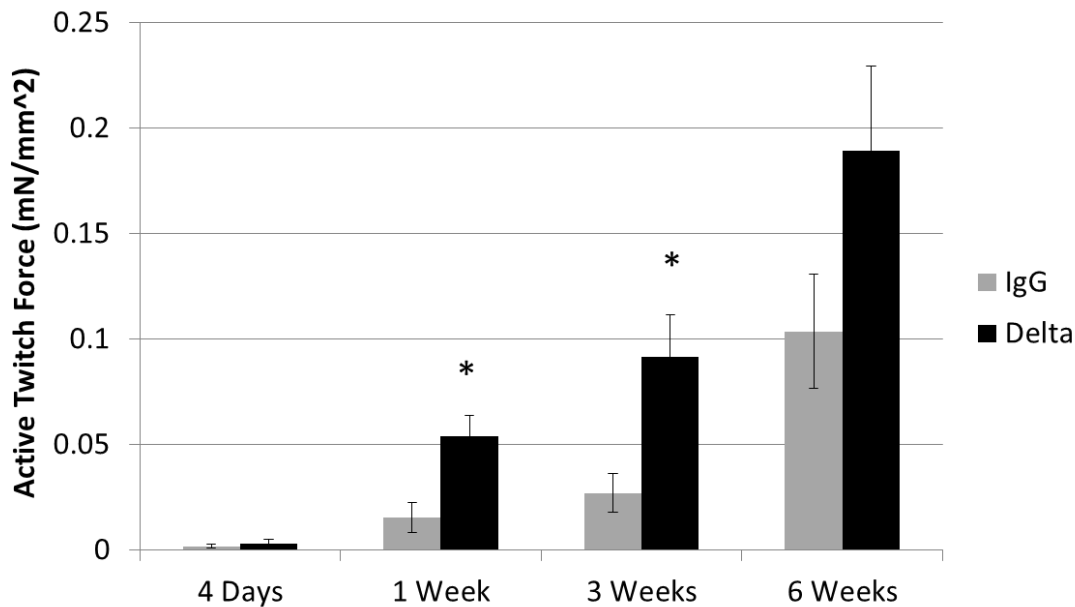
Figure 4.14. Force production in engineered cardiac tissues. Cardiac tissues were formed without MSCs using either IgG control gel or Delta- gel. Cardiac tissues were analyzed for active force production at 4 days, 1 week, 3 weeks, and 6 weeks. * indicates p<0.05.

4.5 Discussion

Previous studies have highlighted the role of Notch signaling in regulating cardiomyocyte proliferation, and achieving this control in the context of stem cell-derived cardiomyocytes would have wide applications both *in vivo* and *in vitro* for regenerative medicine. Although Notch has been successfully activated in cardiomyocytes in various *in vivo* settings [41, 60-62, 74], the use of Notch signaling agonists for *in vitro* culture is limited in that ligands must be immobilized and in many cases oriented in order to elicit a robust signaling response [155, 156]. Previously, this has limited experiments to 2D cell culture without a reliable method to present Notch ligands in a 3D environment. To address this limitation, we first validated a 2D tissue culture platform with oriented, immobilized Delta-1 in 2D and characterized the response of hESC-cardiomyocytes. We next designed a 3D collagen-based hydrogel with oriented and immobilized Delta-1, allowing for the Notch ligand to be presented in 3D, and investigated the ability to promote Notch signaling and subsequently promote cardiomyocyte proliferation.

In contrast to the 2D surfaces, which begin to lose signal activity within 2-3 days after cell plating, the 3D hydrogel platform continued to activate Notch signaling for up to 2.5 weeks after cell seeding into tissues. This corresponds to a robust increase in total Notch signal gained from the 3D system compared to 2D over a 2 week period of *in vitro* culture, prolonging the impact of Notch in the 3D environment. As observed in Figure 4.11, there was a slight delay in the onset of Notch signaling in the 3D gels compared to 2D. We suspect that this delay in signaling is due to the time needed for cells to attach and remodel the collagen matrix. Because Notch signaling is believed to require tension to initiate downstream signaling, we suspect that the appropriate

tension isn't achieved in the 3D collagen gel until the collagen fibers have been crosslinked and remodeled. In our system, the initial collagen gelation occurs between 30 and 120 minutes at which point the tissues have solidified enough to not be disrupted with the addition of media, however this also varies depending on the cellular density as well as the collagen concentration. At this early timepoint, the cells remain rounded and have not yet spread to attach to the collagen, which is typically observed soon after plating in 2D culture. However over the next few days, the collagen matrix continues to undergo remodeling by the hESC-cardiomyocytes, and we suspect that this process is in part responsible for the delayed signal response. The ability of cells to migrate through and remodel the collagen matrix may also explain the extended Notch activation in the 3D context. Although this has not been explicitly addressed in these studies, we suspect that the cardiomyocytes are exposed to more Delta-1 ligand as they migrate through the porous collagen scaffold, lengthening the exposure to the Notch ligand. Further studies are needed to confirm this and evaluate the level of migration and matrix remodeling in this context.

Although we anticipated an increase in cardiomyocyte proliferation in response to Delta-1 in 3D, we were surprised by the increase in active force production in the Notch groups at early timepoints. Our initial hypothesis was that hESC-cardiomyocytes formed in engineered cardiac tissues using Notch-modified hydrogels would show an early proliferative phase compared to IgG controls, during which time the proliferative cardiomyocytes would be relatively immature. As these immature cardiomyocytes would likely be smaller, more glycolytic, and less contractile during the proliferative phase, we expected that they would be unable to significantly contribute to force production. Thus, we anticipated an increase in cell number over time along with a subsequent increase in tissue force production as the cells began to mature over the next few

weeks. This is in contrast to the results shown here, which indicate an increase in force production within the first week in Delta-1 tissues without MSCs (Figure 4.14). One possible explanation for this unexpected result is that the increase in cell density observed with Delta-1 (Figure 4.13) was sufficient to contribute to force production even within the first week after tissue formation. This could be due to strictly an increase in cell number, or possibly a change in overall tissue stiffness due to a higher cellular density within the tissues. Another possibility is that Delta-1 is altering the phenotype of hESC-cardiomyocytes in a way that promotes tissue force production such as collagen remodeling, alignment, or electrical coupling ability. These possibilities were not explicitly addressed in these studies but cannot be ruled out for their contribution to force production. It is also interesting to note that in tissues formed with stromal cells, Delta-1 seems to promote an additional increase in tissue density than what was seen without stromal cells. Stromal cells have often been added as a supporting cell type in engineered cardiac tissues to promote alignment and increase force production [135, 136, 161]. These results suggest that Delta-1 may be sufficient for promoting tissue alignment and force production without the need for a supporting cell population.

Although collagen-1 scaffolds were ultimately chosen as the ideal scaffold material for immobilizing Delta-1, a variety of other biomimetic materials were tested in preliminary experiments (data not shown). The most successful of these was decellularized porcine ECM, with which were able to achieve comparable Notch activation (data not shown). Decellularized ECM is a promising alternative biomimetic material to collagen, as it has already been approved for clinical applications [169-171] and has been successfully delivered via needle and catheter to form a porous network that promotes cell infiltration *in vivo* [172, 173]. Other materials tested

included fibrin, hyaluronic acid, and a self-assembling Notch peptide material [41]. This approach has also been adapted to functionalize PL-CHO photoreversible, patterned hydrogels in collaboration with the Deforest Lab [174].

4.6 Summary

Gaining control over cardiomyocyte proliferation could have broad implications to the field of cardiac regenerative medicine and hESC-cardiomyocyte cell therapy. In this chapter, we developed a Notch-signaling platform to enhance the proliferation of hESC-cardiomyocytes both in 2D cell culture and in 3D engineered cardiac tissue. Culturing hESC-cardiomyocytes on 2D surfaces with immobilized Delta-1 resulted in a significant and dose-dependent increase in cardiomyocyte proliferation relative to control surfaces. We then developed 3D hydrogels with immobilized Delta-1 by using modifying carbodiimide chemistry to modify collagen and bind the ligand in an oriented manner. By immobilizing the Notch ligand Delta-1 in this 3D scaffold, we were able to activate the Notch signaling pathway over 2.5 weeks in culture. Importantly, this increase in Notch signaling increased the proliferation of stem cell-derived cardiomyocytes and increased tissue density in engineered cardiac tissues. Taken collectively, the studies described in this chapter establish a system to modulate Notch signaling and enhance cardiomyocyte proliferation *in vitro* in both 2D tissue culture and in 3D engineered cardiac tissues. This 3D Notch signaling gel is translated into *in vivo* therapeutic studies in Chapter 5

.

Chapter 5: Therapeutic Notch-signaling hydrogel for myocardial repair after ischemia/reperfusion injury

5.1 Abstract

Current transplantation techniques for stem cell-derived cardiomyocytes are hindered by small graft size and limited cell retention, with only a fraction of transplanted cells remaining in the surviving graft. Enhancing the proliferation of transplanted cardiomyocytes *in vivo* is a promising therapeutic strategy to overcome this limitation. Here, a Notch signaling collagen-based hydrogel is used as a vehicle for cardiomyocyte transplantation in the infarcted rat myocardium. Five million hESC-derived cardiomyocytes are resuspended in a modified collagen gel with the immobilized Notch ligand Delta-1 or IgG control, and are injected into the infarcted myocardium using a 26g needle. Four weeks after transplantation, βMHC^+ human graft area is significantly increased by 3-fold in the Notch group compared to controls, with grafts occupying $3.0 \pm 0.6\%$ and $1.0 \pm 0.2\%$ of the infarct region in the Delta-1 and IgG groups, respectively (p = 0.026). When normalized to left ventricular area, graft size increased by 3.4-fold with grafts covering $1.0 \pm 0.3\%$ and $0.3 \pm 0.1\%$ of the left ventricle in the Delta-1 and IgG control group, respectively (p=0.045). Proliferation of hESC-derived cardiomyocytes was also significantly increased in the Delta-1 group, with $10.9 \pm 0.5\%$ of proliferating $BrdU^+/\beta MHC^+$ graft cells compared to $4.8 \pm 0.5\%$ of $BrdU^+/\beta MHC^+$ graft cells in IgG controls (p<0.0001). Neovascularization within the βMHC^+ graft area was also increased by 4.4-fold in the Delta-1 group compared to the IgG control group (p=0.04). Collectively, these results demonstrate the Notch hydrogel as a therapeutic approach to enhance graft size by promoting cardiomyocyte proliferation and stimulating an endogenous repair response in the host myocardium.

5.2 Rationale

Despite the tremendous progress that has been made in developing cell therapy for heart repair, one of the remaining limitations is small graft size. Limited engraftment has been previously described as a major hurdle to overcome in the development of cell transplantation therapies for heart repair. Studies indicate that over 50% of transplanted cells are lost within the first day after transplant, with the remaining graft size further declining to less than 15% of initial transplant number over the next 3 months [2]. In order to facilitate the clinical translation and scalability of hESC-cardiomyocyte cell therapy, there is a need for methods to enhance graft size and to minimize the number of cardiomyocytes required for transplantation.

Promoting cell cycle activity of transplanted cells after engraftment is one approach to achieve a larger graft size, because cell division in a percentage of implanted hESC-cardiomyocytes *in vivo* could result in an increase in the number of human cells within the graft. However controlling cardiomyocyte proliferation *in vitro* and *in vivo* has been challenging. Previous studies have suggested that manipulating the Notch signaling pathway regulates cardiomyocyte proliferation [41, 60-62, 74], however these studies are limited by their lack of transient and spatial control over Notch signaling. Additionally, while cardiomyocyte proliferation following myocardial injury is a pre-requisite to obtaining endogenous functional repair, cardiomyocytes must be able to exit the cell cycle and undergo physiological hypertrophy to meet the force production demands of the heart. We suspect that the balance between proliferation and maturation will be critical, which we hypothesized could be accomplished with a localized, transient Notch signal. In Chapter 4, we demonstrated the signal response curve of the collagen gel with an immobilized

94

Notch ligand that elicited a robust signaling response that waned after 2.5 weeks *in vitro*. This Notch-signaling hydrogel was designed to be compatible with *in vivo* delivery as an injectable material, and is investigated here in conjunction with the implantation of hESC-cardiomyocytes.

In contrast to macro-scale engineered tissues, injectable biomaterials that gel *in situ* are an appealing approach for heart repair because they can be delivered in a minimally-invasive procedure [175, 176]. Many injectable materials have been investigated for myocardial tissue engineering and transplantation including fibrin, alginate, self-assembling peptides, chitosan, and hyaluronic acid [175], however few studies have modified the materials to immobilize ligands or proteins in order to manipulate cellular signaling. Hydrogels derived from extracellular matrix (ECM) components and collagen-based hydrogels are particularly appealing for cardiac repair, because they are biocompatible, biodegradable, are compatible with needle and catheter delivery [175], and have been FDA-approved for numerous clinical applications [177]. Because they already exist as a natural component of the native tissue, natural hydrogels can be readily remodeled by the cells as they infiltrate the porous network [173, 175].

The research in this chapter combines the proliferative response of cardiomyocytes to Notch signaling (Chapter 4) and the benefits of intramyocardial implantation for hESC-cardiomyocyte therapy (Chapter 3) to address a major challenge in the field. We hypothesized that the Notch signaling gel would provide a powerful therapeutic delivery strategy to enhance the engraftment of hESC-derived cardiomyocytes in two ways: 1) by promoting the proliferation of engrafted cardiomyocytes after transplantation 2) by stimulating an endogenous cardiac repair response in the host myocardium via Notch signaling. We have previously shown that hESC-derived

cardiomyocytes proliferate in response to Delta-1 when immobilized in a 3D collagen matrix (Chapter 4), and this collagen gel was designed to be compatible with needle delivery of hESC-cardiomyocytes *in vivo*. In the results described below, we demonstrate increased graft size and enhanced cardiomyocyte proliferation in response to the transplanted Delta-1 Notch signaling hydrogel.

5.3 Methods and Scientific Strategy

RUES2 hESC-Cardiomyocyte Culture and Differentiation

RUES2 hESCs were maintained in culture on Matrigel™ in mouse embryonic fibroblast (MEF)-conditioned media with 5 ng/ml basic fibroblast growth factor (bFGF) as previously described [45]. To induce differentiation, cells were plated in a high-density monolayer, pre-treated with 1 μM CHIR99021, and induced with 100 ng/ml Activin A and 1x Matrigel in RPMI-1640 with B27 Supplement minus insulin. Media was changed to RPMI-1640 with B27 Supplement minus insulin supplemented with 1 μM CHIR99021 and 5 ng/ml BMP4 after 18 hrs. Two days later media was changed again and supplemented with XAV939 for an additional 48 hours. Starting at day 7, cells were fed every 2 days with RPMI-1640 supplemented with B27 Supplement containing insulin. For long-term storage cardiomyocytes were cryopreserved on day 21-24 and thawed 2-3 days prior to implantation to allow for recovery [137]. The day prior to cryopreservation, cells were heat shocked for 1 hour at 42°C. After a 1 hr pretreatment with 10 μM ROCK inhibitor Y-27632, cardiomyocytes were harvested by a brief incubation with EDTA

and dispersed into single cells using 0.25% trypsin in EDTA. Cells were washed and resuspended in CryoStor, added to cryovials, and frozen to -80°C in a controlled rate freezer before transfer to liquid nitrogen. To thaw, cryovials were agitated briefly at 37°C, collected in RPMI-1640 supplemented with 200 U/ml DNAse, and washed with basal media. Cardiomyocytes were replated onto Matrigel-coated culture dishes in RPMI-1640 with B27-insulin and supplemented with 10 μM Y-27632. Flow cytometry for cardiac troponin T (1:100, Thermo Scientific) was used to characterize cardiomyocyte population purity after cardiac differentiation and again at the time of harvest for implantation.

Modified Collagen gels with Immobilized Delta-1

Notch signaling gels were formed as described previously (Chapter 4). This collagen-based biomaterial platform allows for the manipulation of Notch signaling in a 3D environment, as previously described in engineered cardiac tissue constructs, but was also designed to be compatible with *in vivo* delivery. Briefly, rat tail collagen type 1 was dissolved in 0.1% acetic acid and was further diluted to 2.5 mg/ml using RPMI. The collagen was reacted with sterile-filtered 1-ethyl-3-(dimethylaminopropyl)carbodiimide hydrochloride (EDC)/*N*-sulfo-hydroxysuccinimide (sulfo-NHS) with 10x RPMI on ice for 1 hour with periodic mixing. After 1 hour, 20 mM 2-mercaptoethanol (2-ME) was added, the pH is adjusted to 7.0 − 7.2 using 1M NaOH, and 200 μg/ml anti-human IgG (Fc specific) is added. This intermediate solution is incubated for 48 hrs at 4°C, followed by the addition of 100 μg /ml Delta-1 or IgG and a 24 hr incubation at 4°C.

Luciferase-based Analysis of Notch Signaling

To confirm the bioactivity of the Notch-gels that were implanted, luciferase-based analysis of Notch signaling response was performed on all gel preparations as described in Chapter 4. Briefly, U20S CSL-luciferase/renilla cells were engineered to express constitutively active renilla and firefly luciferase under control of the CSL (CBF1, Su(H), and Lag-1) expression (U20S CSLluc/ren)). U20S CSLluc/ren cells were maintained in DMEM supplemented with 10% FBS, 2 mM l-glutamine, and 100 units/ml penicillin/ 100 µg/ml streptomycin, and passaged at 80% confluence using 0.25% trypsin-EDTA. After gel modification was complete, engineered tissues were formed in wells of a 96 well-plate using 25k U20S CSLluc/ren cells in 30 µl of IgG- or Delta-modified collagen. After 72 hrs in culture, media was removed and 200 µl of 1X Passive Lysis Buffer (Promega) was added to lyse cells during a 10 min incubation. Gels and buffer were triturated and underwent 2-3 repetitive freeze/thaw cycles at -80°C, followed by additional trituration using a handheld tissue homogenizer. The Dual-Luciferase Reporter Cells protocol (Promega) was used to measure luciferase activity, again as described in Chapter 4. First, 20 µl per sample was loaded in triplicate into optical 96-well plates, background fluorescence was recorded, and 20 µl of Luciferase Assay Reagent II (LARII) was added to each well to record firefly luciferase luminescence. Next, 20 µl of Stop and Glo Reagent was then added to each well and luminescence was recorded to analyze renilla expression. All firefly luciferase data was normalized to renilla luminescence for each sample (with background subtraction), and expressed as the fold expression over the corresponding IgG control (normalized to 1).

Pro-Survival Cocktail Treatment During Cell Culture in vitro

For one set of experiments, we investigated the effect of pro-survival cocktail on Notch signaling *in vitro* using the U20S luciferase assay described above. For these experiments, U20S cells were resuspended in DMEM containing the pro-survival cocktail (described in [45, 124] and in Chapter 3) which includes 100 μM ZVAD (benzyloxycarbonyl-Val-Ala-Asp(O-methyl)-fluoromethyl ketone), 50 nM Bcl-X$_L$ BH4, 200 nM cyclosporine A, 100 ng/mL IGF-1, and 50 μM pinacidil. In these studies and in the implantation studies including the pro-survival cocktail, the 50% vol/vol Matrigel was replaced with the modified collagen gel (immobilized with IgG or Delta-1). The cell and gel mixture was pipetted into wells of a 96-well plate following our standard protocol. To mimic the daily cyclosporine injections that are given to rats during the first week after implantation, engineered tissues had a daily media change using standard culture media supplemented with 200 nM cyclosporine A. The cyclosporine amount was calculated by estimating the blood volume in the rat and estimating the bioavailability of cyclosporine A in the bloodstream after subcutaneous injection [4, 178]. Lee et al has reported that the blood volume in a standard lab rat can be estimated by the equation below:

Blood Volume = 0.06*(body weight in grams) + 0.77

Given that our experimental rats weigh around 300 g at the time of surgery, this estimates blood volume to be 18.77 ml as shown below:

$$18.77 = 0.06 * 300g + 0.77$$

Each daily injection of cyclosporine A is 30 μl of a 600 μM stock concentration in 18.77 ml of

99

blood, which equates to 3.3 µM cyclosporine A in the bloodstream. However, this estimation is too high because not all of the cyclosporine A injected subcutaneously is delivered to the heart through the bloodstream, as is begins to be metabolized and is not all transported into the heart. In a previous study by our group [4], guinea pigs were treated with 15 mg/kg of cyclosporine A for 7 days followed by 3 weeks of daily subcutaneous injections at a lower dose of 7.5 mg/kg. Cyclosporine in the blood was measured on day 28 to be 838 ± 64 µg/l, equating to roughly 700 nM. Using these values as guidelines, we estimated the cyclosporine concentration in the blood of a 300g rat after daily doses of 2.5 mg/kg injections (0.75 mg/day) would be around 233 µM. This calculation closely matched our standard *in vitro* cyclosporine treatment of 200 µM for the pro-survival cocktail protocol. Thus, 200 nM was chosen as the final cyclosporine A concentration to use in cell culture media for daily media changes.

Cell and Gel Preparation for Implantation

The morning of implantation surgeries, hESC-cardiomyocytes were harvested as described above. These cardiomyocytes were day 21-28 from the initiation of differentiation, and had been previously cryopreserved and allowed to recover for 2-3 days unless otherwise noted. After harvest and cell count, cardiomyocytes were resuspended in sterile RPMI-1640 supplemented with 1x HEPES, 1x growth factor-reduced Matrigel (solution was first brought to a neutral pH with 1M NaOH) and the cells are kept on ice. The modified collagen solution (prepared as described above) was then mixed 1:1 with the resuspended cell solution, bringing the final collagen concentration to 1.5 mg/ml. The cell and gel mixture was stored on ice until implantation. For some early studies, pro-survival cocktail was used to mix 1:1 with the modified collagen for implantation. These methods have been described in detail in Chapter 3, as well as

in the previous paragraph. As per the pro-survival cocktail, animals received daily subcutaneous injections of 0.75 mg cyclosporine A for 7 days, starting the day prior to implantation. Pro-survival cocktail was used during the experiments described in Chapter 5.4.2 but was omitted in all subsequent experiments.

Feasibility Study of Gel-only Implantation Experiments

To demonstrate the feasibility of needle delivery and *in situ* thermal gelation within the myocardial wall, the modified collagen gel was transplanted into the LV wall of uninjured rat hearts. Collagen was modified with EDC:NHS chemistry and bound with anti-IgG antibody, as described in Chapter 3 and in the methods section above, and diluted to either 1 mg/ml or 2 mg/ml to be injected with a 25 or 26-gauge needle. To better visualize the injected gel, collagen was dyed with 0.4 wt% Trypan blue before being loaded into a syringe for implantation (Figure 5.1). Female Sprague Dawley rats were anesthetized with 2.5-5% isofluorane, intubated and mechanically ventilated, and the chest was opened aseptically after an intradermal injection of 2 mg/kg lidocaine and 1 mg/kg bupivacaine at the incision site. Each rat received two 40 μl injections of modified collagen with an 8-0 suture used to identify the injection site in the wall of the left ventricle. After implantation the chest was covered and the animal was monitored under 3% isofluorane for 30 min, followed by euthanasia and heart harvest. The heart was rinsed in PBS, fixed overnight in 4% paraformaldehyde, sectioned, and processed for paraffin-embedding and histology.
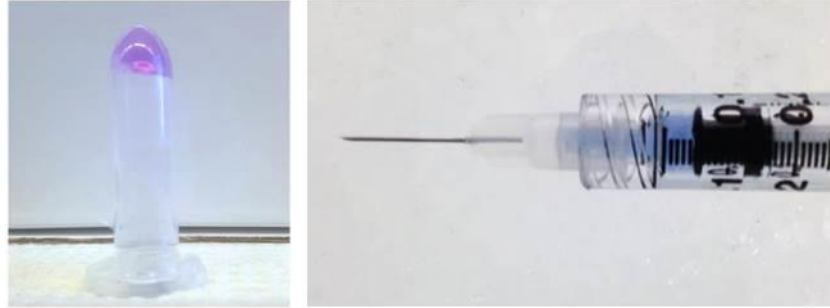
Figure 5.1. Modified collagen gel is compatible with needle delivery. The collagen is dyed with Trypan Blue for easier visualization. At 37°C the collagen solidifies, shown here in an inverted 2.0 ml Eppendorf tube (left). The collagen solution (kept on ice) is loaded into a 1cc syringe and is compatible with delivery through a 26g needle (right).

Gel-only Engraftment and Notch-mediated Response in Uninjured Hearts

These experiments are described in Chapter 5.4.1, and this pilot study was designed to gain initial insight to the therapeutic potentials of the Notch-gel and to further demonstrate the feasibility of transplantation. Collagen was modified with EDC:NHS chemistry and bound with anti-IgG antibody, followed by overnight incubation with Delta-1 or IgG as described above. This modified collagen with immobilized Delta-1 or IgG (control) was transplanted into the myocardial wall of uninjured rat hearts (experimental timeline is shown in Figure 5.2). Sprague Dawley athymic rats were anesthetized and operated on as described in the feasibility study above (and described in more detail in the following section). Each rat received two 40-50 µl injections of 1.5 mg/ml modified collagen with a 26-gauge needle and an 8-0 purse-string suture. After implantation the chest was closed and the animal was monitored during recovery. Post-operative care followed IACUC protocols, and animals received 50 mg/kg BrdU via intraperitoneal injection daily until euthanasia at day 4 or 7. Animal weight was monitored during the experiment. Following euthanasia, the heart was collected, rinsed in PBS, fixed overnight in 4% paraformaldehyde, sectioned, and processed for paraffin-embedding and

histology. Histological methods are described in the immunohistochemical analysis section below. As a quality control, an aliquot of the same batch of prepared Notch-gels were used for *in vitro* Notch analysis in 3D tissues using CSLluc/ren cells, formed the same day of implantation. 3D gels were lysed at day 4 to be analyzed for luciferase expression using the Promega kit as described above.
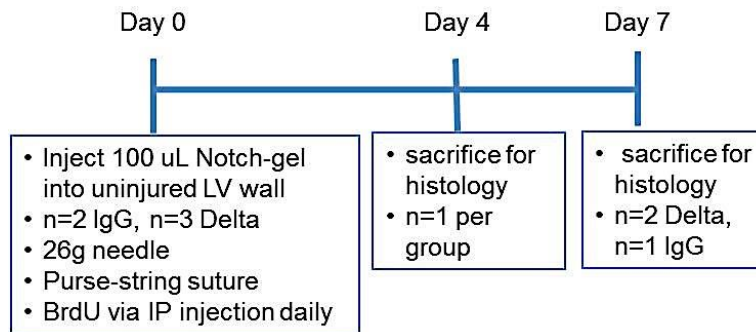
Figure 5.2. Experimental timeline for pilot study. Modified collagen Notch-gel was implanted into uninjured hearts, and animals were sacrificed at either day 4 or day 7 after implantation.

Ischemia and Reperfusion Injury with Cell and Gel Implantation

All animal procedures were performed in accordance with the US NIH Policy on Humane Care and Use of Laboratory Animals and the UW Institutional Animal Care and Use Committee (IACUC). Male Sprague Dawley athymic rats (8 weeks old, 250 – 300 g) were weighed and anesthetized with an IP injection of 90 mg/kg ketamine and 6 mg/kg xylazine, intubated, and mechanically ventilated. Core body temperature was maintained near 37°C by placing the rat on a warming pad and monitoring rectal temperature every 15 min. A local block of 2 mg/kg lidocaine and 1 mg/kg bupivacaine was injected at the incision site intradermally prior to surgery start. A thoracotomy was performed to expose the heart, and ischemia was induced by occluding

the left descending coronary artery with a 7-0 suture for 60 min followed by reperfusion. The chest was closed aseptically and animal recovery was monitored. A dose of 1 mg/kg sustained-release buprenorphine was given subcutaneously before rehousing the animals the same evening. All animals received post-operative care twice-daily for two days following surgery. Four days after I/R, rats were again weighed and given a predose of 0.05 mg/kg buprenorphine (not sustained release) at least 1 hr prior to surgery start. Animals were then anesthetized with 2.5-5% isofluorane, mechanically ventilated, and a second thoracotomy was performed to expose the heart. For the initial implantation studies described in Chapter 5.4.2, $10x10^6$ RUES2 hESC-cardiomyocytes were delivered in 90 µl of either the IgG-collagen (control) or Delta-1-collagen. This was implanted using 2-3 injections in the infarct region and border zone of the myocardium using a 26g needle. The chest was closed aseptically, recovery was monitored, and 1 mg/kg sustained release buprenorphine was administered subcutaneously as described previously. Again, all animals received post-operative care twice-daily for two days followed by monitoring 3-4 times per week until their endpoint. For these studies, pro-survival cocktail was included in the cell and gel preparation, and animals received daily subcutaneous injections of 0.75 mg/kg cyclosporine A for one week. BrdU was administered via intraperitoneal injection at 10 mg/kg on days 1, 4, 7, and 14 post-implantation. This experimental timeline is outlined in Figure 5.3.
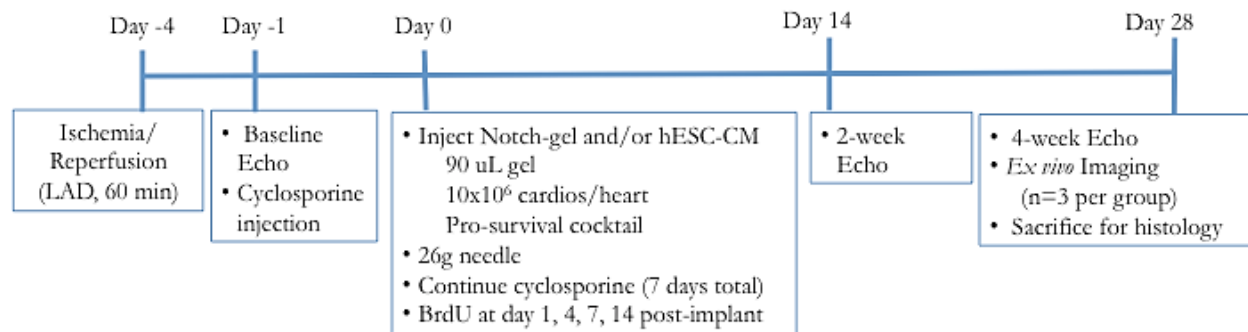
Figure 5.3. Experimental timeline for *in vivo* implantation studies described in Chapter 5.4.2. At day -4, a 60 min ischemia/reperfusion injury was induced and heart function was measured using echocardiography. Four days after injury, animals underwent a second thoracotomy and the Notch-modified collagen gel was implanted with 10×10^6 hESC-cardiomyocytes along with pro-survival cocktail. Daily injections of cyclosporine A were given for 7 days, as per the pro-survival cocktail protocol. Echocardiography was also performed at 2 weeks and 4 weeks, with a subset of hearts undergoing *ex vivo* imaging after sacrifice. All hearts were collected for histology at 4 weeks after implantation.

This implantation protocol was redesigned in a series of pilot studies (Chapter 5.4.3) to produce the final optimized implantation protocol used for the studies described in Chapter 5.4.4. For these experiments, 5×10^6 RUES2 hESC-cardiomyocytes were delivered in two 35 µl injections of either the IgG-collagen (control) or Delta-1-collagen in the infarct region of the myocardium using a 26g needle. After the chest was closed aseptically, animal recovery was monitored, and recovery and post-operative care was performed as described above. No pro-survival cocktail was used in these experiments, and thus there were no daily cyclosporine A injections. Animals still received BrdU injections as described above, underwent echocardiography for analysis of heart function, and were sacrificed at 4 weeks post-implantation. The experimental timeline for these studies is shown in Figure 5.4.

Day -4	Day -1	Day 0	Day 14	Day 28

| Ischemia/ Reperfusion (LAD, 60 min) | • Baseline Echo | • Inject Notch-gel + hESC-CM
• **BrdU at D1, D4, D7, D14** | • 2-week Echo | • 4-week Echo
• Sacrifice for histology |
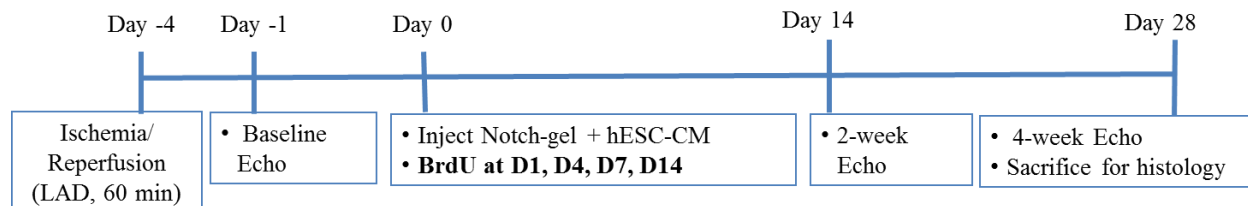
Figure 5.4. Experimental timeline for *in vivo* implantation studies. I/R injury was induced and baseline echocardiography was performed to assess heart function after injury. Four days after injury, a second thoracotomy was performed and the Notch-modified collagen gel was implanted with 5×10^6 hESC-cardiomyocytes. Echocardiography was performed at 2 wks and 4 wks. Animals were sacrificed and hearts were collected for histology at 4 wks.

Echocardiography

Heart function was assessed by echocardiography at baseline 4 days after infarction and at 2 and 4 weeks post-engraftment. Animals were lightly anesthetized with 1-2.5% isoflurane, and the left ventricular (LV) end diastolic dimension (LVEDd), LV end systolic dimension (LVEDd), and heart rate were recorded. Fractional shortening (%FS) was calculated using the equation and analysis method shown in Figure 5.5.

$$\%FS = 100 \times \left(\frac{LVEDd - LVESd}{LVEDd} \right)$$
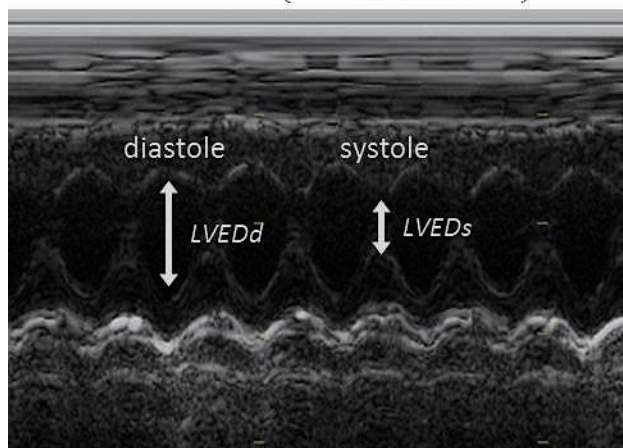
Figure 5.5. Heart function is evaluated by fractional shortening (%FS), which is analyzed using echocardiography. The equation above is used to calculate %FS, where LVEDd = LV end diastolic dimension and LVESd = LV end systolic dimension.

Immunohistochemical Analysis

Histological studies were performed following published protocols by our group [3, 72, 78, [45] and described in Chapters 3.3 and 4.3. Animals were sacrificed at their terminal endpoint of 4 weeks after implantation using a lethal overdose of Beuthasol administered via intraperitoneal injection. Hearts were collected, washed in cold PBS, and perfused with 150 mM KCl. During this time, a small sample of intestine was collected from each animal to serve as a BrdU positive control. The tissues were fixed in 4% paraformaldehyde overnight, sectioned, processed, and stained with the appropriate primary and secondary antibodies. Infarcted myocardium was visualized using picrosirius red with a fast green counterstain, and picrosirius red area was normalized to left ventricular area. Human cardiomyocyte grafts were identified by staining for β-myosin heavy chain (βMHC) (hybridoma supernatant, ATCC #CRL-2046) and visualized using either Alexa Fluor-488 goat anti-mouse (1:100, Molecular Probes) or an avidin-biotin goat anti-mouse antibody (1:100, Vector Labs) developed with diaminobenzadene (Vector Labs). To analyze BrdU incorporation, slides were first stained with the βMHC primary antibody described above and then treated with 1.5 N HCl, followed by overnight incubation with anti-BrdU-POD primary antibody (1:40, Roche). Slides were then incubated with the appropriate secondary antibodies, which was typically Alexa Fluor-488 goat anti-mouse (1:100, Molecular Probes) for βMHC and AF594-tyramide (Alexa Fluor) for BrdU. Cardiomyocyte proliferation was assessed by counting double-labeled $BrdU^+/βMHC^+$ cells, analyzed on images obtained on a Nikon confocal microscope. Vasculature was identified using CD31/PECAM-1 primary antibody (1:100, Novus) and macrophages/monocytes were visualized using CD68 primary antibody (1:100, Serotec). Preliminary experiments used isolectin staining to visualize vascularization, with the caveat being that isolectin can also label macrophages (this can be discerned by

counting only open lumen structures as vasculature). Lectin staining was performed by blocking slides and incubating with GSL-IB4 Fluorescein (1:100) for 1 hr followed by cover slipping with Vectashield containing DAPI. To directly assess remaining gel, implanted Notch-gel was visualized by incubation with a rabbit anti-goat secondary antibody (biotinylated and developed by DAB for brightfield microscopy, or with AF-594 for immunofluorescent imaging) to label the covalently-bound goat anti-human IgG protein (the protein that binds IgG or Delta-1 to the collagen).

Ex Vivo Fluorescent GCaMP3 Imaging

A subset of hearts from the studies in Chapter 5.4.2 (experimental timeline shown in Figure 5.3) were analyzed using *ex vivo* fluorescent imaging to confirm electrical integration of the graft with host myocardium. These procedures followed the protocols outlined in the methods section of Chapter 3. Briefly, animals were sacrificed with a lethal overdose of Beuthasol and hearts were collected and mounted on a Langendorff apparatus as described previously [45]. 2,3-butanedione monoxime (BDM, 20 mM) was used to mechanically arrest the heart, and the epicardial GCaMP3 fluorescent signal and ECG was recorded. Grafts were electrically paced via electrode insertion in the atria, and data analysis was performed as described in Chapter 3.

Alu qPCR-Based Graft Detection Experiments

Quantitative PCR can be used to detect the amount of human specific sequences compared to rat sequences after the implantation of human cells into the rat heart. This method offers a quantitative approach to measure the total number of human cells engrafted with high specificity. For these experiments, an ischemia/reperfusion injury was induced in male Sprague Dawley rats,

and $10\text{x}10^6$ RUES2 hESC-cardiomyocytes were implanted four days later. Two sham-operated negative controls did not receive any cell injection. Surgical procedures, cell and gel preparation, and implantation procedures followed the protocols defined above. No pro-survival cocktail was included in these experiments. Animals were sacrificed 2 weeks after implantation and hearts were harvested as described previously. Hearts were washed in PBS to remove excess blood, and stored in cold PBS while remaining hearts were harvested. Hearts were then trimmed to remove aorta and excess fat while keeping the atria and ventricles intact, dabbed dry with sterile gauze, and weighed. Hearts were then placed into labeled 2.0 ml cryotubes and snap frozen by placing the tubes into liquid nitrogen followed by storage at -80°C. All surgical necropsy tools were cleaned with PBS and ethanol between animals to avoid cross-contamination between samples. To serve as a known cell control, hESC-cardiomyocytes from the same subset of cells used for implantation were thawed using the protocols described previously, counted, pelleted, and snap frozen at -80°C.

Genomic DNA extraction from tissues was performed using the DNeasy Blood & Tissue Kit (Qiagen). Heart tissues and cell pellets were thawed at room temperature, and tissues were weighed, cut into 8 tissue pieces, and placed into labeled 5 mL tubes containing 600 µl of sterile PBS. Tissues were homogenized using the TissueRuptor (Qiagen) until the tissue was well-homogenized. Proteinase K (1:20 total volume) and RNase A (1:100 total volume) were added to each sample, tubes were vortexed briefly, and then incubated for 2 minutes at room temperature. As per the Qiagen protocol, Buffer AL (1x volume) was added to each tube, and samples were incubated overnight at 56°C. Following the DNeasy Blood & Tissue Kit protocol, 400 µl of lysate was mixed with 200 µl of ethanol and added to a spin column. This was followed by

washes with Buffer AW1 and AW2, along with an additional centrifugation step to dry the membrane. Nuclease-free water (Life Technologies) was used to elute the DNA and concentration was measured on a NanoDrop (Thermo Scientific). These samples along with known cardiomyocyte DNA standards as a control and sham-operated hearts, were set up in duplicate wells of 96-well PCR plates with SYBR green (Applied Biosystems) and human Alu Primers (Forward: GTC AGG AGA TCG AGA CCA TCC C, Reverse: TCC TGC CTC AGC CTC CCA AG). The samples were analyzed on a CFX Connect qPCR machine (BioRad) with an annealing temperature of 63°C. Data is represented as either mean Cq values or extrapolated to present total picograms of human DNA using the cell standard curve as a reference for calculations.

Animal Sample Size Justification

The goal of studies described here were to identify differences between groups using histology as a primary endpoint, and also to closely assess safety and feasibility of this newly-developed therapeutic treatment. By histology, n=8 per group allows for detection of a 2-fold increase in graft size, even with variable engraftment. For example, power calculations indicate n=7/group is sufficient to detect a change in graft size from 3% to 6% of the scar area, with a standard deviation of 2% (2-sided, alpha = 0.05, power = 0.80). This also allowed us to exclude n=1/group if needed due to animal death or exclusion by infarct size. However, n=8 per group is not powered to be sufficient for identifying significant changes in functional improvement. Future studies aimed at addressing functional improvement as a primary endpoint will use n=15 per group for an echocardiography-based functional endpoint. These calculations are consistent with previous observations, and represent an adequate sample size to identify functional

improvement by echocardiography. For example, a similarly-designed study by our group detected a 9% decrease in fractional shortening in the control group compared to no decrease in cell-treated groups, which was significant and detected with n=15-16/group [124]. Our rationale for animal numbers was based on these previous studies by our group and aided by power calculations.

Statistical Measurements

ImageJ was used to perform all image analysis and measurements, and statistical analysis was performed using Excel or Prism Graphpad. Statistical significance (p<0.05) was determined using a two-tailed Student's t test assuming unequal variance. All values are reported as means with error bars representing SEM.

5.4 Results

5.4.1. Gel-only Implantation into Uninjured Myocardium

Modified Collagen is Injected into the Myocardial Wall and Gels In Situ

We first conducted a feasibility study to demonstrate needle delivery and *in situ* thermal gelation within the myocardial wall. The modified collagen gel with immobilized IgG (and dyed with Trypan Blue for visualization) was transplanted into the left ventricular (LV) wall of uninjured rat hearts and allowed to gel for 30 min prior to tissue harvest. After harvest, dyed gel was visible near the suture indicating the injection site (arrow and outline, Figure 5.6), which was the

first indication that transplanted gel remained in the LV wall. Histological analysis confirmed the *in situ* gelation, and acellular graft regions could be easily identified by picrosirius red and hematoxylin and eosin (H&E) staining. This feasibility study demonstrated successful Notch-gel transplant via 1cc syringe and 26g needle and subsequent gelation in the LV wall.
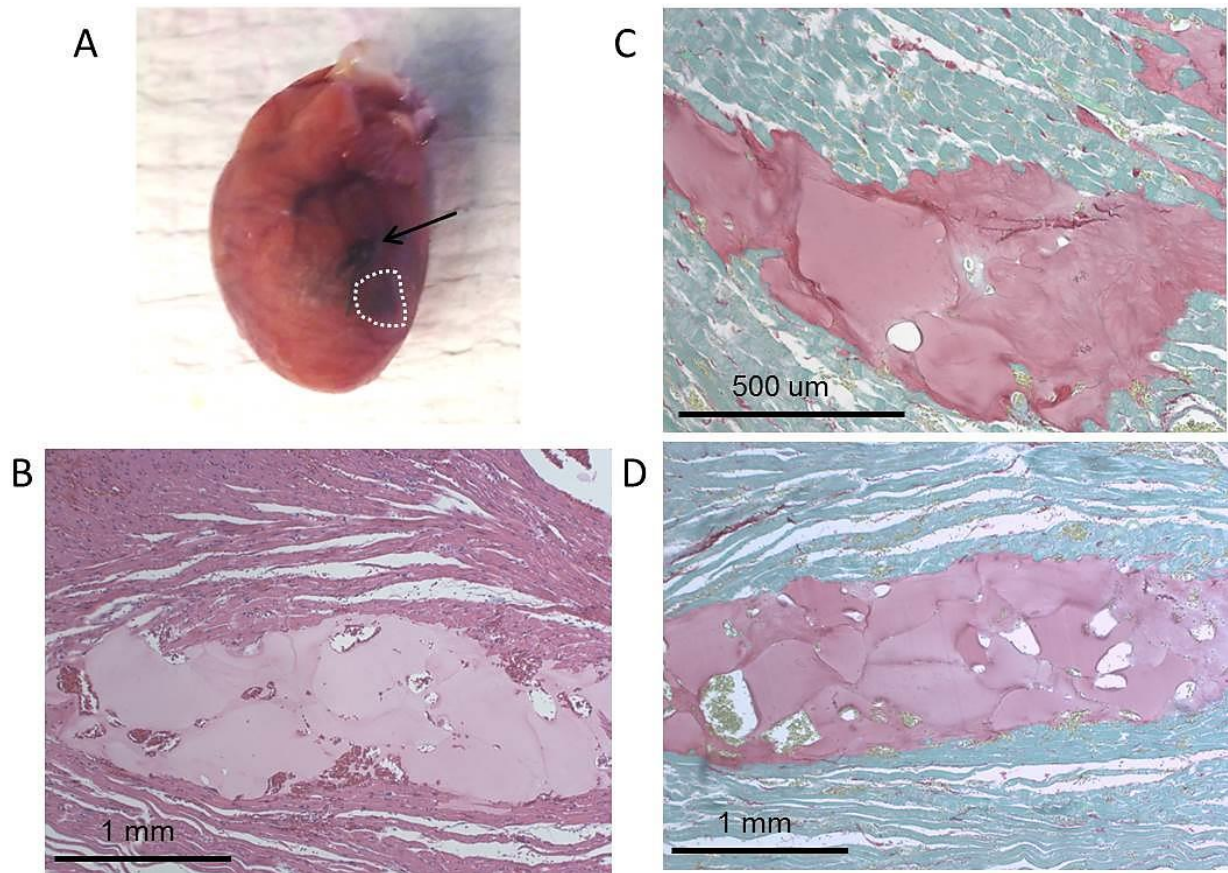
Figure 5.6. *In vivo* needle delivery feasibility study identifies gel in the myocardium 30 min after implantation. Modified collagen gel was dyed and injected into the LV wall, and hearts were harvested after a 30 min gelation period. (A) The dyed gel (outlined) could be seen through the epicardial surface located apically to the suture (arrow) which was used to identify the injection site. (B) Engrafted gels could be identified in the myocardial wall after hematoxylin and eosin (H&E) staining as acellular grafts. Collagen is visible as the light pink region, and healthy myocardium is dark pink. Scale bar = 1 mm. (C, D) The collagen-based gel is easily identified by picrosirius red/fast green staining (collagen = red, myocardial tissue = green). Erythrocytes are identified as yellow-green cells.

Modified Notch Gel is Retained in Uninjured Myocardium at 4 and 7 Days

The first pilot experiment was designed to assess gel retention and remodeling after implantation into uninjured myocardium (Figure 5.2), with primary endpoints at four days and one week. Because enhanced Notch signaling after cardiac injury has been shown to promote neovascularization and reduce fibrosis [75], host vascularization into the hydrogel was quantified as well as the inflammatory response by monocytes, macrophages, and fibroblasts in the gel and surrounding myocardium. Firstly, to validate the Notch signaling response of implanted Delta-1 collagen gels, tissues were formed *in vitro* using CSLluc/ren reporter cells and harvested at day 4 for luciferase analysis, consistent with the first experimental animal timepoint (sacrifice at days 4 and 7). Notch-gels were bioactive and induced a 4.0 ± 0.13 fold increase in normalized luciferase expression compared to the transplanted IgG control gel (Figure 5.6, $p<0.0001$).
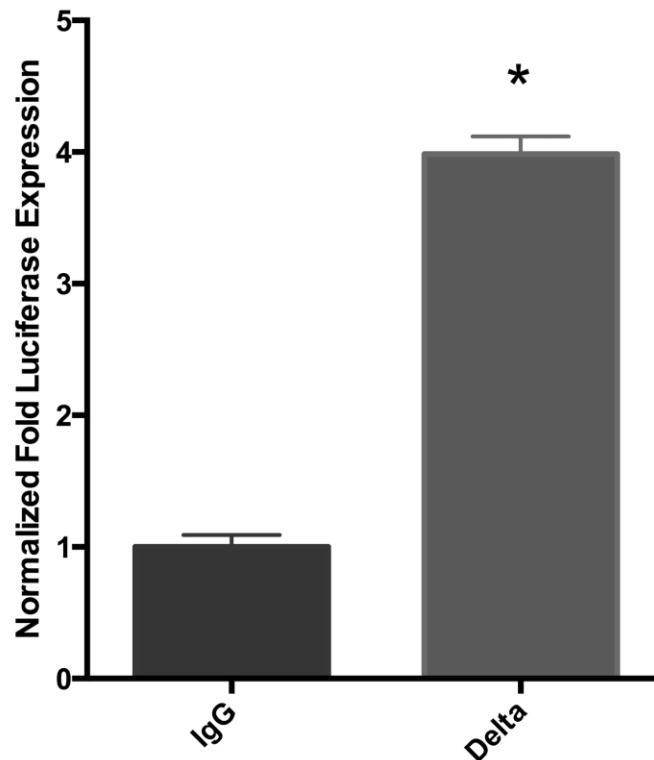
Figure 5.6. EDC:NHS modified collagen with immobilized Delta-1 used for the pilot experiment was bioactive and promoted Notch signaling by luciferase reporter analysis. * $p<0.0001$.

Notch-gels are Remodeled and Cellularized in the Uninjured Heart

Implanted collagen was identified in 5 of 5 hearts regardless of harvest timepoint post-transplantation (n=3 at day 0, n=1 at day 4, n=3 at day 7). Implanted collagen underwent noticeable remodeling, as observed by the transition from the rounded and acellular implants found at day 0 to the finger-like grafts infiltrating the myofibers at day 7 (Figure 5.7). Infiltrating cells were found within the collagen graft at days 4 and 7, which we suspect to be primarily macrophages, fibroblasts, and endothelial cells.
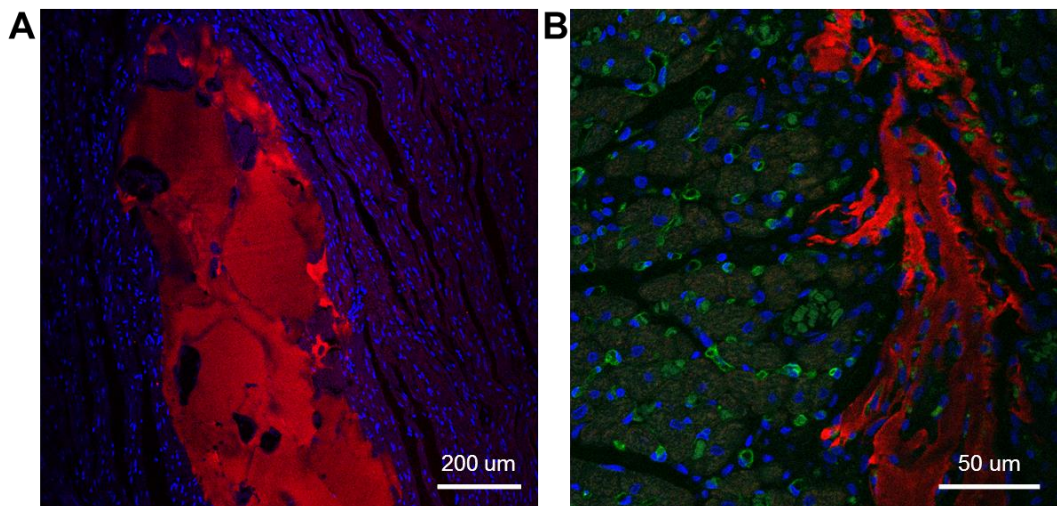
Figure 5.7. Implanted Notch-gels are retained at 1 week within uninjured myocardium. Notch-gels are visualized by donkey α-goat AF-594, labeling the anti-IgG covalently bound to the EDC:NHS-modified collagen. (A) At day 0 the grafts are acellular and retain most of its injected shape (graft = red, nuclei = blue, scale = 200 μm). (B) By day 7 the graft is infiltrated with cells and has undergone significant remodeling. Open lumens labeled by lectin staining indicates vascularization near the graft region. (graft = red, vessels = green, nuclei = blue, scale = 50 μm).

Proliferative Cells are Found Throughout the Gel Region and Surrounding Myocardium

Given the proliferative response to Delta-1 observed in Chapter 3, we assessed the ability of host cells to proliferate in response to a localized Delta-1 signal. Animals received daily intraperitoneal injections of BrdU until their endpoint. BrdU$^+$ cells were identified throughout the graft region and in the adjacent myocardium one week after transplantation of the Notch-gel with immobilized Delta-1 ligand (Figure 5.8). There was evidence of BrdU$^+$/α-actinin$^+$ proliferating rat cardiomyocytes (indicated by white arrows) in the myocardium directly adjacent to the Notch-gel, although identification of these cells was rare and it was difficult to discern these from interstitial cells. Many proliferative non-cardiac cells (BrdU$^+$/α-actinin$^-$) were identified between myofibers, which we suspect to be primarily macrophages and fibroblasts, not rat cardiomyocytes. This proliferative non-cardiac population was localized to the graft region (Figure 5.8D, E) with low levels of BrdU$^+$ cells found in the remote myocardium (i.e. in the right ventricle or in the left ventricle basal to the injection site, Figure 5.8C). Quantitative analysis of BrdU$^+$ cells shows that at day 4, $34.7 \pm 1.8\%$ of cells within the graft were proliferating in Delta-1 gels, compared to $32.4 \pm 1.5\%$ and $37.3 \pm 2.3\%$ at day 7 in IgG control and Delta-1 gels, respectively. Overall cell proliferation in the adjacent myocardium peaked at day 7 and was similar between IgG and Delta-1 gels ($7.4 \pm 1.1\%$ at day 4 in Delta-1 gels, compared to $17.4 \pm 2.2\%$ and $17.0 \pm 1.7\%$ at day 7 in IgG and Delta-1 gels, respectively, Figure 5.8F). Proliferative rates in the remote myocardium were lower in all groups, and all BrdU$^+$ cells in the remote myocardium appear to be non-myocytes. Due to the low animal numbers and rare occurrence of proliferating host cardiomyocytes, we could not complete more detailed analysis on cardiomyocyte-specific proliferation compared to the IgG control gel (n=1 at day 7 for IgG; n=1 at day 4, n=2 at day 7 for Delta-1).
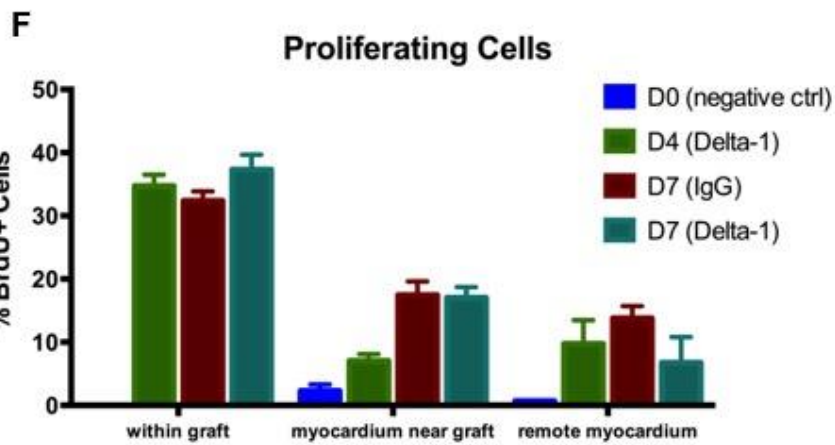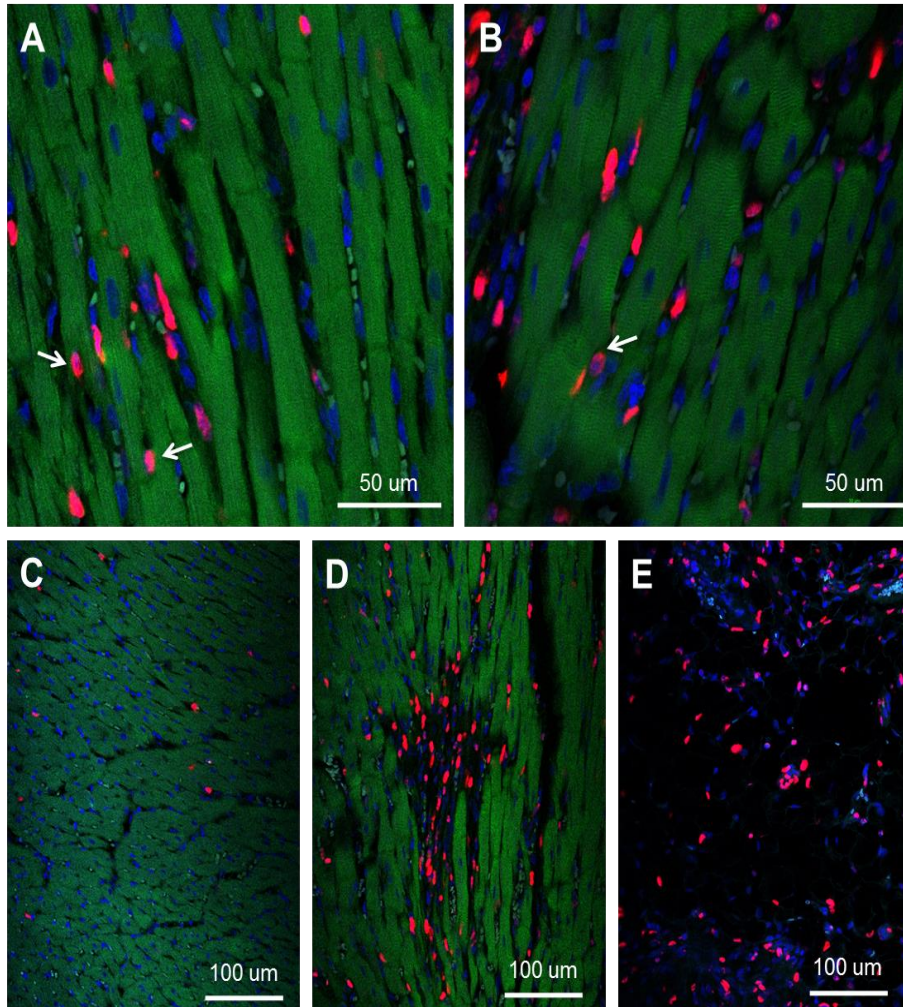
Figure 5.8. Proliferating cells shown in Delta-1-gel hearts at day 7, are stained for BrdU (red) and alpha-actinin (green). BrdU^{+} cells are identified in adjacent myocardium (A, B, scale = 50 µm), at low levels in remote myocardium (C), and at high levels within the graft region (D, E, scale = 100 µm). (F) Quantification of total BrdU^{+} cells at D0, D4, and D7.

Transplanted Notch-gels Induce an Inflammatory Response in the Myocardium

Monocytes and macrophages were identified by histological staining for CD68 after transplanting the Notch-gel into uninjured rat hearts (Figure 5.9). While there are few CD68^{+} cells identified anywhere in the heart between 30 min to 2 hrs post-implantation (6.5 ± 2.6% of total cells, n=3), there was a striking macrophage infiltration in the gel regions at day 4 (Figure 5.9). The vast majority of CD68^{+} cells are localized to the graft region (41.4 ± 1.9% of total cells in Delta-1 gels) but were also present at lower levels epicardially and in the interstitial tissue. This inflammatory population declined by day 7 to 20.0 ± 4.5% in Delta-1 gels, consistent with the timing of the wound healing and inflammatory response observed in the rat heart after ischemic injury. There was monocyte and macrophage infiltration in the hearts after implantation, however it is promising that the population of inflammatory cells is declining by day 7. We were unable to draw any definitive conclusions regarding the role of Delta-1 vs IgG in CD68^{+} cell recruitment due to small animal numbers in this pilot study (n=1 IgG), but preliminary results indicate higher macrophage levels at day 7 in IgG compared to Delta-gels (33.4 ± 2.0% in IgG, 20.0 ± 4.5% in Delta-1 gels, error bars refer to differences across various tissue sections analyzed for each rat).
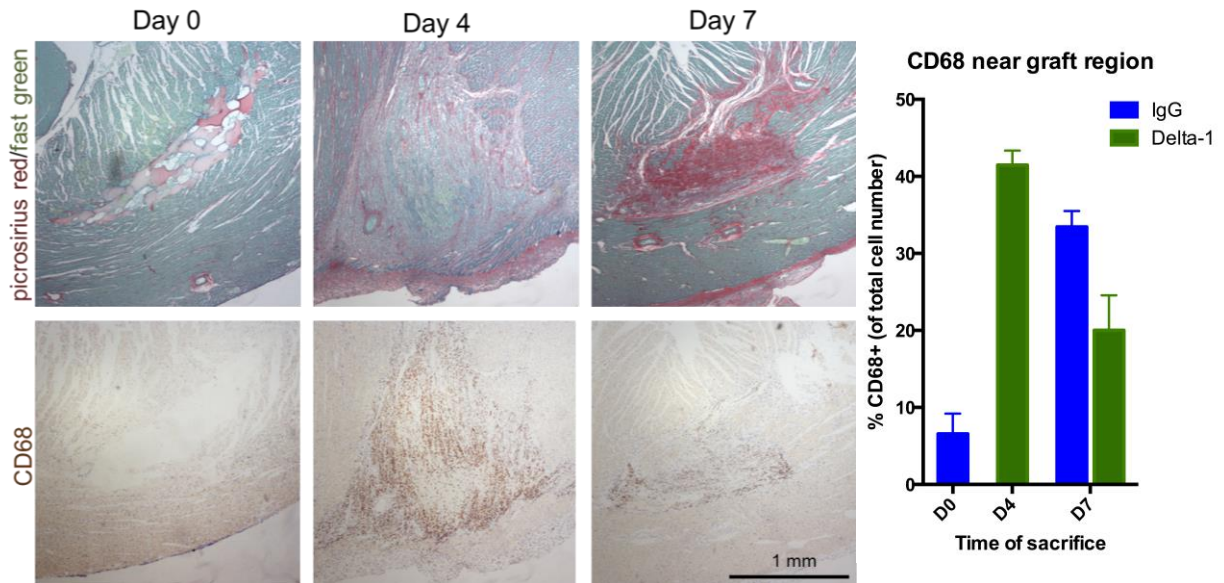
Figure 5.9. Monocyte and macrophage recruitment to the graft region is indicated by CD68 staining in hearts after transplantation of the acellular Notch gel (bottom panel). Picrosirius red/fast green stain (top panel) was used to identify collagen in the LV wall. Scale bar = 1 mm. (Right) CD68^{+} cells are quantified in histological sections, near the graft region at D0, D4, and D7.

5.4.2 Notch-gel with hESC-cardiomyocyte transplantation in I/R-injured hearts

HESC-Cardiomyocytes are Transplanted into Myocardium using the Notch-gel as a Vehicle

The *in vitro* results in Chapter 4 indicated that we were able to achieve a Notch-dependent proliferative response in hESC-cardiomyocytes when cultured in Delta-1-collagen gels. We hypothesized that this increased proliferation would remain *in vivo* when the gel and cardiomyocytes were transplanted into the injured rat myocardium, ultimately resulting in a larger graft area. Following the initial feasibility study and the pilot study testing gel-only implantation, our first set of cell implantation experiments followed protocols similar to those published previously by our group for transplanting hESC-cardiomyocytes into the rat heart [45,

124]. For these experiments, the modified collagen (IgG control or Delta-1) was used as a 50:50 vol/vol component of the injection vehicle for the transplanted hESC-cardiomyocytes. For these experiments, 10×10^6 hESC-cardiomyocytes were implanted into the I/R-injured myocardium with pro-survival cocktail [124] and either IgG control or Delta-1 modified gel (Table 5.1).

Group	Animals	Endpoint	Injectate	Cells
IgG Control	8	4 weeks	Collagen-IgG + PSC	10×10^6 hESC-CM
Delta	8	4 weeks	Collagen-Delta1 + PSC	10×10^6 hESC-CM

Table 5.1. Experimental outline for Notch-gel implantation with hESC-cardiomyocytes in I/R-injured rat hearts. Transplanted cardiomyocytes were cryopreserved and thawed prior to implantation, as per our usual experimental protocols.

The implanted gel was analyzed to confirm a Notch-signaling response of 3.1 ± 0.2-fold increase in Notch-mediated luciferase expression in Delta-1 groups compared to IgG controls (p=0.02, Figure 5.10A), which is expressed as the average fold increase across the 3 implantation preparations. Implanted cardiomyocytes were $90.5 \pm 0.4\%$ cTnT$^+$ by flow cytometry, indicating a highly pure population of hESC-cardiomyocytes (Figure 5.10B, C).
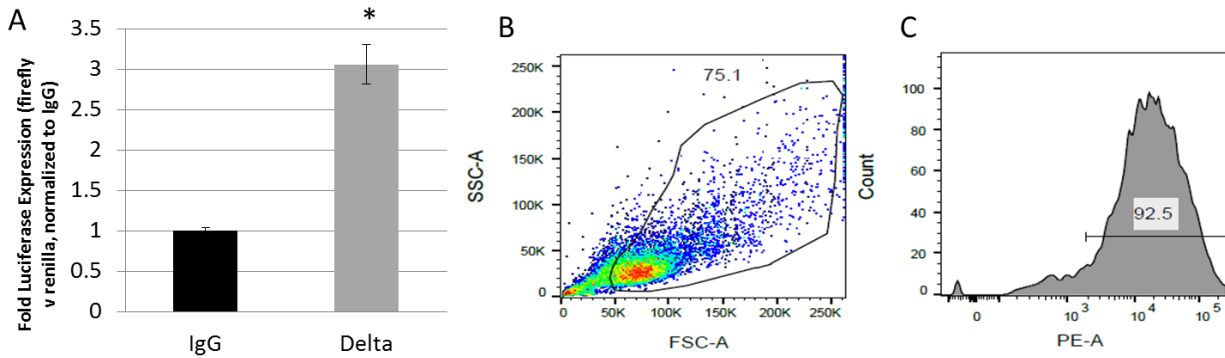
Figure 5.10. Analysis of cell and gel implant material prior to transplantation. (A) Implanted Delta-1 gels produced a Notch-mediated increase in luciferase expression. Data is expressed as fold increase of firefly vs renilla luciferase, normalized to IgG controls. * indicates p<0.05. (B) Flow cytometry analysis of implanted cardiomyocytes. Forward Scatter (FSC) and Side Scatter (SSC) are used to identify a population of single cells (outline), which identifies 75.1% of events. (B) A PE-labeled secondary antibody is used to detect cTnT$^+$ cells, and data is shown at right as a histogram of PE expression. Compared to negative gating determined using an isotype control, 92.5% of single cell events express cTnT-PE.

Human myocardial grafts are identified in both groups

After 4 weeks human myocardial grafts were identified by histology in both groups, as indicated by staining for beta myosin heavy chain (βMHC, Figure 5.11A, B). Graft size was 0.6 ± 0.3% and 0.3 ± 0.1% normalized to left ventricular (LV) area in the IgG groups and Delta groups, respectively (Figure 5.11C). There was no significant difference in graft size between groups, however we did notice an unexpected amount of variability in graft size between animals, which was present in both groups. Of the 7 animals in each group, 5 in each group had a total graft size 0.5% of the left ventricle or less, including 2 animals in the Delta-1 group that had no detectable graft and 2 animals in the control group with grafts smaller than 0.04% of the left ventricle. In contrast, 2 animals in the control group had grafts larger than 1% of the left ventricular area while the remaining 5 animals had grafts less than half that size. We anticipate this variability in graft area is due to variability in initial cell retention upon engraftment, which could have precluded our ability to identify differences in graft size that were related specifically to the

120

effect of Delta-1 in the gel. Based on our *in vitro* data (Chapter 4), we hypothesized that the

hESC-cardiomyocytes implanted within the Delta-1 gel would have increased cell cycle activity

compared to those implanted in IgG control gels. After histological analysis of BrdU

incorporation in transplanted cardiomyocytes, we observed an increase in cardiomyocyte

proliferation in Delta-1 groups ($1.8 \pm 0.3\%$ compared to $4.6 \pm 0.7\%$ proliferation in IgG and

Delta-1 groups, respectively, $p=0.018$, Figure 5.11D).
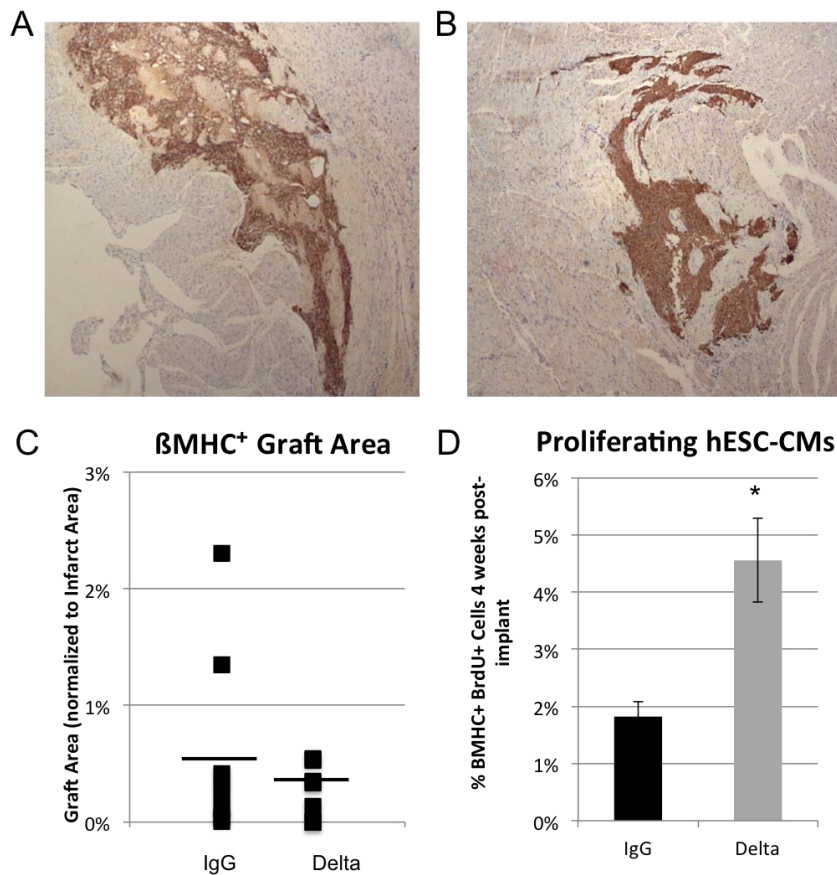
Figure 5.11. Human cardiomyocytes are identified 4 weeks after implantation into I/R-injury. Grafts are identified by staining for βMHC (brown) and counterstained with hematoxylin after implantation with (A) IgG gel and (B) Delta-1 gel. (C) Graft area is normalized to infarct area. Each box indicates the total graft area within one heart, normalized to infarct area with horizontal lines indicating the group average. There was no statistical difference in average graft area between IgG and Delta groups. (D) Proliferation of engrafted hESC-cardiomyocytes was analyzed by quantifying double positive βMHC$^+$/BrdU$^+$ cells in the myocardium. * indicates $p<0.05$.

No functional Differences were Observed Between Groups

Impact on heart function was evaluated using echocardiography, however no significant differences were identified between groups (Figure 5.12D). Fractional shortening measurements at day 0 after injury but prior to cell implantation were $28.0 \pm 1.1\%$ in the IgG group and $27.2 \pm 1.9\%$ in the Delta-1 group (p=0.71), indicating similar injury profiles for both groups at baseline. At two weeks post-implantation fractional shortening was $25.7 \pm 1.1\%$ in the IgG group and $26.8 \pm 1.4\%$ in the Delta-1 group (p=0.55), and at four weeks was $27.7 \pm 0.69\%$ and $25.6 \pm 1.2\%$ in the IgG and Delta-1 groups, respectively (p=0.17). Infarct area analysis by histology showed no significant differences in average infarct area normalized to left ventricular area (Figure 5.12C). While there were no statistical differences detected by fractional shortening or average infarct area, there was variability within groups. We found that this tended to correlate with graft size as our previous work suggested in Chapter 3 [45], where larger grafts tended to be identified in hearts with smaller infarcts. As shown in Figure 5.12A, infarct labeled by picrosirius red was relatively small and large graft regions can be identified within the myocardium, in contrast to the tissue shown in Figure 5.12B where there is a large infarct spanning from the apex to the base of the heart. No graft was identified in this heart.
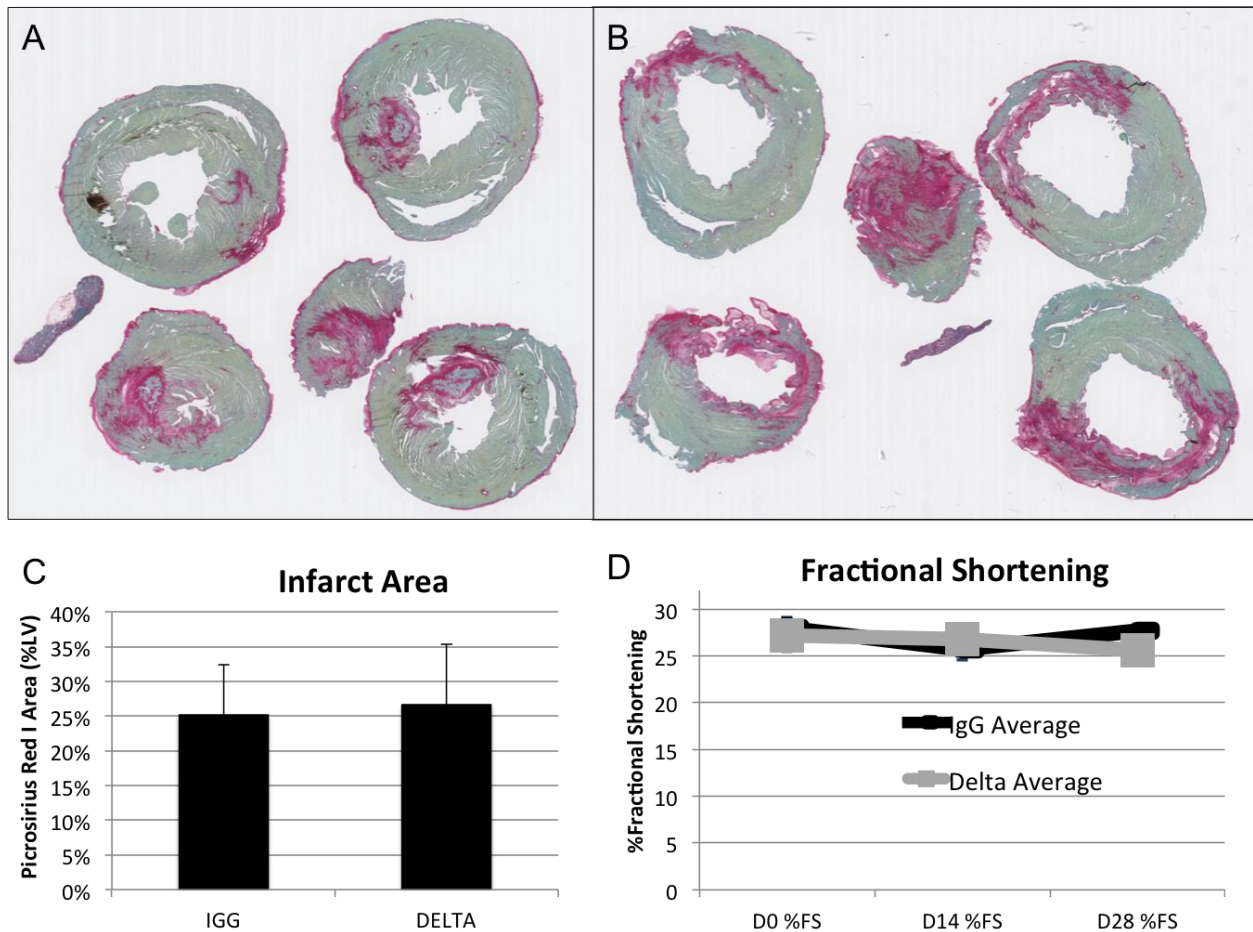
Figure 5.12. No significant differences were observed in average heart function or fibrosis between groups. Variability in infarct size was observed across both implantation groups. (A) In some hearts infarcts were small and the corresponding graft area was larger than average. Picrosirius red (red) labels infarct area and fast green counterstain (green) identifies healthy myocardium. In this heart, graft regions can be identified as light green pockets of healthy, compact tissue within the scar region. (B) In other hearts, infarcts were large and in many of these hearts (as shown in this example) did not have detectable graft regions in the tissue sections analyzed. (C) Infarct area analysis shows no significant differences in scar size by histology (measuring picrosirius red infarct area, normalized to left ventricular area) at 4 weeks. (D) Heart function was evaluated by echocardiography at baseline after injury, and at 2 and 4 weeks post-implantation. Data is presented as the group average fractional shortening for IgG (black) and Delta-1 (gray).

Safety and Feasibility Demonstrated in Both Experimental Groups

Although there were no adverse effects noted in early pilot studies, it was important to carefully assess the safety and feasibility of implanting the EDC:NHS collagen-based gel (with IgG and Delta-1 ligands) into the infarcted rat myocardium for a 1-month endpoint. These studies have never been performed prior to the experiments described in this chapter and differ from our standard implantation protocols by including the injectable collagen-based Notch material. There were no serious adverse effects noted after implantation of the cells and gel into the infarcted heart. We also closely monitored animal weight gain after surgery, and there were no significant differences in animal weight at any timepoint throughout the experiment (Figure 5.13A). At baseline, bodyweight was 298 ± 5 grams and 288 ± 5 grams for IgG and Delta-1 groups, respectively (p=0.22), which declined in the four days following surgery to 283 ± 4 and 269 ± 5 grams for IgG and Delta-1, respectively (p=0.07). This drop in weight following surgery is expected and is within our acceptable range of post-operative weight loss. By two weeks animals had recovered to their pre-surgical weight of 308 ± 5 and 302 ± 5 grams (IgG and Delta-1, respectively, p=0.46). While there were no differences in absolute body weight, there was a significant difference in the percent body weight gain during the cell and gel treatment protocol, with Delta-1 rats gaining $25.4 \pm 1.5\%$ of their pre-surgical weight compared to $19.1 \pm 1.8\%$ in the IgG rats (p=0.02, Figure 5.13B). There was no difference in lung weight or lung to body weight ratio (Figures 5.13C, D) between groups.
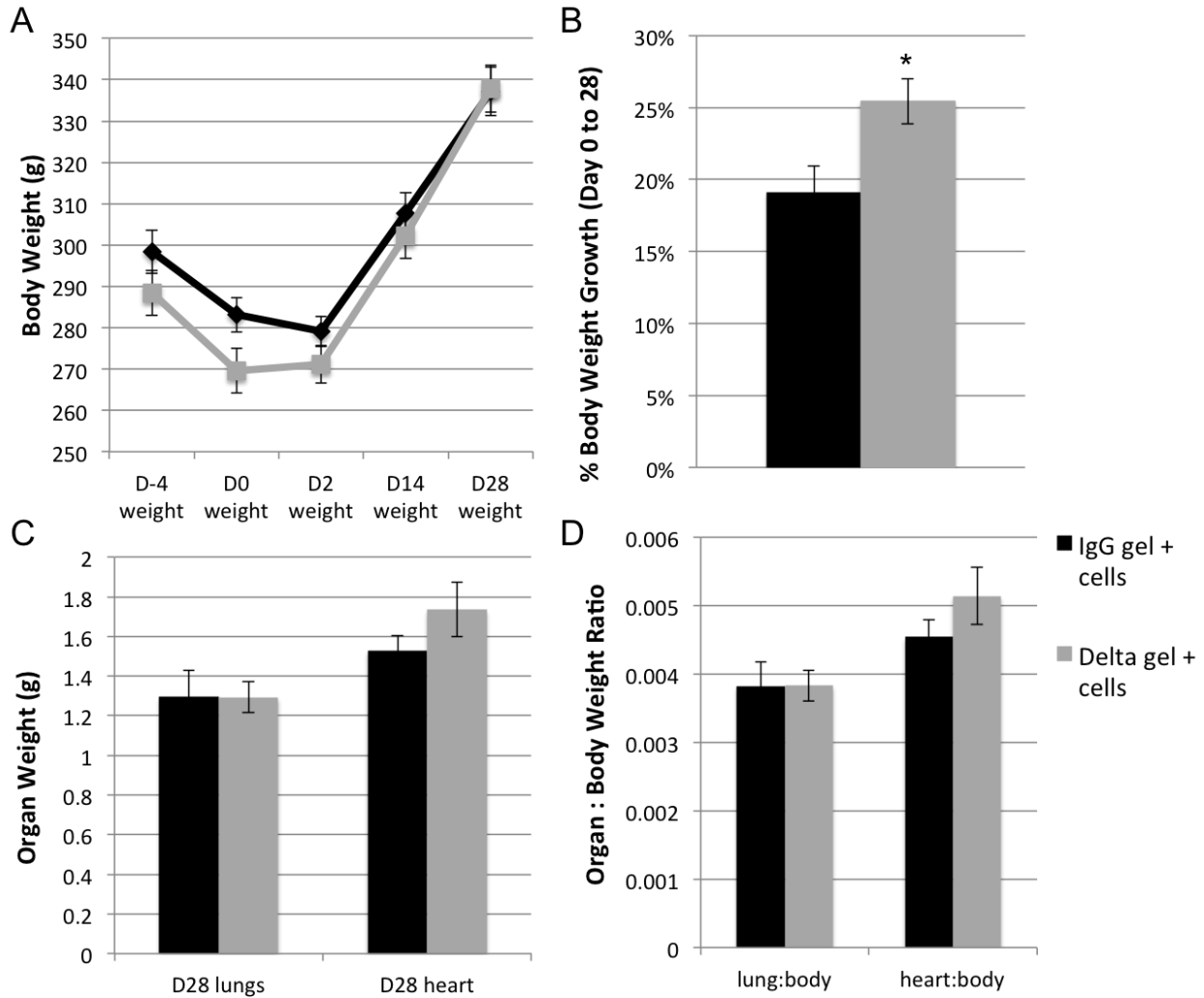
Figure 5.13. No significant differences in animal weight between groups during the experiment. (A) Body weight measured in grams at D-4 (I/R injury), D0 (implantation), D2, D14, and D28 (final endpoint). The observed drop in weight after surgery is within our acceptable range of post-operative weight loss. (B) Percent body weight gain, measured as the change between D0 and D28 weight. (C) Lung and heart weights at D0 and D28. (D) Ratios of lung to body weight and heart to body weight at 4 weeks show an increased trend for weight and heart to body weight ratio in the Delta-1 rats compared to the IgG control groups.

5.4.3 Redesigned Pilot Studies to Improve Effect of Delta-1 on hESC-cardiomyocyte Graft Size

In vitro analysis indicates effect of pro-survival cocktail on Notch signaling

As described above, we did observe a significant increase in hESC-cardiomyocyte proliferation after implantation of cells within the Delta-1 group compared to IgG control. However, based on our *in vitro* data this was a more modest increase than expected. Surprisingly, we did not see any subsequent increase in graft size, which is what would be expected from an observed increase in proliferation. This caused us to rethink our animal model and redesign our experimental protocols. One key difference between the *in vitro* tissue engineering experiments and the animal studies described above is the inclusion of pro-survival cocktail [124]. It has recently been suggested that one of the pro-survival cocktail components, cyclosporine A, inhibits Notch signaling [179], and we were concerned that this may have impacted our animal study results. Thus, we designed an *in vitro* experiment to test the effect of pro-survival cocktail on Notch signaling within our modified collagen gels.

Engineered tissues were formed using U2OS CSL luc/ren Notch reporter cells and either Delta-1 or IgG gels as described previously, and were treated with the standard pro-survival cocktail protocol as outlined in the methods section. Pro-survival cocktail treatment significantly reduced the Notch signaling response in the Delta-1 gels compared to standard media treatment, resulting in an 11.8 ± 0.14-fold increase in Notch with media treatment compared to only a 6.13 ± 0.52-fold increase after pro-survival cocktail treatment (p=5.6E-05, Figure 5.14). There was no observed increase in Notch signaling in the IgG gels, and as such there was no detectable impact on Notch signaling in the IgG control gels (1.0 ± 0.05 vs 0.05 ± 0.03-fold increase in luciferase

expression after standard media culture and pro-survival cocktail treatment, respectively (p=0.37). These differences were consistent for Delta-1 gels formed with the standard ligand concentration as well as a lower-concentration gel, where fold luciferase expression decreased from 13.9 ± 0.69 to 8.12 ± 0.21 after pro-survival cocktail treatment (p=0.0002).
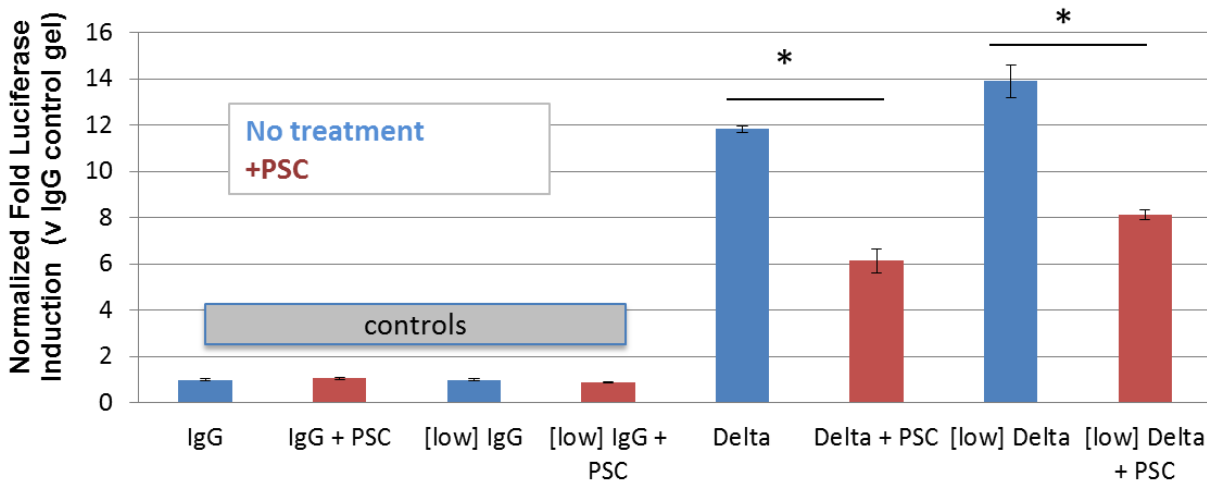
Figure 5.14. Pro-survival cocktail inhibits Notch signaling by luciferase analysis *in vitro*. Engineered tissues were formed using the U2OS CSL luc/ren Notch reporter cell line and modified collagen gels with either Delta-1 or IgG control (using a standard ligand concentration, or a low dose of ligand). Tissues were treated with pro-survival cocktail (PSC, red bars) or standard media (no treatment, blue bars). Control gels (IgG) are labeled by the gray horizontal bar. * indicates $p<0.05$.

Pilot studies designed to further test differences between in vitro and in vivo protocols

After finding that pro-survival cocktail was likely having a negative effect on our designed Notch signaling platform for *in vivo* therapeutic applications, we set out to perform a series of *in vivo* pilot studies to further test the differences between our *in vitro* tissue engineering protocols and our established implantation protocols. These pilot studies are outlined in Table 5.2. All pilot studies were performed without the use of pro-survival cocktail, and all tissues were harvested at

either 7 or 14 days (as listed below) instead of the 4 week endpoint used previously. The first pilot study – "Alu Graft Detection" was designed to use qPCR-based detection of human Alu sequences to quantify graft size, and implanted $10x10^6$ hESC-cardiomyocytes directly after thaw into I/R-injured myocardium (this is similar to our previously-described protocols). The remaining 3 pilot studies implanted hESC-cardiomyocytes that had been previously cryopreserved but were thawed and allowed to recover prior to implantation (referred to as "fresh cells"). For these studies, a second Delta-1 group was added to test a lower dose of Delta-1 ligand in the modified collagen gel.

Pilot Name	Injury Model	Endpoint	Groups	# Cells	PSC?
#1 – Alu Graft Detection	I/R	2 weeks	IgG, Delta	10M (frozen)	No
#2 – Fresh cells in I/R	I/R	2 weeks	IgG, [low] Delta, Delta	5M (fresh)	No
#3 – Uninjured Model	Uninjured	2 weeks	IgG, [low] Delta, Delta	3M (fresh)	No
#4 – 1 week uninjured	Uninjured	1 week	IgG, [low] Delta, Delta	5M (fresh)	No

Table 5.2. Pilot studies for *in vivo* cell and gel implantation experiments.

Human Alu sequence-based graft detection after implantation into I/R-injured hearts (Pilot 1)

Given the increase in cardiomyocyte proliferation but the lack of a detectable increase in graft size in Chapter 5.4.2, we hypothesized that we needed a more sensitive graft detection method.

While histological tissue sectioning and immunohistochemical staining is often used to quantify graft size, this approach is limited in that only five cross-sectional profiles of the tissue are analyzed, after slicing the heart in 2 mm thick sections. Thus, while the analyzed cross-sections are assumed to be representative of the remaining tissue, it is possible that graft area is excluded from these measurements depending on graft localization between the 2 mm cross sections of tissues. Another method of graft detection that has been previously described in the mouse heart is to use qPCR to detect human-specific Alu sequences from the implanted human cardiomyocytes [146]. This method of graft detection offers a sensitive assay to detect the total amount of human DNA present in the rodent heart, regardless of graft localization. Using this along with a standard curve, it is possible to extrapolate the number of human cells present in the rodent tissue.

For these studies, 10×10^6 hESC-cardiomyocytes were suspended in the Notch gel (or IgG control) and implanted directly after thaw into I/R-injured myocardium, without any pro-survival cocktail. The implanted cardiomyocytes were >90% cTnT$^+$, as indicated by flow cytometry, and implanted Notch Delta-1 gels produced a 5.0 ± 0.26-fold increase in luciferase expression compared to IgG control gels (p=7.6E-07, Figure 5.15).
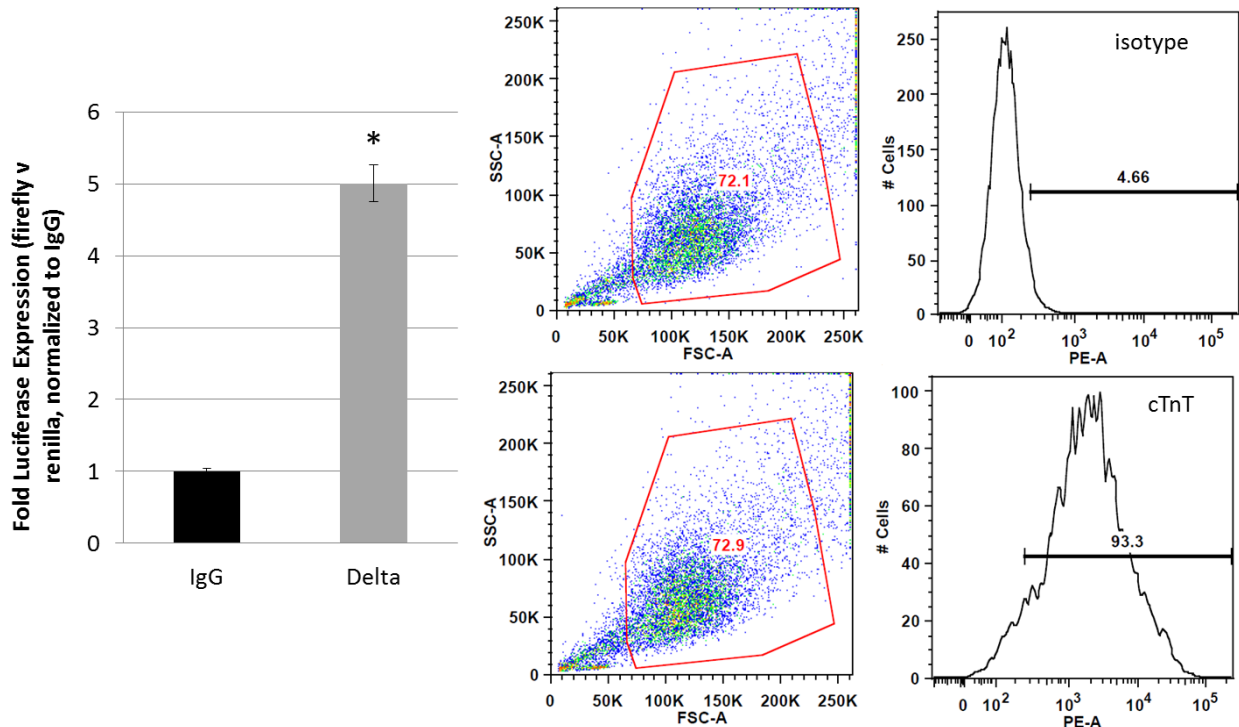
Figure 5.15. Input gel and cell characterization for Alu sequence detection pilot study. Implanted gels bound with Delta-1 produced a Notch-mediated increase in luciferase expression (left). Data is shown as fold increase of firefly vs renilla luciferase, and normalized to IgG controls. Implanted hESC-cardiomyocytes were greater than 90% cTnT+ by flow cytometry. The cell population Forward Scatter (FSC) and Side Scatter (SSC) plots are shown on the left. Cardiac troponin T (cTnT) is detected by PE, where data is shown at right as a histogram of PE expression. The isotype control (top panel) is used as a negative gating control to show 93.3% of single cell events express cTnT.

Two weeks after implantation, hearts were harvested and qPCR analysis was performed as described in the methods section of this chapter. Known numbers of hESC-cardiomyocytes were used to make a standard curve, ranging from 0 to 10,000 pg (in 100 ng DNA). The known amount of human Alu is plotted against the raw Cq value and fitted to the following curve: $y = 8E+07e^{-0.693}$, R=0.99971 (Figure 5.16). The mean Cq values for each cell standard and each heart are plotted, where a high Cq value equates to a lower measured amount of human DNA. Considering the raw Cq values, the blank samples have Cq values of around 31; this is true for

the blank cell standard as well as sham-operated control hearts, which received no human cells (average Cq value for these blank and sham samples was 31.8 ± 0.1). The remaining hearts implanted with human cells in the Notch gel have Cq values that fall along the standard cell control curve (Figure 5.16).
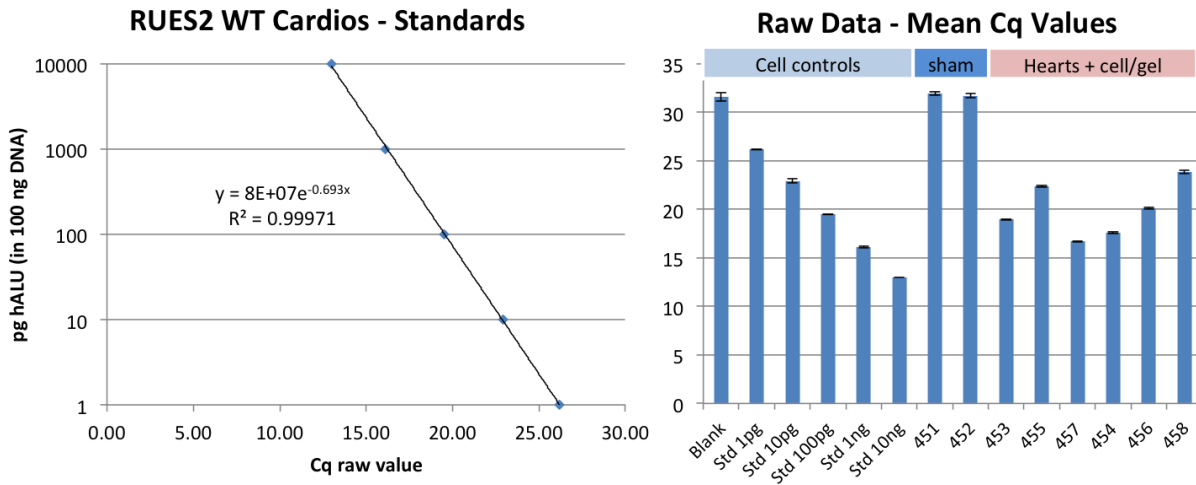
Figure 5.16. Cell standard curve of known DNA amounts was used to identify the total human DNA amount present in rat hearts. Picograms of human ALU transcripts present in 100 ng of DNA are plotted against raw Cq values for curve fitting (left). Raw Cq values correspond to the amount of human DNA present in the samples (right). The first 6 bars represent the standard curve plotted in the left chart, and the remaining data are raw Cq values for each heart. Sham-operated controls (identification numbers 451 and 452) did not receive any human cell injection, and their Cq values similar to those found in the blank control.

The mean Cq values were then extrapolated using the standard cell curve to determine the total amount of human DNA present in each heart. These values are plotted in Figure 5.17, first showing the amount in each heart and then as a group average for all IgG and Delta-1 hearts, respectively. Similar to what we observed in the experiments described above in Chapter 5.4.2, there was no difference in graft size between IgG and Delta-1 groups. Average calculated DNA

amounted to 11.6E+05 ± 8.5E+05 pg and 6.2E+05 ± 4.6E+05 pg in the IgG and Delta-1 groups, respectively. Similar to our previous results there was variability in engraftment for both groups, with detected DNA varying between roughly 100 pg to over 2 mg for each group. This variability can be observed in Figure 5.17A. Based on the findings of this pilot study, we decided additional changes were needed to further optimize our implantation protocol, as well as our graft detection protocol. Given the variability and loss of structural information in the Alu detection endpoint, we decided to use histological analysis of BrdU incorporation as the primary endpoint in the remaining pilot studies.
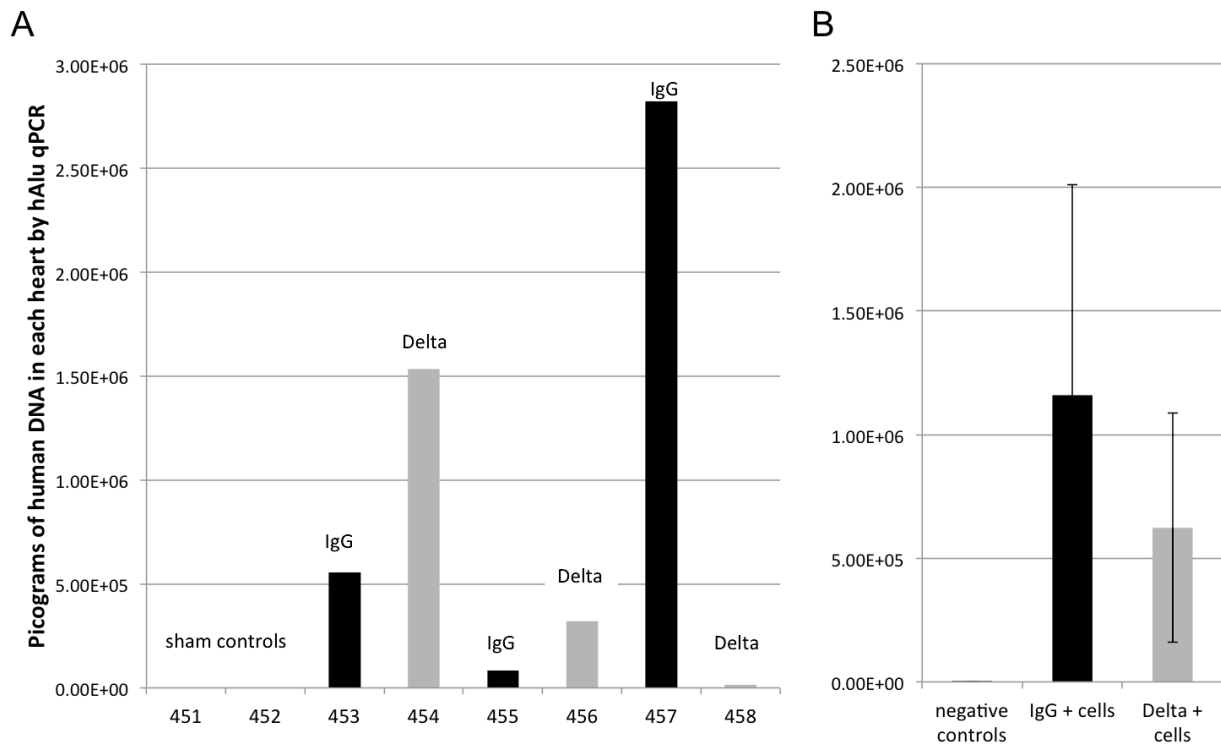
Figure 5.17. Human DNA detected in rat hearts 2 weeks after engraftment. Total detected picograms of human DNA by hALU qPCR is shown for each heart (left), and group averages are shown (right) with no significant differences in graft size between groups.

Pilot studies using histology as the primary endpoint

Based on the findings of initial pilot study described above, we decided that additional changes were still needed to optimize our implantation protocol. We also found that while the Alu detection assay was sensitive, losing structural graft information made this analysis less informative because there was no context about scar area or graft localization within the scar or healthy myocardium. Thus, the remaining three pilot studies were designed to use histology as the primary endpoint, particularly BrdU incorporation and βMHC^+ graft area. The details of these pilot studies were outlined in Table 5.2, but the primary variables tested included cell implant number, Delta-1 ligand dose, injury model, and endpoint. All three studies used fresh hESC-cardiomyocytes (as opposed to directly thawed after cryopreservation), and all three studies were performed without the use of pro-survival cocktail.

The second pilot study tested implanting cells and the modified gel into I/R-injured hearts, whereas the third and fourth pilot studies used uninjured hearts for implantation. Picrosirius red with fast green counterstain was used to identify regions of fibrosis in the hearts after sacrifice (Figure 5.18). The left panel in Figure 5.18 shows higher levels of fibrosis as expected with the injury, with scar covering an average of 27.4%, 15.5%, and 21.0% of the left ventricular area in the IgG, low Delta-1, and high Delta-1 groups respectively (n=2 per group, no statistics performed, Figure 5.20A). Although there was no ischemia/reperfusion injury induced in Pilot #3 or #4, isolated regions of fibrotic tissues can be identified in these tissues. In Pilot #3, in which tissues were harvested 2 weeks after implantation, fibrotic area was 10.3%, 7.5%, and 9.3% of the left ventricle in IgG, low Delta-1, and high Delta-1 groups respectively (n=2 per group, no statistics performed). In Pilot #4 with a 1 week endpoint, fibrotic area was measured at

9.6%, 11.3%, and 13.6% of the left ventricle in IgG, low Delta-1, and high Delta-1 groups respectively (n=2 per group, no statistics performed). This data is summarized in Figure 5.20A. The fibrosis identified in the uninjured hearts is likely due to a combination of an injury response due to the needle-based implantation and thoracotomy, as well as an inflammatory response to the implanted materials.
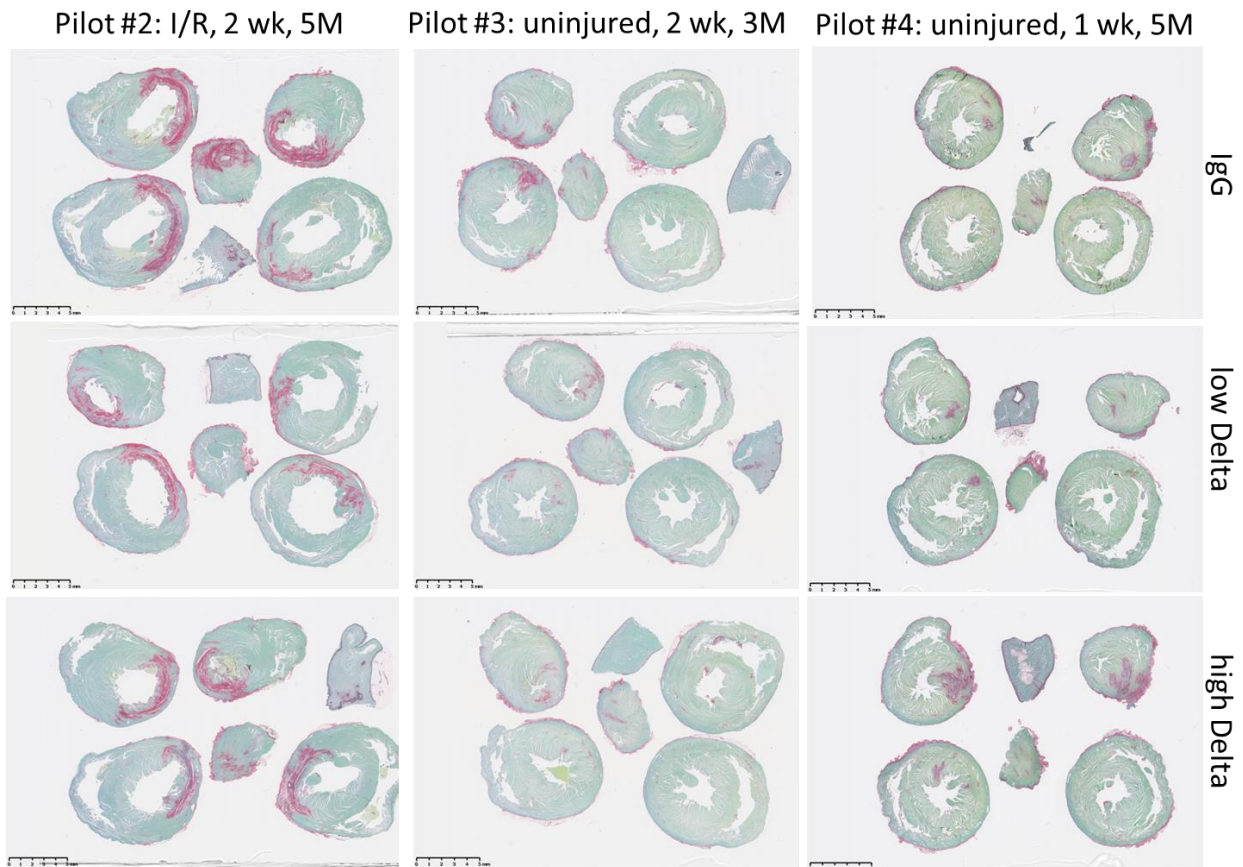
Figure 5.18. Fibrosis is identified in the myocardium by picrosirius red for histology-based pilot studies. Collagen is stained with picrosirius red (red) and healthy myocardium is counterstained with fast green (green). From left to right, columns are separated by pilot study #2, #3, and #4. From top to bottom, rows indicate cells were implanted in the IgG control gel, a low-dose Delta-1 gel, or the standard dose Delta-1 gel. (Left) Pilot study #2 implanted $5x10^6$ hESC-cardiomyocytes 4 days after an ischemia/reperfusion injury, and tissues were harvested 2 weeks following implantation. (Middle) Pilot study #3 implanted $3x10^6$ hESC-cardiomyocytes in uninjured hearts, and tissues were harvested 2 weeks later. (Right) Pilot study #4 implanted $5x10^6$ hESC-cardiomyocytes in uninjured hearts, with tissues harvested at 1 week post-implantation. Scale bars = 5mm.

Human cardiomyocyte grafts are identified in all hearts regardless of pilot study

Human myocardial grafts were identified by histological staining for beta myosin heavy chain following terminal endpoints of either 1 or 2 weeks (Figure 5.19). As expected, cardiomyocyte grafts were found in all samples, regardless of which pilot study or treatment group was used. Considering the sum total graft area, the largest grafts were found in Pilot study #2, where 5×10^6 hESC-cardiomyocytes were transplanted into I/R-injured hearts (Figure 5.20B). This protocol is most similar to our standard implantation protocols, with the following differences: half the number of implanted cells, fresh instead of frozen cells, and a 2-week endpoint. In Pilot #2, there was a trend of larger grafts in the Delta-1 group (Figure 5.20B). The average total graft area across all tissue sections analyzed was 0.66 mm^2, 0.24 mm^2, and 0.96 mm^2 for the IgG, low Delta-1, and Delta-1 groups respectively (n=2 per group, no statistics performed). This trend was also replicated in pilot #4 (the only difference in implantation was I/R vs uninjured myocardium), with average graft areas of 0.41 mm^2, 0.25 mm^2, and 0.69 mm^2 in the IgG, low Delta-1, and Delta-1 groups respectively (no statistics performed). Interestingly, this trend was not observed in pilot #3 with fewer cells implanted into uninjured heart for a 1-week endpoint (graft area was 0.31 mm^2, 0.12 mm^2, and 0.18 mm^2 for IgG, low Delta-1, and Delta-1 groups). These trends in graft size were maintained when graft area was normalized to left ventricular area (Figure 5.20C). Pilot study #2 resulted in grafts that covered 0.44%, 0.15%, and 0.72% of the left ventricular area after implanting 5×10^6 cardiomyocytes in IgG, low Delta-1, or Delta-1 gels, respectively. Pilot study #3 resulted in the smallest graft areas of 0.19%, 0.07%, and 0.21% of the left ventricle after implanting 3×10^6 cardiomyocytes into uninjured hearts for 1 week. Pilot study #4 followed the trend of the second pilot study, with graft area covering 0.50%, 0.34%, and 0.59% of the left ventricle. Graft size was also normalized to fibrotic area (Figure 5.20D),

135

however this normalization is most relevant for the second pilot study where cells and gel was implanted into I/R-injured myocardium (grafts covered 1.80%, 0.78%, and 3.35% of the scar area in IgG, low Delta-1, and Delta-1 groups, respectively). Interestingly, regardless of pilot study the smallest grafts were generally observed in the samples with a low concentration of Delta-1.
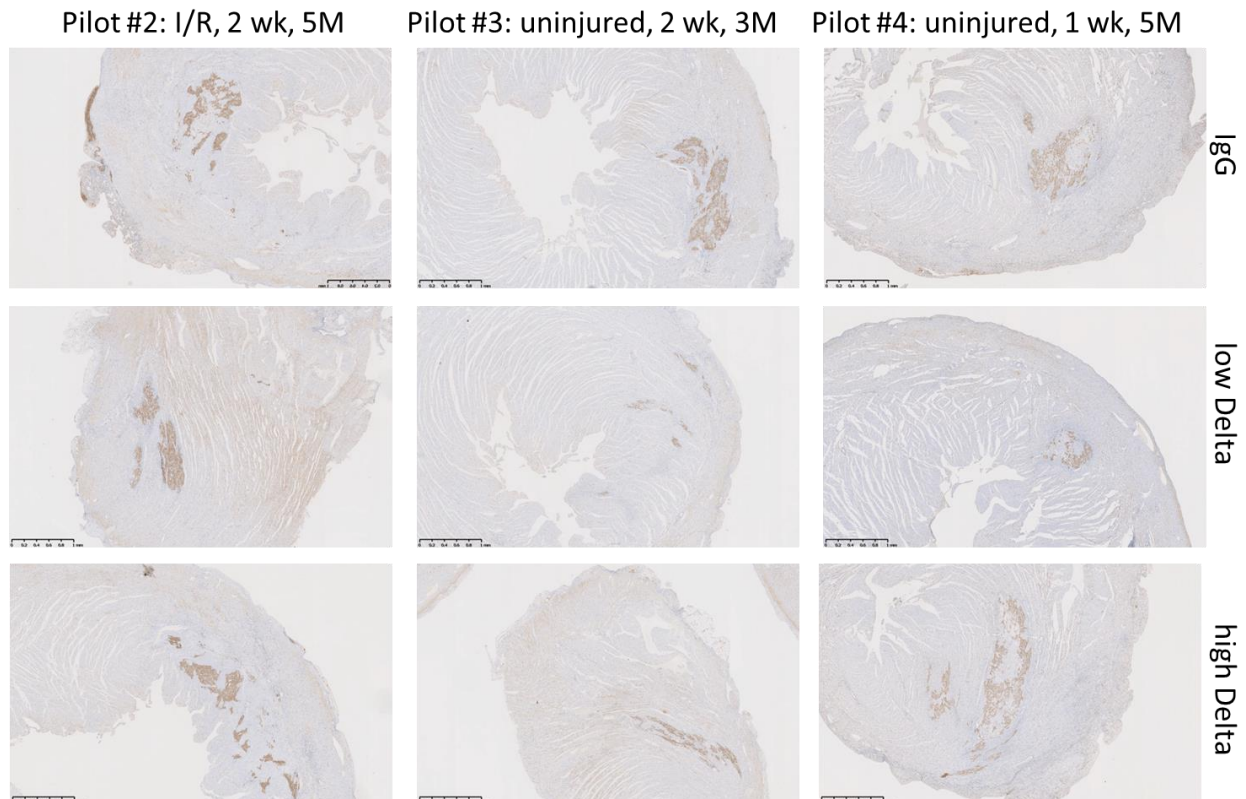
Figure 5.19. Human cardiomyocyte grafts were identified in all hearts regardless of implantation group or model. Transplanted human cardiomyocytes are identified with βMHC and visualized with DAB (brown) with a hematoxylin counterstain to quantify graft area. From left to right, columns include pilot studies #2, #4, and #4. From top to bottom, rows define gel implantation group of either IgG control gel, a low-dose Delta-1 gel, or the standard dose Delta-1 gel. (Left) In pilot study #2, $5x10^6$ hESC-cardiomyocytes were implanted in modified gel 4 days after an ischemia/reperfusion injury with tissue harvest 2 weeks later. (Middle) Pilot study #3 implanted $3x10^6$ hESC-cardiomyocytes into uninjured myocardium with tissue harvest 2 weeks following implantation. (Right) Pilot study #4 transplanted $5x10^6$ hESC-cardiomyocytes again into uninjured hearts but with tissue harvest after 1 week. Scale bars = 1mm.
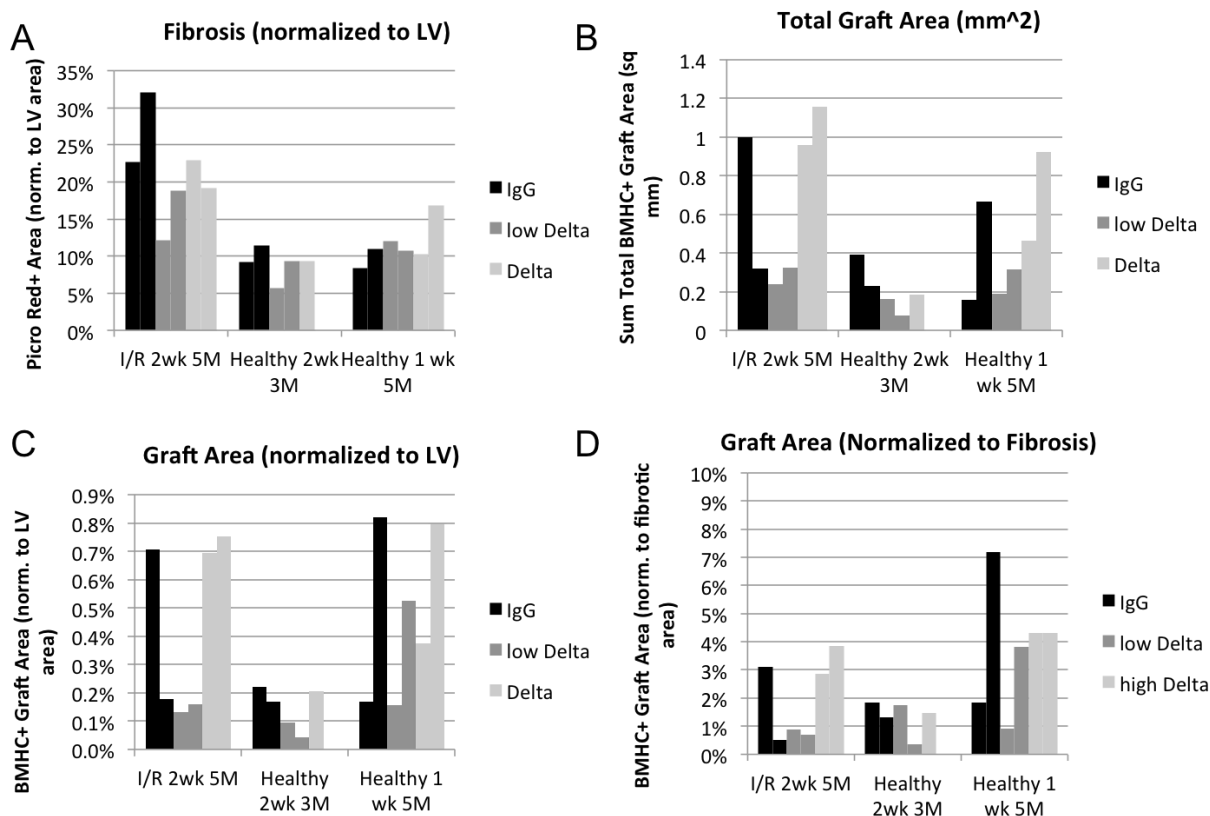
Figure 5.20. Fibrosis and graft size across all groups in the pilot studies. (A) Fibrosis was quantified by analyzing picrosirius red area and then normalizing to left ventricular area. (B) Sum total of βMHC$^+$ graft area across all analyzed tissue sections. (C) βMHC$^+$ graft area is normalized to left ventricle area. (D) Graft area is normalized to fibrotic tissue area.

HESC-cardiomyocyte proliferation in pilot studies

Human cardiomyocyte proliferation was analyzed by counting double-positive BrdU and βMHC$^+$ cells identified in the myocardium. Quantification of graft proliferation is summarized in Figure 5.21. There was an increase in cardiomyocyte proliferation when cells were implanted in Delta-1 gels compared to IgG controls, which was identified in both uninjured and I/R-injured hearts at the 2 week endpoint. In pilot study #2, hESC-cardiomyocyte proliferation was 9.5 ± 2.2% for IgG, 9.3 ± 2.5% for low Delta-1, and 15.7 ± 1.7% for Delta-1 group, resulting in a 6.2%

increase in proliferation between IgG control and Delta-1. A similar increase was observed in pilot #3, where hESC-cardiomyocyte proliferation was increased by 6.0% between the IgG control and Delta-1 groups. However there was a lower level of proliferation observed in the IgG group, which we suspect was due to an overall lower baseline level of proliferation in the uninjured heart tissue compared to after an ischemic injury. Proliferation in this study was 4.1 ± 0.5% for IgG, 8.0 ± 0.1% for low Delta-1, and 10.1 ± 2.2% for Delta-1.
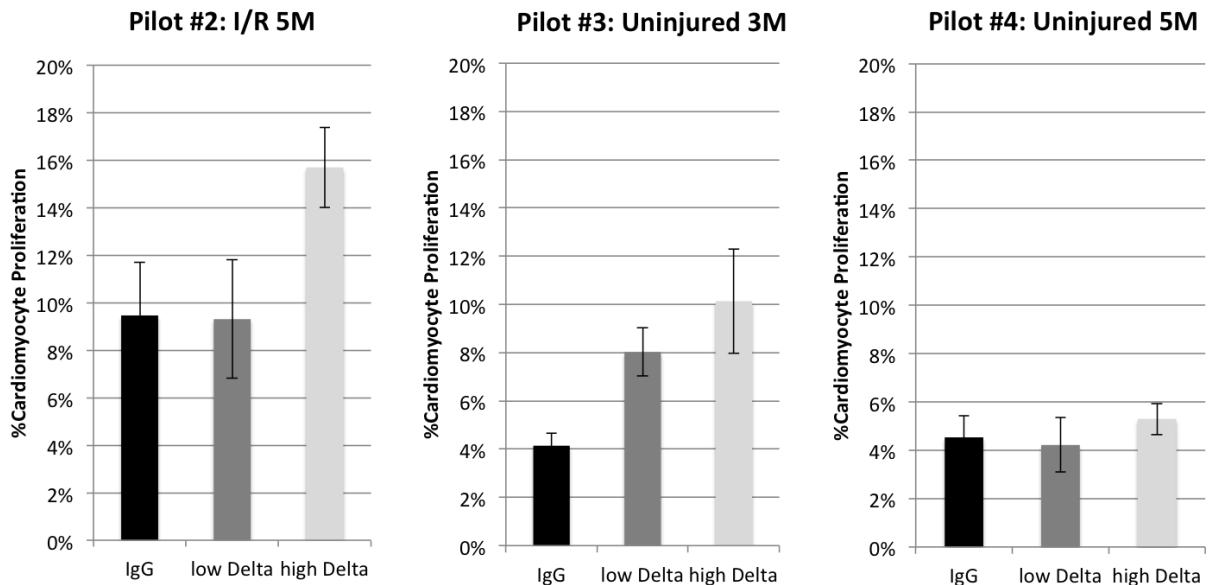
Figure 5.21. HESC-cardiomyocyte proliferation is analyzed in the myocardium after implantation. Proliferating human cardiomyocytes are assessed by quantifying double positive BrdU and βMHC^+ cells in the myocardium. IgG = black bars, low concentration Delta-1 = dark gray bar, Delta-1 = gray bar. Each bar corresponds to the average proliferation rate across 8-15 confocal images of the n=2 animals in each group (n=2 animals per group for every pilot study with the exception of Pilot #3, where n=1 for the Delta-1 group).

5.4.4 Optimized Protocol Designed after Successful Results in Pilot Study #2

Considering all of the pilot study results collectively, the second pilot study produced the most promising results in terms of graft size and cardiomyocyte proliferation. In this section, we

summarize the major findings from this particular pilot study. Only data from the IgG control group and the standard Delta-1 ligand dose group are presented in this section (see Chapter 5.4.3 for results from the low Delta-1 concentration group). The pilot study protocol in this section guided the major findings of Chapter 5, where the data is described in Chapter 5.4.5. In this second pilot study, five million hESC-cardiomyocytes were transplanted four days after I/R injury in either IgG or Delta-1 modified gel, and tissues were harvested after 2 weeks. This protocol is the most similar to what was described in Chapter 5.4.2, which was adapted from our standard cell implantation protocols. The major differences between the studies in Chapter 5.4.2 and pilot study #2 are:

1) Cardiomyocytes were not implanted directly after thawing following cryopreservation, but rather thawed 2-3 days prior to implantation to allow time for recovery.

2) 5 million cells were transplanted instead of the standard 10 million cell protocol.

3) No pro-survival cocktail was used.

Graft area is increased with Delta-1 gel implantation in pilot study #2

Scar area was identified by picrosirius red staining with a fast green to counterstain to label healthy myocardium, and area was quantified using Image J. In the IgG control group, fibrosis covered an average of 27.4% of the left ventricle compared to only 21.0% of the left ventricle in the Delta-1 group (Figure 5.22). Graft size was higher in the Delta-1 group compared to IgG controls, which was analyzed by quantifying βMHC^+ area. The sum total graft area averaged between the hearts was 0.66 mm^2 and 0.96 mm^2 for the IgG and Delta-1 groups, respectively. When normalized to left ventricular area, grafts covered 0.44% and 0.72% of the left ventricular area in the IgG and Delta-1 groups, respectively. A similar increase in graft size can be observed

by normalizing graft area to scar area, where βMHC^+ grafts covered 3.35% of the infarct area in the Delta-1 group compared to only 1.80% in the IgG control group.
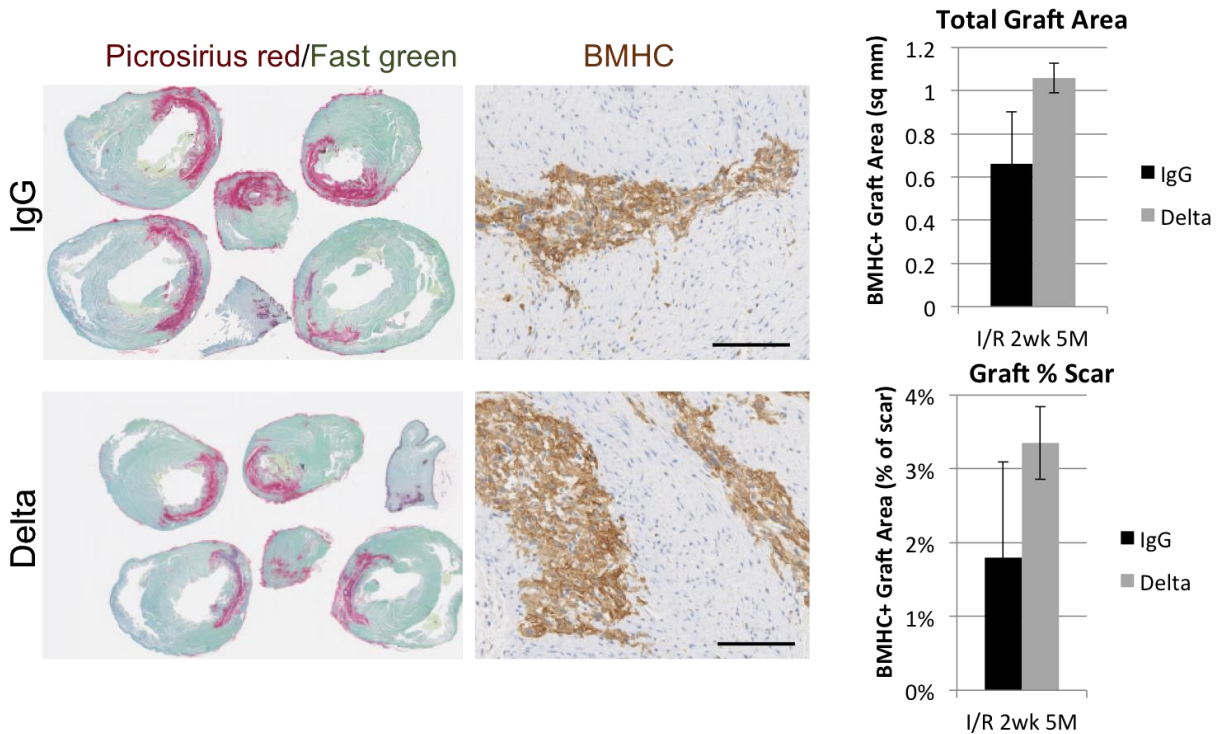
Figure 5.22. Graft area is increased with Delta-1 in the second pilot study. Five million hESC-cardiomyocytes were transplanted four days after I/R injury in either IgG or Delta-1 modified gel, and tissues were harvested after 2 weeks. Scar area is assessed by picrosirius red staining (collagen = red) and fast green to counterstain healthy myocardium (green). Human cardiomyocyte grafts are identified by staining for beta myosin heavy chain (βMHC) and are quantified in Image J. Graft area is expressed as total graft area (square mm) or normalized to fibrotic area. Scale bar = 100 μm.

Trend for decreased inflammation in Delta-1 group

To assess the level of inflammatory response to the implanted cells and gel, monocytes and macrophages were identified by histological staining for CD68 (Figure 5.23). We had previously assessed the level of $CD68^+$ inflammation after transplanting the Notch-gel only (no cells – see Figure 5.9), and preliminary results suggested that inflammation was reduced in the Notch groups. The amount of monocyte and macrophage infiltration in the hearts after implantation was

normalized to picrosirius red area for given regions of interest (inset, Figure 5.23). Similar to previous preliminary results, we observed a decrease in inflammatory cells in the Delta-1 group compared to IgG controls, with CD68$^+$ area amounting to 0.24 ± 0.1% area coverage in Delta-1 (normalized to fibrotic area) compared to 1.02 ± 0.4% in IgG control hearts (Figure 5.23). Data is averaged across all samples within the implant group and includes the apex and apex+1 section (the first apical section and the next histological sectioning plane 2 mm away).
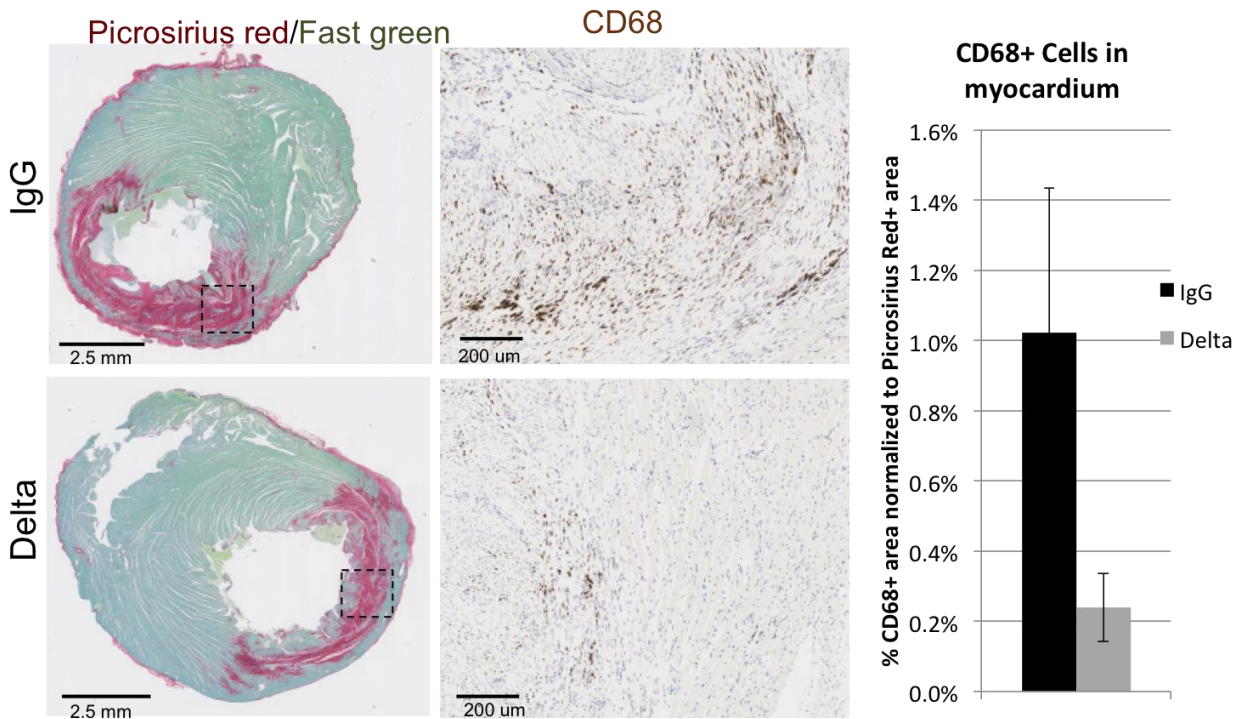
Figure 5.23. Inflammatory response was assessed by CD68 staining. Fibrosis is identified by picrosirius red/fast green staining and serial sections are stained with CD68 (visualized with DAB, brown) to label infiltrating monocytes and macrophages. Inset outlined on picrosirius red/fast green images is shown at a higher magnification in the CD68 panel. CD68$^+$ cell area is normalized to fibrosis and quantified at right. Scale bar = 2.5 mm in left column. Scale bar = 200 µm in middle column.

Increased proliferation in Delta-1 group in pilot study #2

In addition to total graft size, proliferation of hESC-cardiomyocytes after transplantation was the other primary endpoint for the pilot studies. To assess proliferation, animals were given 4 intraperitoneal injections of BrdU (at Day 1, 4, 7, and 14 following implantation), and histology was performed to identify BrdU$^+$/βMHC$^+$ cells in the heart tissue. By quantifying the amount of double-labeled cells in confocal images, we found hESC-cardiomyocyte proliferation was increased by 6.2% when cells were implanted with the Delta-1 gel compared to IgG controls. The total amount of hESC-cardiomyocyte proliferation was 9.5 ± 2.2% for hESC-cardiomyocytes in the IgG control group compared to 15.7 ± 1.7% in the Delta-1 group (Figure 5.24). There were numerous non-myocytes (βMHC$^-$, presumably fibroblasts) that expressed BrdU localized to the infarct region, which were not included in this analysis. This data is shown in Figure 5.24, alongside the data from pilot study #4 for comparison. It is interesting to note that the lowest observed proliferation rate is in uninjured myocardium in the IgG group, and that Delta-1 raises the proliferation rate by 2-fold (pilot study #4). The proliferation rates between this Delta-1 group and the IgG control group in the I/R-injured myocardium are comparable. It has been previously reported that Notch signaling is upregulated after injury [71-74] , which may explain the shift in baseline proliferation in the IgG control group after injury.
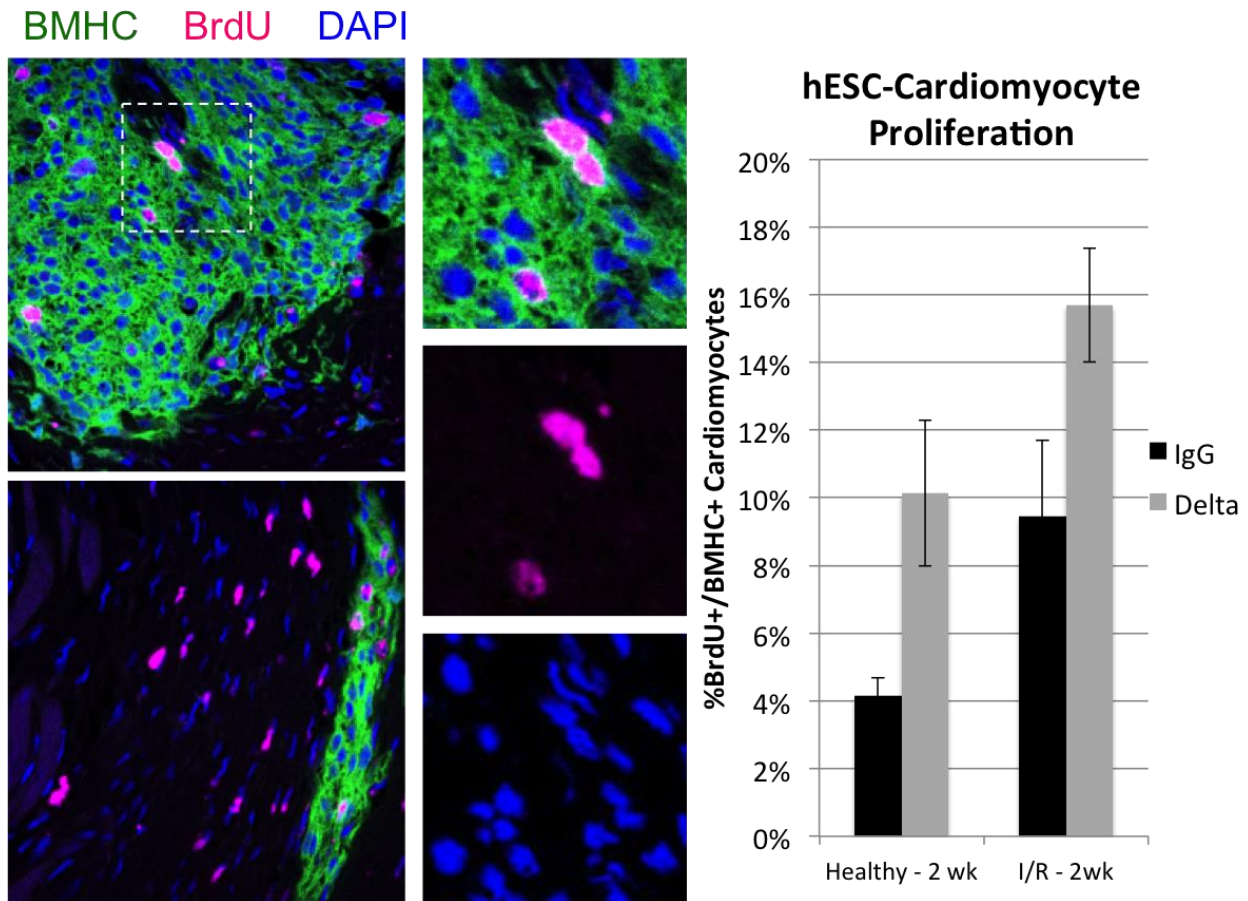
Figure 5.24. Proliferation of transplanted hESC-cardiomyocytes is identified by histology. Tissue sections are stained with antibodies to detect beta myosin heavy chain (βMHC, green), BrdU (pink), and nuclear counterstain of DAPI (blue). Outlined region in upper left panel is enlarged at right. Proliferation rates are quantified and shown, plotted along with the proliferation data from pilot study #4 in uninjured myocardium for reference.

5.4.5 Optimized protocol increases graft size and hESC-cardiomyocyte proliferation

Based on the results described in Chapter 5.4.4, the implantation protocol was redesigned to follow the optimizations used in pilot study #2. Animal numbers were increased to n=8 per group to allow for histology-based detection of differences in graft size (see "Animal Sample Size Justification", Methods Chapter 5.3) and the endpoint was lengthened to 4 weeks instead of 2 weeks. 5×10^6 hESC-cardiomyocytes were suspended in either IgG control or Delta-1 modified collagen gel, and were implanted into the infarct region of the myocardium four days after

ischemia/reperfusion injury. Pro-survival cocktail was not included in this study. The full experimental timeline is outlined in Figure 5.4.

Increased human myocardial graft size after 4 weeks

Picrosirius red staining with a fast green counterstain was used to label collagenous scar tissue and healthy myocardium, respectively (Figure 5.25A, D). Human myocardial graft size was identified by histological staining for beta myosin heavy chain (βMHC) for IgG groups (Figure 5.25B, C) and for Delta-1 (Figure 5.25E, F).
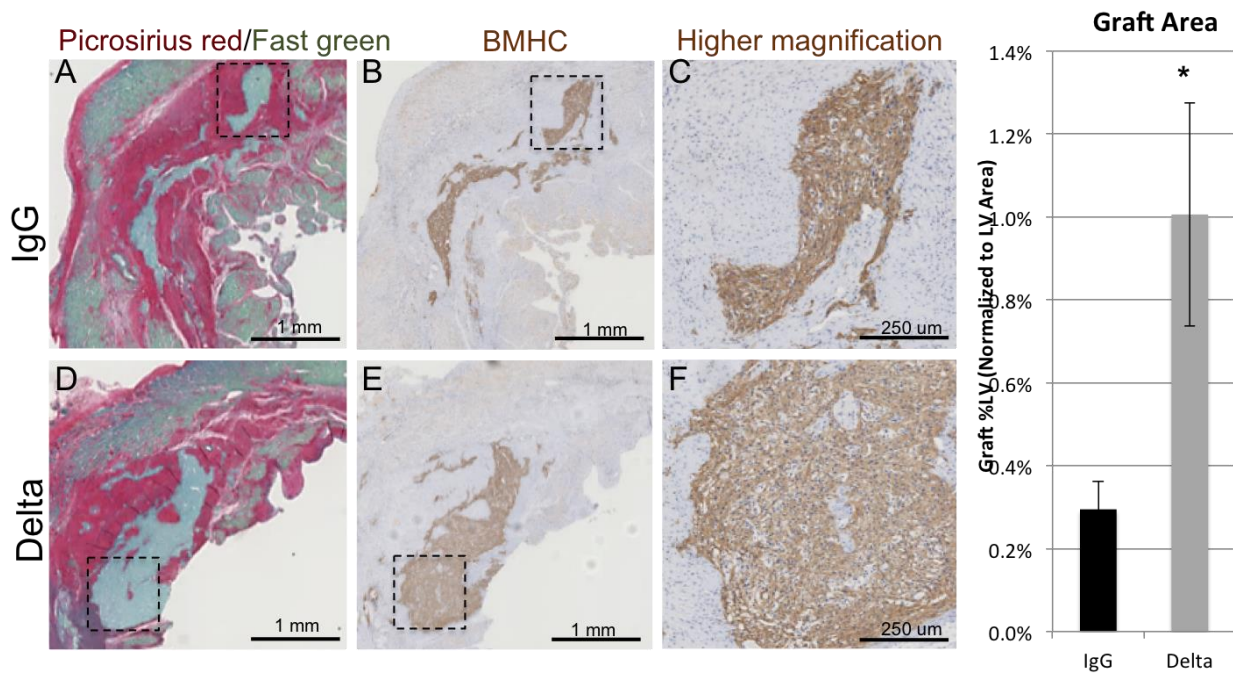
Figure 5.25. Graft area is significantly increased after implantation with Delta-1-gel. Four days after I/R injury, five million hESC-cardiomyocytes were transplanted in either IgG or Delta-1 modified gel, and tissues were harvested after 4 weeks. (A, D) Collagenous scar area is identified by picrosirius red staining (red) with a fast green counterstain to label healthy myocardium (green). Outline identifies region of interest. Scale bar = 1 mm. (B, E) In serial sections, human myocardial grafts are identified by staining for beta myosin heavy chain (βMHC, brown) with hematoxylin counterstain. Scale bar = 1 mm. (C, F) Regions of interest outlined in previous panels are shown at higher magnification with staining for βMHC. Scale bar = 250 μm. (Right) Graft area is expressed normalized to left ventricular area. * indicates $p<0.05$.

There was a significant increase in graft size in the Delta-1 group compared to IgG control. Graft area covered $1.0 \pm 0.3\%$ of the left ventricle in the Delta-1 group compared to only $0.3 \pm 0.1\%$ in IgG controls (p=0.04, Figure 5.25). This corresponds to a 3.3-fold increase in βMHC^+ graft area with Delta-1 modified collagen gel implantation. The sum total graft area was 0.6 ± 0.1 mm^2 and 1.6 ± 0.4 mm^2 for the IgG and Delta-1 groups, respectively (p=0.04, Figure 5.26). There were no significant differences in infarct area at 4 weeks, with fibrosis covering an average of $27.5 \pm 3.2\%$ of the left ventricular area in the IgG control group compared to $29.8 \pm 2.4\%$ in the Delta-1 group (p=0.58, Figure 5.28A). When normalized to infarct area, myocardial grafts covered $1.0 \pm 0.2\%$ and $3.0 \pm 0.6\%$ of the infarct region in the IgG and Delta-1 groups, respectively (p=0.027, Figure 5.26).
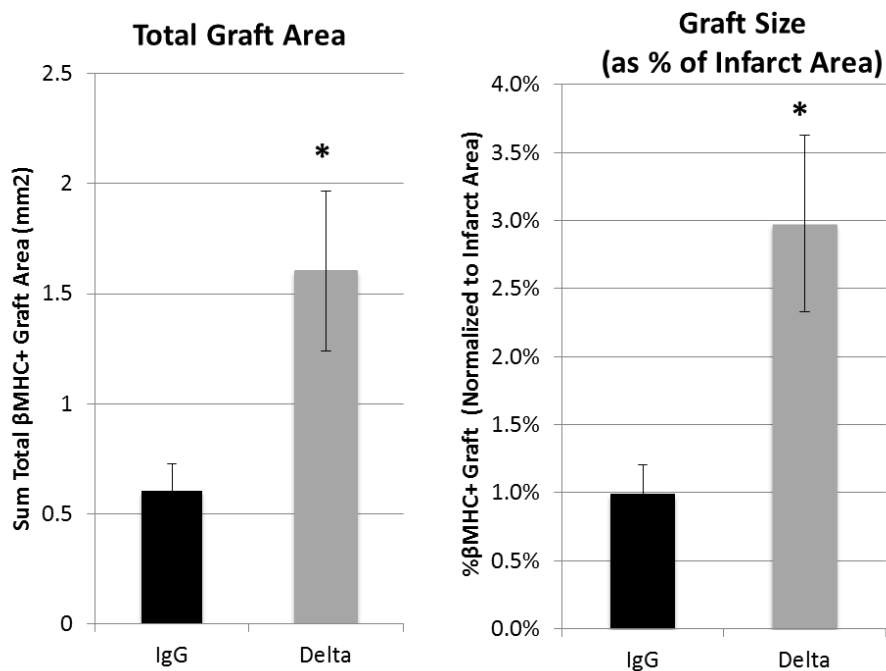
Figure 5.26. Significant increase in human graft area at 4 weeks. Beta myosin heavy chain is used to quantify human graft area. Graft area is expressed as the sum total of grafts measured across histological sections and averaged for each heart (left) and also as percent area normalized to infarct area (right). * indicates p<0.05.

Increased proliferation of hESC-cardiomyocytes after implantation with Delta-1 gel

There was a significant increase in transplanted hESC-cardiomyocyte proliferation in the Delta-1 group compared to IgG control (Figure 5.27). Animals were given 4 doses of BrdU (at Day 1, 4, 7, and 14 following implantation) to assess cell cycle activity *in vivo*, and tissue sections were stained histologically for beta myosin heavy chain and BrdU. The percent of proliferating double-positive BrdU$^+$/βMHC$^+$ cardiomyocytes was $10.9 \pm 0.5\%$ in the Delta-1 group compared to only $4.8 \pm 0.5\%$ in the IgG group, corresponding to a 2.3-fold increase in proliferation ($p=1.27E-05$, Figure 5.27). As we've identified in previous studies, there are many proliferative non-myocytes localized near the graft area, presumably fibroblasts in the scar tissue. These BrdU$^+$/βMHC$^-$ non-myocytes were not included in the proliferative assessment.
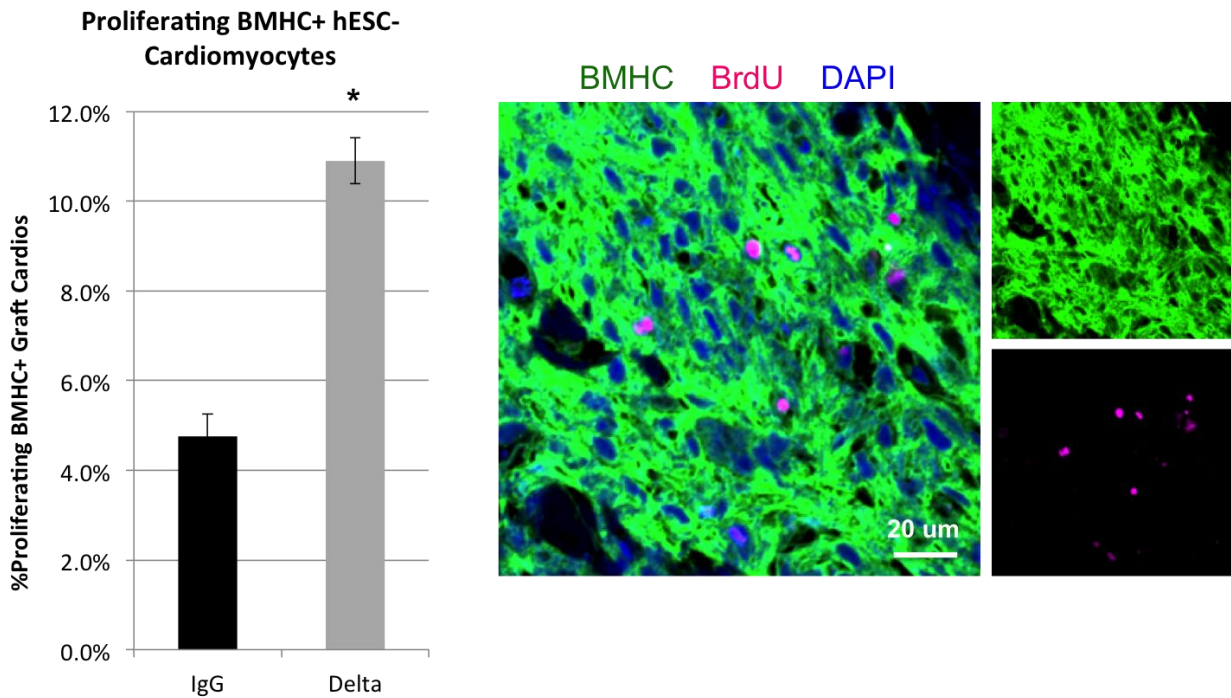
Figure 5.27. Increased proliferation of transplanted hESC-cardiomyocytes in Delta-1 gels. Percent of proliferating double-positive BrdU$^+$/βMHC$^+$ cardiomyocytes is plotted on the left. * indicates $p<0.001$. Heart tissue sections are stained immunohistochemically to detect beta myosin heavy chain (βMHC, green), BrdU (pink), with DAPI nuclear counterstain (blue).

Heart function is maintained in both groups at 4 weeks post-injury

Infarct area and anterior wall thickness were measured by histology to investigate the impact on fibrosis and remodeling between the IgG control and Delta-1 groups (Figure 5.28A, B). There was no significant difference between IgG and Delta-1 groups on anterior wall thickness, with measured wall width of 1.5 ± 0.1 mm, 1.7 ± 0.1 mm, and 2.0 ± 0.1 mm at the apex +2, apex +3, and apex +4 sections in the IgG control group, compared to 1.6 ± 0.2 mm, 1.7 ± 0.1 mm, and 2.1 ± 0.1 mm at the apex +2, apex +3, and apex +4 sections in the Delta-1 group. Wall thickness was measured using picrosirius red and fast green-stained tissue sections (Figure 5.28C, D). Impact on heart function was evaluated using echocardiography, however no significant differences were identified between groups (Figure 5.28E). The average change in fractional shortening between day 0 at baseline after injury compared to at 4 weeks post-implantation were $-2.2 \pm 1.5\%$ in the IgG control group and $-1.1 \pm 2.2\%$ in the Delta group (p=0.96). Although there were no statistical differences in fractional shortening, there was also no significant decrease in function over one month (p=0.15 and p=0.57 for IgG and Delta-1, respectively) which is consistent with previous data from our group indicating that hESC-cardiomyocyte cell therapy after I/R prevents decline in function compared to sham controls [124]. There was also variability in heart function within the groups, which did not correlate with graft area (Figure 5.29). It is important to note that this study was not designed to be powered for a functional endpoint, and to detect differences in heart function by echocardiography a larger group number would be required (see "Animal Sample Size Justification" in Chapter 5.3).

A Average Infarct Area

B Anterior Wall Thickness

C Picrosirius red/Fast green

IgG

D

Delta

2.5 mm

E Fractional Shortening

IgG
IgG Average
Delta
Delta Average
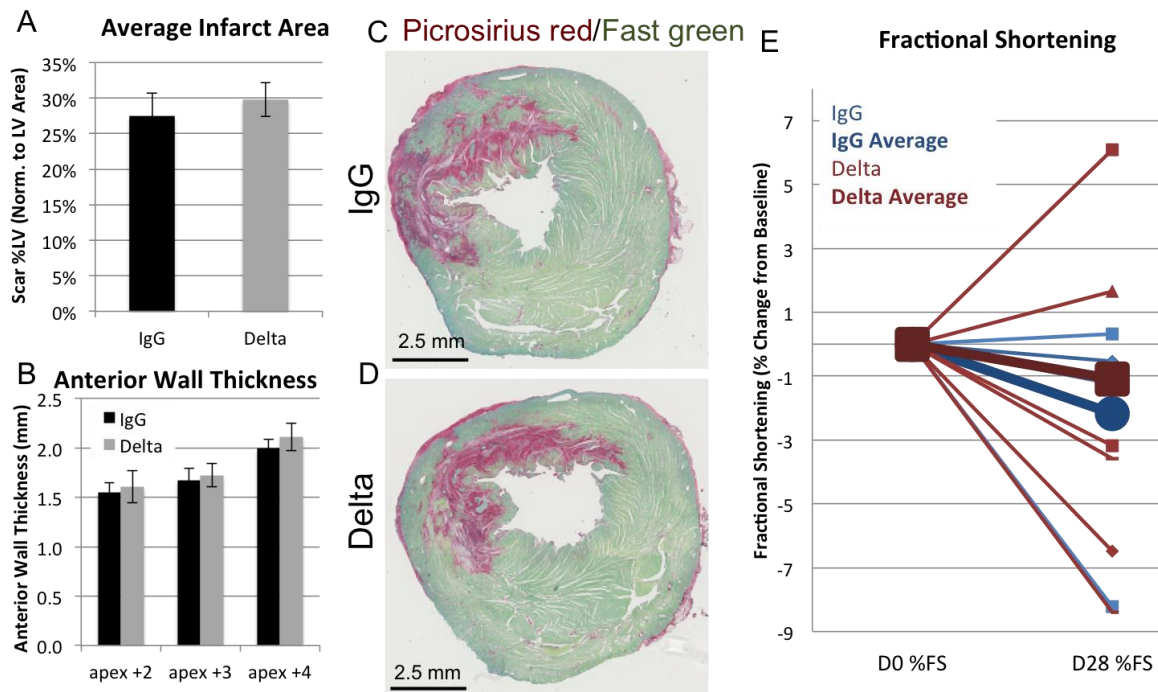
Figure 5.28. No significant differences were observed in heart function between Delta-1 or IgG groups. (A) Average infarct area is assessed by histology and expressed normalized to left ventricular (LV) area at 4 weeks. (B) Anterior wall thickness by histology is shown for various histological tissue sections: apex + 2, apex +3, and apex +4. Each tissue section is 2 mm apart. IgG = black, Delta-1 = gray. Values in mm. (C, D) Picrosirius red and fast green counterstain was used to identify fibrotic regions that are quantified in panel A. Representative images are shown for both IgG (C) and Delta-1 (D). Scale bar = 2.5 mm. (E) Fractional shortening is assessed by echocardiography at baseline (D0) and at 4 weeks (D28) and expressed here as change between D0 and D28. Each heart sample is shown, with IgG samples in blue and Delta-1 samples in red. Group averages are shown in bold.
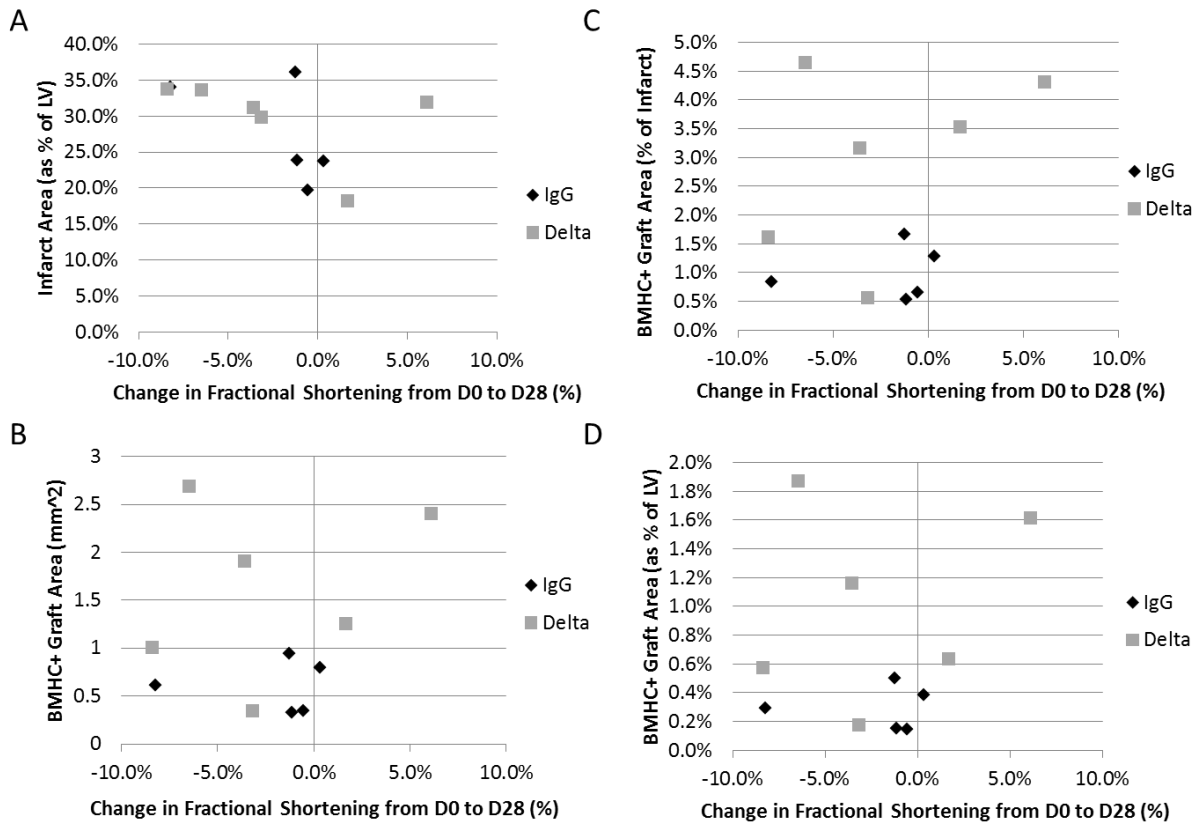
Figure 5.29. Heart function compared to human graft area at 4 weeks. No significant correlations were found between graft area and heart function. (A) Infarct area (measured as a percent of left ventricle area) is plotted against the change in fractional shortening between implantation (Day 0) and the 4-week endpoint (Day 28). (B) βMHC$^+$ graft area (mm^2) is plotted against the change in fractional shortening. (C) βMHC$^+$ graft area normalized to infarct area is plotted against the change in fractional shortening. (D) βMHC$^+$ graft area (normalized to left ventricular area) is plotted against the change in fractional shortening.

Decreasing trend of inflammation in Delta-1 group

The inflammatory response was assessed by measuring monocyte and macrophage levels near the implantation region. Tissue sections were stained for CD68 and visualized using DAB, with the level of CD68$^+$ staining normalized to infarct area (Figure 5.30A-D).
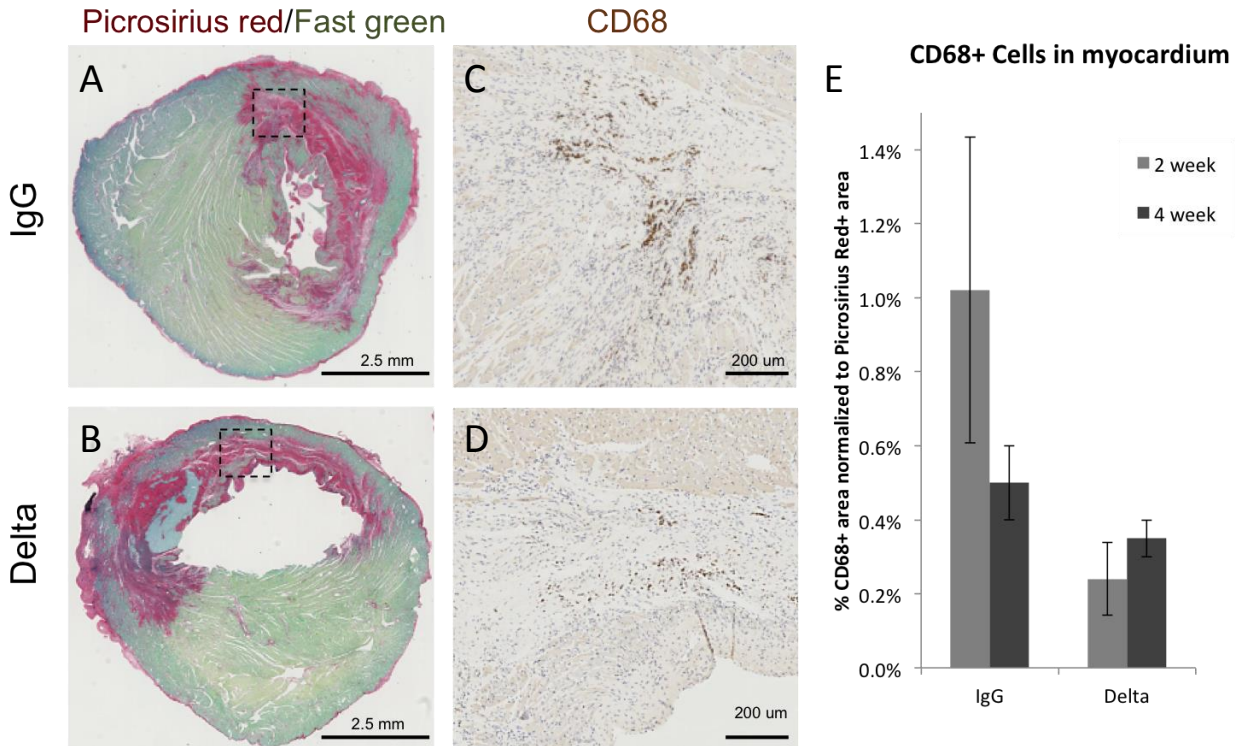
Figure 5.30. Inflammatory response at 4 weeks by CD68 staining normalized to infarct area. (A, B) Infarct regions are identified by picrosirius red/fast green counterstain. Scale bar = 2.5 mm. (C, D) Outlined regions of interest in A, B are shown at higher magnification in C, D. Serial sections are stained with CD68 antibody to label monocytes and macrophages and visualized with DAB (brown). Scale bar = 200 μm. (E) Level of inflammatory response is expressed as CD68^{+} area normalized to scar area by picrosirius red at 2 weeks and 4 weeks.

At 4 weeks, there was a trend of decreased inflammation in the Delta-1 group compared to IgG controls, with CD68^{+} area covering $0.35 \pm 0.05\%$ of the fibrotic area in the Delta-1 group compared to $0.50 \pm 0.10\%$ in the IgG control group (Figure 5.30E). For reference, the level of inflammation at 2 weeks (pilot study #2) is also graphed alongside the 4 week results. Although not statistically significant with this sample size, the trend of decreased CD68^{+} cells in the infarct region is observed at both 2 weeks and 4 weeks following implantation of Delta-1 gel with hESC-cardiomyocytes.

Increased vascularization within the Delta-1 grafts at 4 weeks

Host-derived vessels were identified within the graft and infarct regions in both implantation groups at 4 weeks. Vascularization was assessed by histology for CD31 to label endothelial cells, and only open lumen structures were counted as vessels. Tissue sections were labeled with βMHC and CD31 (Figure 5.31A) and are shown at higher magnification to visualize open lumen structures, which are labeled with white arrows (Figure 5.31B). Graft neovascularization was quantified by counting open CD31^{+} lumen structures within hESC-cardiomyocyte βMHC^{+} graft regions, and normalized to graft area. Delta-1 implants resulted in a 4.4 ± 1.3-fold increase in neovascularization compared to IgG controls (p=0.04, Figure 5.31C).
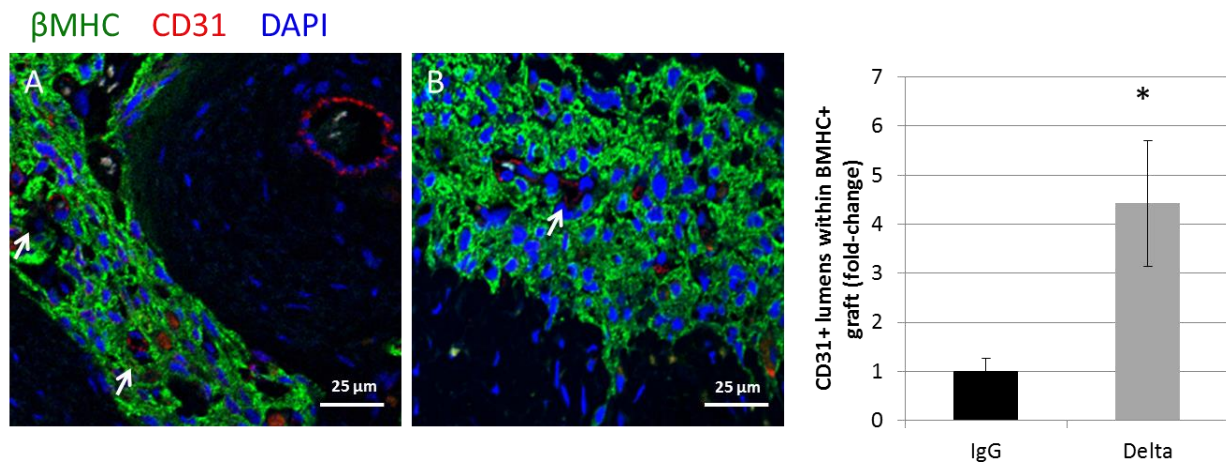
Figure 5.31. Neovascularization within the graft region at 4 weeks. (A, B) Host-derived vessels are identified by staining with CD31 antibody (red) with a double stain for βMHC (green) to identify hESC-cardiomyocyte grafts within the infarct regions. White arrows indicate open lumen structures. (C) Level of neovascularization is quantified as CD31^{+} lumens within βMHC^{+} graft regions, and normalized to βMHC^{+} area.

Graft Area Relative to Previous Results

The studies described in this chapter introduced two datasets regarding the implantation of hESC-cardiomyocytes into ischemia-reperfusion injured rat hearts with 4 week endpoints. These injury and endpoint protocols were similar to the experiments described in Chapter 3, offering insight to the relative engraftment in in these different contexts. To directly compare the relative graft size across these different experimental protocols and implantation groups, the infarct area and graft sizes for these three studies are shown in Figure 5.32. For all columns, the top row indicates infarct area measured histologically by picrosirius red staining and normalized to left ventricular area. The bottom row indicates human myocardial graft area in each implantation group, normalized to left ventricular area. In the first panel, labeled "4 week I/R, 10M cells in PSC" (Chapter 3), infarct area is between ~15-20% of the LV, and average graft area ranges from ~1% of the LV in the cell suspension group to <0.5% in the engineered tissue groups (MTPs = micro tissue particles, patch = epicardial patches). Pro-survival cocktail was used in these experiments, and a total of 10×10^6 cells were implanted in each heart. The middle column, labeled "4 wk, I/R, 10M cells in PSC + Gel," shows data from Chapter 5.4.2, and the final column shows data from Chapter 5.4.5. In both of these experiments, infarct area is relatively higher representing ~25-30% of the left ventricle. In all implant groups except for the Delta-1 group in the right column, graft area comprises roughly 0.5% of the LV, which is comparable to the engineered tissue graft sizes in the first column. Interestingly, implanting 5×10^6 hESC-cardiomyocytes in Delta-1 gels results in comparable graft sizes to those achieved after implanting 10×10^6 cells as a cell suspension, suggesting that similar graft sizes can be reached using half of the input cells in the Delta-1 Notch gel. Consistent with previous studies [180], this trend was not be achieved in IgG control groups by increasing cell number from 5 to 10 million.
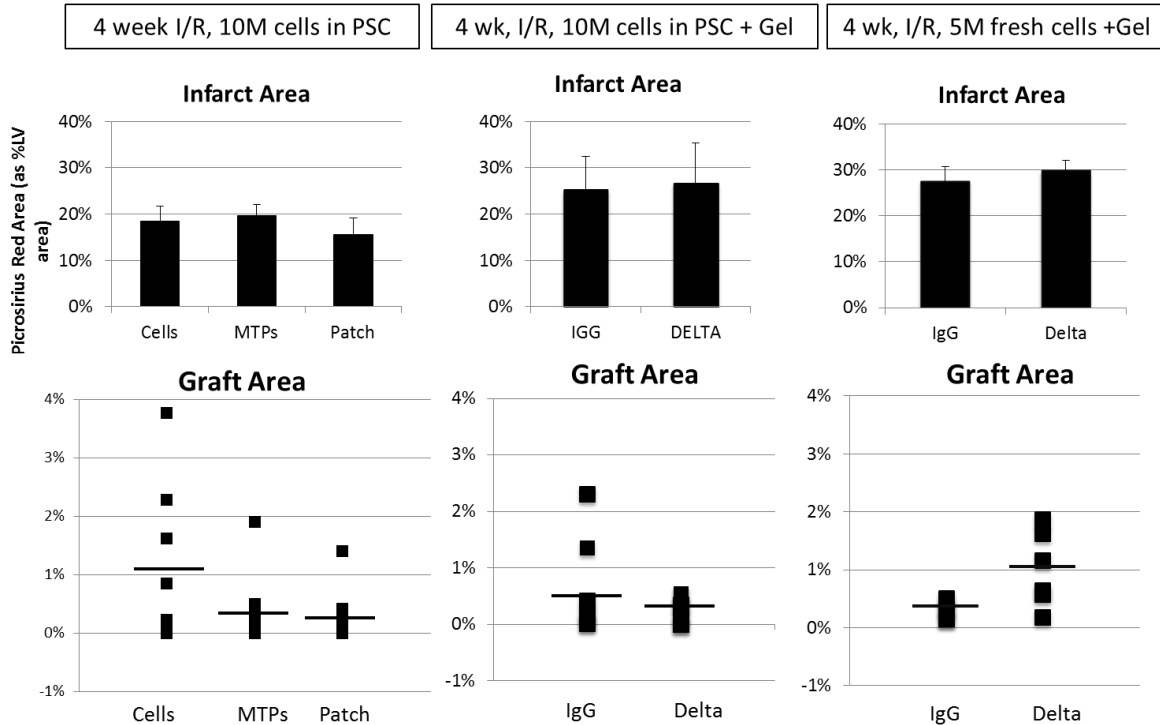
Figure 5.32. Graft size compared across implantation method and animal model. The top row (consistent for all columns) shows infarct area measured using histology for picrosirius red staining to identify collagenous scar. Data is represented as a percentage normalized to left ventricular area. The bottom row shows human myocardial graft area, expressed as a percentage normalized to left ventricular area.

5.5 Discussion

The experiments described in this chapter developed a therapeutic strategy to improve the engraftment of hESC-derived cardiomyocytes into the injured rat myocardium using a Notch-signaling hydrogel as the injectate vehicle. Despite tremendous progress in the field to develop cardiomyocyte cell transplantation therapy for cardiac repair after a myocardial infarction,

current approaches in rodents are limited in their low cell retention and relatively small graft size. These experiments addressed this limitation by promoting the Notch-dependent proliferation of hESC-cardiomyocytes after implantation. We hypothesized that increased proliferation after implantation *in vivo* would subsequently increase graft size at 4 weeks. Following a set of pilot studies *in vivo,* our final optimized protocol of implanting hESC-cardiomyocytes within the Notch-gel with immobilized Delta-1 resulted in a significant increase in graft size, increased hESC-cardiomyocyte proliferation, and increased vascularization within the graft region.

Our first set of implantation studies were designed test whether the Notch-gel could be delivered intramyocardially to gel *in situ* (Figures 5.6, 5.7). These studies demonstrated that the modified collagen Notch-gel could produce stable grafts that remained at one week following implant. We next designed a set of cell and gel implantation studies to assess the biological effect of a localized, transient Notch signal in the ischemic myocardium during hESC-cardiomyocyte cell therapy. These experiments followed adapted protocols previously published by our group for hESC-cardiomyocyte implantation into the I/R-injured rat heart (Chapter 3, [124]). These experiments included the pro-survival cocktail protocol; however the Matrigel component was replaced with the collagen-based Notch hydrogel.

As described in Chapter 5.4.2, we observed a modest increase in hESC-cardiomyocyte proliferation after implantation of cells within the Delta-1 gel compared to IgG control, however we were surprised that there was no subsequent increase in graft size. These results caused us to rethink our approach, and we began to more closely evaluate the differences in cell and gel

preparations between the *in vitro* engineered tissue studies (Chapter 4) and our *in vivo* strategy. One key difference between the *in vitro* tissue engineering experiments and the animal studies described above was the inclusion of the pro-survival cocktail [124]. A recent paper suggested that cyclosporine A (one of the pro-survival cocktail components), inhibited Notch signaling [179], which we confirmed in a series of *in vitro* studies using the U20S Notch-luciferase reporter cell line (Figure 5.14). In the series of *in vivo* pilot studies that followed (Table 5.2), we investigated the following variables that were different between the *in vitro* studies (Chapter 4) and our *in vivo* approach: inclusion of pro-survival cocktail, implanting fresh cardiomyocytes versus direct thaw-to-implant cryopreserved cardiomyocytes, total number of transplanted cells (and therefore the cell density), and rat injury model. In Chapter 5.4.4, we highlighted the results of the most successful pilot study, which was used to determine our optimized implantation protocol. For all experiments moving forward, 5×10^6 RUES2 hESC-cardiomyocytes (previously cryopreserved, but thawed and allowed to recover for 2-3 days) were implanted into the myocardium four days after I/R injury, and no pro-survival cocktail was used.

Using this optimized protocol, we demonstrated that transplantation of the Notch-gel with immobilized Delta-1 in concert with hESC-cardiomyocytes resulted in robust engraftment and limited the number of cells required for transplantation by 50%. Total graft area increased by 3.3-fold compared to control gels (Figure 5.25), and the resulting human myocardial grafts were comparable to the graft sizes we've achieved in previous studies that used 10×10^6 hESC-cardiomyocytes instead of 5×10^6 hESC-cardiomyocytes (Figure 5.32). As hypothesized, hESC-cardiomyocyte proliferation was significantly increased in the Delta-1 group compared to the IgG control group (Figure 5.27), replicating data described in engineered cardiac tissues using

the Delta-1 gels (Chapter 4).

Due the reported evidence of Notch-mediated effects on cardiac repair in mice and zebrafish [70, 71, 73-75], we also hypothesized that the localized, transient Notch signal would stimulate an endogenous repair response in the rat host myocardium. We found that the Delta-1 gel resulted in an increase in neovascularization within the graft region (Figure 5.31), which is consistent with previous reports [75]. We also investigated the effect of Delta-1 on inflammation. Monocytes and macrophages are rapidly recruited to tissue after injury, which is essential for tissue repair [181], however the appropriate resolution of inflammation is critical to limit long-term fibrosis and inflammation after injury. Our preliminary implantation experiments suggested that an inflammatory response was activated upon transplantation of the modified Notch-gels in uninjured tissue (Figure 5.9), and although there were no significant differences in the ischemia/reperfusion injury models there was a trend of decreased inflammation after Delta-1 compared to IgG control gels (Figure 5.30). Based on these results, we suspect that Notch signaling may be accelerating the resolution of inflammation, although no definitive conclusions can be drawn from the current data because there is only histological data at 2 and 4 weeks. Notch signaling has also been implicated in mediating macrophage phenotype between M1 and M2 in cancerous tumors [182], and it is reasonable to suspect that Delta-1 may be affecting this in the injured heart. These phenotypic switches were not studied in these experiments, but and our platform would provide an opportunity to address this in the ischemic myocardium in future studies.

5.6 Future studies to investigate the functional impact of transplanting Delta-1 gel and hESC-cardiomyocytes

Although echocardiography was performed in these 4-week studies to monitor heart function, the experiments were not designed to detect significant differences in functional benefit. The preliminary echocardiography data presented here suggests that both groups (IgG and Delta-1 with hESC-cardiomyocytes) maintained heart function between baseline after infarction and at 4 weeks. This is what we would expect based on previous studies in rats following cell transplantation in a similar animal model [124]. Laflamme et al found that after MI, heart function in rats declined between baseline and 4 weeks in the sham-operated controls, while cardiac cell transplantation resulted in hearts maintaining the level of function over 4 weeks. The experiments here did not include a cell-free control group, which is an important control to detect differences in functional improvement gained from the Delta-1 gel with cell transplantation.

Additionally, despite the larger grafts detected in the Delta-1 group compared to IgG control, preliminary echocardiography results suggest that this increased graft size was not enough to affect heart function relative to IgG controls. There are two potential explanations for this:

1. The proliferative hESC-cardiomyocytes in the Delta-1 group are immature relative to those in the IgG group and are therefore contributing less to global heart function despite the larger graft size.

2. Graft size of the IgG implant group is above the threshold level needed to maintain baseline heart function, thus no additional benefit is gained from the larger graft size in the Delta-1 implant group.

Future studies will address these two points and specifically investigate the functional benefit of implanting hESC-cardiomyocytes within the Delta-1 Notch signaling hydrogel.

Immature hESC-cardiomyocytes

Cardiomyocyte immaturity will be addressed in future studies by using a 3-month endpoint instead of a 1-month endpoint. In doing this, we are allowing additional time for the localized Notch signal to decline, and time for the transplanted hESC-cardiomyocytes to transition from an immature, proliferative state to a more mature cardiomyocyte state. We have previously discussed the importance of achieving this balance between proliferation and maturation (Chapter 5.2), which is one benefit of the Notch signaling gel. *In vivo* maturation of transplanted hESC-cardiomyocytes has been observed between 1 month and 3 months in the non-human primate heart [1], and this maturation process occurs in the rodent heart albeit to a less complete extent [183]. We hypothesize that by extending the experimental endpoint to 3 months, implanted cardiomyocytes will mature over time and contribute more significantly to heart function. We expect that this maturation will allow us to delineate functional differences relative to graft area, which we have shown is increased in the Delta-1 groups.

Graft area and effect on heart function

Our preliminary functional data did not show any correlation between graft area and heart function (Figure 5.29), however both *in vivo* data sets suggested that the cell and gel implants were able to maintain heart function between baseline and 4 weeks (Figures 5.12D, 5.28E). We expect that implanting only the IgG modified collagen gel as a cell-free control group will result

in a decline in function over 1 month and continuing to 3 months, which would show a functional benefit to implanting hESC-cardiomyocytes in both the IgG and Delta-1 groups.

However, we are particularly interested in determining if there is a functional benefit to achieving larger human grafts in the Delta-1 group over the IgG control, so the key question is whether the graft size achievable in our current implantation protocols is above the threshold cell number needed to maintain heart function. Pilot studies described in Chapter 5.4.3 demonstrated that implanting 3×10^6 hESC-cardiomyocytes resulted in relatively smaller yet detectable grafts, although this was analyzed after 2 weeks in the context of uninjured myocardium. A dose-response study has been previously published by our group, which found human myocardial grafts after implanting 5×10^6 and 10×10^6 hESC-cardiomyocytes, but no detectable grafts after implanting only 0.5×10^6 or 1×10^6 cells [180]. However, important caveats to drawing comparisons from this study are that: 1) these cells were only ~15% cTnT$^+$ (compared to >75% cTnT$^+$ here) and our experience is that non-myocytes die off after implantation, 2) cells underwent a harsh Percoll gradient purification step, and 3) cells were implanted into uninjured myocardium where engraftment rates are typically greater. Extrapolating evidence from the pilot studies described in Chapter 5.4.3 and [180], we expect that stable, long-term human grafts can be achieved by implanting a minimum of $2-3 \times 10^6$ hESC-cardiomyocytes. This expectation comes from assuming ~0.75×10^6 cTnT$^+$ cardiomyocytes were implanted in the 5×10^6 group (with 15% cTnT expression) in [180], which is roughly half of the cardiomyocytes implanted using 2×10^6 cells with 75% cTnT purity. Given that these cells will be implanted into ischemic myocardium where engraftment is typically lower, this is a reasonable lower limit for cell implantation. Thus, we hypothesize that decreasing the number of transplanted hESC-

159

cardiomyocytes from 5×10^6 to 2.5×10^6 will allow us to better differentiate functional differences between the two cell implant groups.

Taken collectively, the future experiments will include four groups: 1) IgG gel-only (cell-free control), 2) Delta-1 gel-only (cell-free control), 3) IgG gel + 2.5×10^6 hESC-cardiomyocytes (control), and 4) Delta-1 gel + 2.5×10^6 hESC-cardiomyocytes. Gel-only groups will have n=8 per group, while gel and cell implant groups will have n=15 per group. Animals will be taken to a 3-month endpoint with echocardiography analysis at baseline, 2 weeks, 1 month, 2 months, and 3 months. To keep a consistent cellular density within the gel, the injectate volume will be reduced in half. All other experimental details will follow those outlined for Chapter 5.4.5. We are optimistic that these future studies will further highlight the therapeutic potential of the Notch signaling gel.

5.7. Summary

Stem cell-derived cardiomyocytes have made their way to the forefront of cell therapy approaches for heart repair and have demonstrated promising results in preclinical studies. However, current transplantation techniques are limited by small graft size, with only a small fraction of transplanted cells surviving in the graft long-term. In this chapter, we described a method to enhance the proliferation of transplanted hESC-cardiomyocytes *in vivo* using a Notch signaling collagen-based hydrogel as a vehicle for cell transplantation. After a series of feasibility studies and pilot studies, an optimized implantation protocol was developed. Using this optimized protocol resulted in a significant 3-fold increase in human graft area at 4 weeks after implantation of 5 million hESC-cardiomyocytes in the Delta-1 Notch gel compared to IgG controls. Proliferation of the transplanted human cardiomyocytes was also significantly increased by over 2-fold, suggesting that Notch-mediated cell cycle activity is responsible for the increase in graft size. Neovascularization within the graft was also increased by 4-fold relative to controls and there was a trend of decreased inflammatory response in the Notch-treated group. Taken collectively, these studies establish the Notch-signaling hydrogel as a promising therapeutic approach to promote cell cycle activity of transplanted cardiomyocytes, therefore increasing human myocardial graft size within the infarcted rat ventricle.

Chapter 6. Thesis Summary and Conclusions

Tremendous progress has been made in establishing cell-based therapies for heart repair after myocardial infarction, and stem cell-derived cardiomyocytes have moved towards center stage as the ideal cell source for translational studies. Our group has been leading the field of stem cell-derived cardiomyocyte cell transplantation, and we have demonstrated both long-term engraftment and increased cardiac function after therapy in rodents and large animals. Despite this progress, there are still hurdles to overcome that would help facilitate successful clinical translation of this therapy. The research described in this dissertation used tissue engineering strategies to improve the engraftment of hESC-derived cardiomyocytes to address some of these limitations.

In Chapter 3, we conducted a comparative study to assess the engraftment and electromechanical integration of hESC-cardiomyocytes in the infarcted rat myocardium. Prior to this research, the ability of human cardiomyocytes to electrically and mechanically integrate with rodent myocardium using various delivery methods including cell suspensions and bulk engineered tissues had not been well understood. The results from this chapter demonstrated for the first time that human cardiomyocytes could electrically integrate with the rat host myocardium and beat in synchrony to rates over 6 Hz. We demonstrated that this coupling ability was restricted to intramyocardially-delivered cells, which could be injected either as a cell suspension or as engineered cardiac micro-tissues. However, graft size remained relatively small across all delivery methods, so we changed our research focus to investigate methods to increase graft size.

Current transplantation methods have been shown to only retain a small fraction of transplanted cells after implantation, which requires transplanting an excess of cells into the myocardium. To address this limitation, we sought out methods to increase cell cycle activity of hESC-cardiomyocytes after transplantation, using cardiomyocyte proliferation as a strategy to improve graft size. Towards this goal, in Chapter 4, we developed a Notch-signaling platform to promote the proliferation of hESC-cardiomyocytes in 2D and in 3D. This collagen-based hydrogel was used for *in vitro* tissue engineering studies, and results showed that hESC-cardiomyocyte proliferation was significantly increased in engineered cardiac tissues formed with the Notch gel.

Given the proliferative cell response to Notch within the hydrogel, we hypothesized that this platform would promote hESC-cardiomyocyte proliferation when the Notch gel was used as a vehicle for cell delivery into the injured myocardium. In Chapter 5, we translated the Notch gel into *in vivo* studies and demonstrated that this method resulted in a significant increase in graft area and in cardiomyocyte proliferation. The Notch-gel also led to a response in the host myocardium, as evidenced by an increase in graft neovascularization and a decreased trend of inflammation. Thus, the collagen-based hydrogel with immobilized Delta-1 was established as an effective delivery method for transplanting stem cell-derived cardiomyocytes into the infarcted myocardium.

Taken collectively, the research described in this dissertation significantly contributes to the field of cell therapy for cardiac regeneration by implementing tissue engineering strategies to improve standard cell transplantation methods.

Vita

Kaytlyn Gerbin grew up in Campbellsport, WI, a rural Wisconsin town surrounded by farmland and good cheese. She completed her Bachelors of Science at the University of Wisconsin-Madison in Mathematics with applied courses in Biology and Medicine. As an undergraduate researcher, she worked with Dr. Stephen Kennedy to understand the role of charged proteins in electromediated drug delivery, under the mentorship of Dr. Susan Hagness, Dr. John Booske, and Dr. William Murphy. She moved to Seattle, Washington in 2011 to pursue her PhD in Bioengineering at the University of Washington. When not working her research, Kaytlyn enjoys spending her free time with her husband Ely in the mountains of the Pacific Northwest. She enjoys trail and ultrarunning, snowboarding and backcountry splitboarding, mountaineering, and climbing.

6.0 References

1. Chong, J.J., et al., *Human embryonic-stem-cell-derived cardiomyocytes regenerate non-human primate hearts.* Nature, 2014. **510**(7504): p. 273-7.
2. Muller-Ehmsen, J., et al., *Survival and development of neonatal rat cardiomyocytes transplanted into adult myocardium.* J Mol Cell Cardiol, 2002. **34**(2): p. 107-16.
3. Gerbin, K.A. and C.E. Murry, *The winding road to regenerating the human heart.* Cardiovasc Pathol, 2015. **24**(3): p. 133-140.
4. Shiba, Y., et al., *Human ES-cell-derived cardiomyocytes electrically couple and suppress arrhythmias in injured hearts.* Nature, 2012. **489**(7415): p. 322-5.
5. Porrello, E.R. and E.N. Olson, *A neonatal blueprint for cardiac regeneration.* Stem Cell Research, 2014. **13**(3, Part B): p. 556-570.
6. Berks-Cardiologists, *Congestive Heart Failure.* http://berkscardiologists.com/congestive-heart-failure-chf/, 2016.
7. Bray, S.J., *Notch signalling: a simple pathway becomes complex.* Nat Rev Mol Cell Biol, 2006. **7**(9): p. 678-89.
8. WHO, W.H.O., *Cardiovascular Diseases (CVDs).* http://www.who.int/mediacentre/factsheets/fs317/en/, 2016. **accessed 10Nov2016**.
9. Arroyo, L.H. and R.T. Lee, *Mechanisms of plaque rupture.* Cardiovascular Research, 1999. **41**(2): p. 369-375.
10. Go, A.S., et al., *Heart disease and stroke statistics--2013 update: a report from the American Heart Association.* Circulation, 2013. **127**(1): p. e6-e245.
11. Murray, C.J.L., et al., *Disability-adjusted life years (DALYs) for 291 diseases and injuries in 21 regions, 1990–2010: a systematic analysis for the Global Burden of Disease Study 2010.* The Lancet, 2012. **380**(9859): p. 2197-2223.
12. Laflamme, M.A. and C.E. Murry, *Heart regeneration.* Nature, 2011. **473**(7347): p. 326-35.
13. Anversa, P., et al., *Regenerating new heart with stem cells.* J Clin Invest, 2013. **123**(1): p. 62-70.
14. Senyo, S.E., et al., *Mammalian heart renewal by pre-existing cardiomyocytes.* Nature, 2013. **493**(7432): p. 433-6.
15. Sun, Y., et al., *Cardiac remodeling by fibrous tissue after infarction in rats.* Journal of Laboratory and Clinical Medicine, 2000. **135**(4): p. 316-323.
16. Virag, J.I. and C.E. Murry, *Myofibroblast and endothelial cell proliferation during murine myocardial infarct repair.* Am J Pathol, 2003. **163**(6): p. 2433-40.
17. Jugdutt, B.I., M.J. Joljart, and M.I. Khan, *Rate of collagen deposition during healing and ventricular remodeling after myocardial infarction in rat and dog models.* Circulation, 1996. **94**(1): p. 94-101.
18. Perricone, A.J. and R.S. Vander Heide, *Novel therapeutic strategies for ischemic heart disease.* Pharmacological Research, 2014. **89**(0): p. 36-45.
19. Brown, R.D., et al., *The cardiac fibroblast: therapeutic target in myocardial remodeling and failure.* Annu Rev Pharmacol Toxicol, 2005. **45**: p. 657-87.
20. Kikuchi, K. and K.D. Poss, *Cardiac regenerative capacity and mechanisms.* Annu Rev Cell Dev Biol, 2012. **28**: p. 719-41.

21. Poss, K.D., L.G. Wilson, and M.T. Keating, *Heart regeneration in zebrafish.* Science, 2002. **298**(5601): p. 2188-90.

22. Wang, J., et al., *The regenerative capacity of zebrafish reverses cardiac failure caused by genetic cardiomyocyte depletion.* Development, 2011. **138**(16): p. 3421-30.

23. Jopling, C., et al., *Zebrafish heart regeneration occurs by cardiomyocyte dedifferentiation and proliferation.* Nature, 2010. **464**(7288): p. 606-9.

24. Kikuchi, K., et al., *Primary contribution to zebrafish heart regeneration by gata4(+) cardiomyocytes.* Nature, 2010. **464**(7288): p. 601-5.

25. Porrello, E.R., et al., *Transient regenerative potential of the neonatal mouse heart.* Science, 2011. **331**(6020): p. 1078-80.

26. Porrello, E.R., et al., *Regulation of neonatal and adult mammalian heart regeneration by the miR-15 family.* Proc Natl Acad Sci U S A, 2013. **110**(1): p. 187-92.

27. Behfar, A., et al., *Cell therapy for cardiac repair--lessons from clinical trials.* Nat Rev Cardiol, 2014. **11**(4): p. 232-46.

28. Hansson, E.M. and U. Lendahl, *Regenerative medicine for the treatment of heart disease.* J Intern Med, 2013. **273**(3): p. 235-45.

29. Hare, I.H.S.J.M., *Key developments in stem cell therapy in cardiology.* Regenerative Medicine, 2012. **7**(6): p. 17-24.

30. Malliaras, K. and E. Marban, *Cardiac cell therapy: where we've been, where we are, and where we should be headed.* Br Med Bull, 2011. **98**: p. 161-85.

31. Haraguchi, Y., et al., *Regenerative therapies using cell sheet-based tissue engineering for cardiac disease.* Cardiol Res Pract, 2011. **2011**: p. 845170.

32. Vunjak-Novakovic, G., et al., *Bioengineering heart muscle: a paradigm for regenerative medicine.* Annu Rev Biomed Eng, 2011. **13**: p. 245-67.

33. Thomson, K.S., et al., *Prevascularized microtemplated fibrin scaffolds for cardiac tissue engineering applications.* Tissue Eng Part A, 2013. **19**(7-8): p. 967-77.

34. Radisic, M., et al., *Functional assembly of engineered myocardium by electrical stimulation of cardiac myocytes cultured on scaffolds.* Proc Natl Acad Sci U S A, 2004. **101**(52): p. 18129-34.

35. Boudou, T., et al., *A microfabricated platform to measure and manipulate the mechanics of engineered cardiac microtissues.* Tissue Eng Part A, 2012. **18**(9-10): p. 910-9.

36. Tulloch, N.L., et al., *Growth of engineered human myocardium with mechanical loading and vascular coculture.* Circ Res, 2011. **109**(1): p. 47-59.

37. Madden, L.R., et al., *Proangiogenic scaffolds as functional templates for cardiac tissue engineering.* Proc Natl Acad Sci U S A, 2010. **107**(34): p. 15211-6.

38. Coulombe, K.L., et al., *Heart regeneration with engineered myocardial tissue.* Annu Rev Biomed Eng, 2014. **16**: p. 1-28.

39. Roberts, M.A., et al., *Stromal Cells in Dense Collagen Promote Cardiomyocyte and Microvascular Patterning in Engineered Human Heart Tissue.* Tissue Eng Part A, 2016. **22**(7-8): p. 633-44.

40. Tous, E., et al., *Injectable acellular hydrogels for cardiac repair.* J Cardiovasc Transl Res, 2011. **4**(5): p. 528-42.

41. Boopathy, A.V., et al., *The modulation of cardiac progenitor cell function by hydrogel-dependent Notch1 activation.* Biomaterials, 2014. **35**(28): p. 8103-8112.

42. Futakuchi-Tsuchida, A. and C.E. Murry, *Human myocardial grafts: do they meet all the criteria for true heart regeneration?* Future Cardiol, 2013. **9**(2): p. 151-4.

43. Maher, K.O. and C. Xu, *Marching towards regenerative cardiac therapy with human pluripotent stem cells.* Discov Med, 2013. **15**(85): p. 349-56.

44. Shiba, Y., et al., *Electrical Integration of Human Embryonic Stem Cell-Derived Cardiomyocytes in a Guinea Pig Chronic Infarct Model.* J Cardiovasc Pharmacol Ther, 2014. **19**(4): p. 368-381.

45. Gerbin, K.A., et al., *Enhanced Electrical Integration of Engineered Human Myocardium via Intramyocardial versus Epicardial Delivery in Infarcted Rat Hearts.* PLoS ONE, 2015. **10**(7): p. e0131446.

46. Buja, L.M. and D. Vela, *Cardiomyocyte death and renewal in the normal and diseased heart.* Cardiovasc Pathol, 2008. **17**(6): p. 349-74.

47. Mollova, *Cardiomyocyte proliferation contributes to heart growth in young humans.* PNAS, 2013. **110**(4): p. 1446–1451.

48. Bergmann, O., et al., *Evidence for cardiomyocyte renewal in humans.* Science, 2009. **324**(5923): p. 98-102.

49. Engel, F.B., et al., *p38 MAP kinase inhibition enables proliferation of adult mammalian cardiomyocytes.* Genes Dev, 2005. **19**(10): p. 1175-87.

50. Chaudhry, H.W., et al., *Cyclin A2 mediates cardiomyocyte mitosis in the postmitotic myocardium.* J Biol Chem, 2004. **279**(34): p. 35858-66.

51. Pasumarthi, K.B., et al., *Targeted expression of cyclin D2 results in cardiomyocyte DNA synthesis and infarct regression in transgenic mice.* Circ Res, 2005. **96**(1): p. 110-8.

52. Engel, F.B., et al., *FGF1/p38 MAP kinase inhibitor therapy induces cardiomyocyte mitosis, reduces scarring, and rescues function after myocardial infarction.* Proc Natl Acad Sci U S A, 2006. **103**(42): p. 15546-51.

53. Bersell, K., et al., *Neuregulin1/ErbB4 signaling induces cardiomyocyte proliferation and repair of heart injury.* Cell, 2009. **138**(2): p. 257-70.

54. Raya, A., et al., *Activation of Notch signaling pathway precedes heart regeneration in zebrafish.* Proc Natl Acad Sci U S A, 2003. **100 Suppl 1**: p. 11889-95.

55. de la Pompa, J.L. and J.A. Epstein, *Coordinating tissue interactions: Notch signaling in cardiac development and disease.* Dev Cell, 2012. **22**(2): p. 244-54.

56. Gemberling, M., et al., *Nrg1 is an injury-induced cardiomyocyte mitogen for the endogenous heart regeneration program in zebrafish.* eLife, 2015. **4**: p. e05871.

57. Polizzotti, B.D., et al., *Neuregulin stimulation of cardiomyocyte regeneration in mice and human myocardium reveals a therapeutic window.* Science Translational Medicine, 2015. **7**(281): p. 281ra45.

58. Tian, Y., et al., *A microRNA-Hippo pathway that promotes cardiomyocyte proliferation and cardiac regeneration in mice.* Science Translational Medicine, 2015. **7**(279): p. 279ra38.

59. Nemir, M., et al., *The Notch pathway controls fibrotic and regenerative repair in the adult heart.* European Heart Journal, 2014. **35**(32): p. 2174-2185.

60. Campa, V.M., et al., *Notch activates cell cycle reentry and progression in quiescent cardiomyocytes.* J Cell Biol, 2008. **183**(1): p. 129-41.

61. Collesi, C., et al., *Notch1 signaling stimulates proliferation of immature cardiomyocytes.* J Cell Biol, 2008. **183**(1): p. 117-28.

62. Tung, Jason C., et al., *Engineered Biomaterials Control Differentiation and Proliferation of Human-Embryonic-Stem-Cell-Derived Cardiomyocytes via Timed Notch Activation.* Stem Cell Reports, 2014. **2**(3): p. 271-281.

63. Harper, J.A., et al., *Notch signaling in development and disease.* Clin Genet, 2003. **64**(6): p. 461-72.

64. Baron, M., *An overview of the Notch signalling pathway.* Semin Cell Dev Biol, 2003. **14**(2): p. 113-9.

65. Kopan, R. and M.X. Ilagan, *The canonical Notch signaling pathway: unfolding the activation mechanism.* Cell, 2009. **137**(2): p. 216-33.

66. Hsieh, J.J.-D., et al., *CIR, a corepressor linking the DNA binding factor CBF1 to the histone deacetylase complex.* Proceedings of the National Academy of Sciences, 1999. **96**(1): p. 23-28.

67. Iso, T., L. Kedes, and Y. Hamamori, *HES and HERP families: multiple effectors of the Notch signaling pathway.* J Cell Physiol, 2003. **194**(3): p. 237-55.

68. Croquelois, A., et al., *Control of the adaptive response of the heart to stress via the Notch1 receptor pathway.* The Journal of Experimental Medicine, 2008. **205**(13): p. 3173-3185.

69. Krebs, L.T., et al., *Haploinsufficient lethality and formation of arteriovenous malformations in Notch pathway mutants.* Genes Dev, 2004. **18**(20): p. 2469-73.

70. Kratsios, P., et al., *Distinct roles for cell-autonomous Notch signaling in cardiomyocytes of the embryonic and adult heart.* Circ Res, 2010. **106**(3): p. 559-72.

71. Gude, N.A., et al., *Activation of Notch-mediated protective signaling in the myocardium.* Circ Res, 2008. **102**(9): p. 1025-35.

72. Ferrari, R. and P. Rizzo, *The Notch pathway: a novel target for myocardial remodelling therapy?* European Heart Journal, 2014. **35**(32): p. 2140-2145.

73. Zhang, R., et al., *In vivo cardiac reprogramming contributes to zebrafish heart regeneration.* Nature, 2013. **498**(7455): p. 497-501.

74. Zhao, L., et al., *Notch signaling regulates cardiomyocyte proliferation during zebrafish heart regeneration.* Proc Natl Acad Sci U S A, 2014. **111**(4): p. 1403-8.

75. Li, Y., Y. Hiroi, and J.K. Liao, *Notch Signaling as an Important Mediator of Cardiac Repair and Regeneration after Myocardial Infarction.* Trends in Cardiovascular Medicine, 2010. **20**(7): p. 228-231.

76. Li, Y., et al., *Notch1 in bone marrow-derived cells mediates cardiac repair after myocardial infarction.* Circulation, 2011. **123**(8): p. 866-76.

77. Menasché, P., et al., *Myoblast transplantation for heart failure.* The Lancet, 2001. **357**(9252): p. 279-280.

78. Orlic, D., et al., *Bone marrow cells regenerate infarcted myocardium.* Nature, 2001. **410**(6829): p. 701-5.

79. Strauer, B.E., *Repair of Infarcted Myocardium by Autologous Intracoronary Mononuclear Bone Marrow Cell Transplantation in Humans.* Circulation, 2002. **106**(15): p. 1913-1918.

80. Simari, R.D., et al., *Bone marrow mononuclear cell therapy for acute myocardial infarction: a perspective from the cardiovascular cell therapy research network.* Circ Res, 2014. **114**(10): p. 1564-8.

81. Murry, C.E., L.J. Field, and P. Menasche, *Cell-based cardiac repair: reflections at the 10-year point.* Circulation, 2005. **112**(20): p. 3174-83.

82. Wollert, K.C., et al., *Intracoronary autologous bone-marrow cell transfer after myocardial infarction: the BOOST randomised controlled clinical trial.* Lancet, 2004. **364**(9429): p. 141-8.

83. Meyer, G.P., et al., *Intracoronary bone marrow cell transfer after myocardial infarction: eighteen months' follow-up data from the randomized, controlled BOOST (BOne marrOw transfer to enhance ST-elevation infarct regeneration) trial.* Circulation, 2006. **113**(10): p. 1287-94.

84. Schächinger, V., et al., *Intracoronary Bone Marrow–Derived Progenitor Cells in Acute Myocardial Infarction.* New England Journal of Medicine, 2006. **355**(12): p. 1210-1221.

85. Assmus, B., *Transplantation of Progenitor Cells and Regeneration Enhancement in Acute Myocardial Infarction (TOPCARE-AMI).* Circulation, 2002. **106**(24): p. 3009-3017.

86. Leistner, D.M., et al., *Transplantation of progenitor cells and regeneration enhancement in acute myocardial infarction (TOPCARE-AMI): final 5-year results suggest long-term safety and efficacy.* Clin Res Cardiol, 2011. **100**(10): p. 925-34.

87. Schachinger, V., et al., *Transplantation of progenitor cells and regeneration enhancement in acute myocardial infarction: final one-year results of the TOPCARE-AMI Trial.* J Am Coll Cardiol, 2004. **44**(8): p. 1690-9.

88. Clifford, D.M., et al., *Stem cell treatment for acute myocardial infarction.* Cochrane Database Syst Rev, 2012. **2**: p. CD006536.

89. Simari, R.D., et al., *Development of a network to test strategies in cardiovascular cell delivery: the NHLBI-sponsored Cardiovascular Cell Therapy Research Network (CCTRN).* J Cardiovasc Transl Res, 2010. **3**(1): p. 30-6.

90. Perin, E.C., et al., *Effect of transendocardial delivery of autologous bone marrow mononuclear cells on functional capacity, left ventricular function, and perfusion in chronic heart failure: the FOCUS-CCTRN trial.* JAMA, 2012. **307**(16): p. 1717-26.

91. Traverse, J.H., et al., *LateTIME: a phase-II, randomized, double-blinded, placebo-controlled, pilot trial evaluating the safety and effect of administration of bone marrow mononuclear cells 2 to 3 weeks after acute myocardial infarction.* Tex Heart Inst J, 2010. **37**(4): p. 412-20.

92. Traverse, J.H., et al., *Effect of intracoronary delivery of autologous bone marrow mononuclear cells 2 to 3 weeks following acute myocardial infarction on left ventricular function: the LateTIME randomized trial.* JAMA, 2011. **306**(19): p. 2110-9.

93. Traverse, J.H., et al., *Effect of the use and timing of bone marrow mononuclear cell delivery on left ventricular function after acute myocardial infarction: the TIME randomized trial.* JAMA, 2012. **308**(22): p. 2380-9.

94. Surder, D., et al., *Intracoronary injection of bone marrow-derived mononuclear cells early or late after acute myocardial infarction: effects on global left ventricular function.* Circulation, 2013. **127**(19): p. 1968-79.

95. Mathur, *BAMI. The Effect of Intracoronary Reinfusion of Bone Marrow-derived Mononuclear Cells(BM-MNC) on All Cause Mortality in Acute Myocardial Infarction.* ClinicalTrials.gov NCT01569178, Barts & London NHS Trust. Accessed 10/13/2014.

96. Dominici, M., et al., *Minimal criteria for defining multipotent mesenchymal stromal cells. The International Society for Cellular Therapy position statement.* Cytotherapy, 2006. **8**(4): p. 315-7.

97. Bianco, P., et al., *The meaning, the sense and the significance: translating the science of mesenchymal stem cells into medicine.* Nat Med, 2013. **19**(1): p. 35-42.

98. Dimmeler, S., J. Burchfield, and A.M. Zeiher, *Cell-based therapy of myocardial infarction.* Arterioscler Thromb Vasc Biol, 2008. **28**(2): p. 208-16.

99. Chen, S.L., et al., *Effect on left ventricular function of intracoronary transplantation of autologous bone marrow mesenchymal stem cell in patients with acute myocardial infarction.* Am J Cardiol, 2004. **94**(1): p. 92-5.

100. Heldman, A.W., et al., *Transendocardial mesenchymal stem cells and mononuclear bone marrow cells for ischemic cardiomyopathy: the TAC-HFT randomized trial.* JAMA, 2014. **311**(1): p. 62-73.

101. Hare, J.M., et al., *Comparison of allogeneic vs autologous bone marrow-derived mesenchymal stem cells delivered by transendocardial injection in patients with ischemic cardiomyopathy: the POSEIDON randomized trial.* JAMA, 2012. **308**(22): p. 2369-79.

102. Bartunek, J., et al., *Cardiopoietic stem cell therapy in heart failure: the C-CURE (Cardiopoietic stem Cell therapy in heart failURE) multicenter randomized trial with lineage-specified biologics.* J Am Coll Cardiol, 2013. **61**(23): p. 2329-38.

103. Murry, C.E., N.J. Palpant, and W.R. MacLellan, *Cardiopoietry in motion: primed mesenchymal stem cells for ischemic cardiomyopathy.* J Am Coll Cardiol, 2013. **61**(23): p. 2339-40.

104. Abdel-Latif A, B.R., Tleyjeh IM, Montori VM, Perin EC, Hornung CA, Zuba-Surma EK, Al-Mallah M, Dawn B, *Adult bone marrow-derived cells for cardiac repair: a systematic review and meta-analysis.* Arch Intern Med, 2007. **167**(10): p. 989-97.

105. Agbulut, O., et al., *Comparison of human skeletal myoblasts and bone marrow-derived CD133+ progenitors for the repair of infarcted myocardium.* J Am Coll Cardiol, 2004. **44**(2): p. 458-63.

106. Li, T.S., et al., *Direct comparison of different stem cell types and subpopulations reveals superior paracrine potency and myocardial repair efficacy with cardiosphere-derived cells.* J Am Coll Cardiol, 2012. **59**(10): p. 942-53.

107. Beltrami, A.P., et al., *Adult cardiac stem cells are multipotent and support myocardial regeneration.* Cell, 2003. **114**(6): p. 763-76.

108. Tallini, Y.N., et al., *c-kit expression identifies cardiovascular precursors in the neonatal heart.* Proc Natl Acad Sci U S A, 2009. **106**(6): p. 1808-13.

109. Zaruba, M.M., et al., *Cardiomyogenic potential of C-kit(+)-expressing cells derived from neonatal and adult mouse hearts.* Circulation, 2010. **121**(18): p. 1992-2000.

110. van Berlo, J.H., et al., *c-kit+ cells minimally contribute cardiomyocytes to the heart.* Nature, 2014. **509**(7500): p. 337-341.

111. Bolli, R., et al., *Cardiac stem cells in patients with ischaemic cardiomyopathy (SCIPIO): initial results of a randomised phase 1 trial.* Lancet, 2011. **378**(9806): p. 1847-57.

112. Lancet, T., *Expression of concern: the SCIPIO trial.* The Lancet, 2014. **383**(9925): p. 1279.

113. Smith, R.R., et al., *Regenerative potential of cardiosphere-derived cells expanded from percutaneous endomyocardial biopsy specimens.* Circulation, 2007. **115**(7): p. 896-908.

114. Malliaras, K., et al., *Intracoronary Cardiosphere-Derived Cells After Myocardial Infarction: Evidence of Therapeutic Regeneration in the Final 1-Year Results of the CADUCEUS Trial (CArdiosphere-Derived aUtologous stem CElls to reverse ventricUlar dySfunction).* J Am Coll Cardiol, 2014. **63**(2): p. 110-22.

115. Makkar, R.R., et al., *Intracoronary cardiosphere-derived cells for heart regeneration after myocardial infarction (CADUCEUS): a prospective, randomised phase 1 trial.* Lancet, 2012. **379**(9819): p. 895-904.

116. Takehara, N., et al., *Controlled delivery of basic fibroblast growth factor promotes human cardiosphere-derived cell engraftment to enhance cardiac repair for chronic myocardial infarction.* J Am Coll Cardiol, 2008. **52**(23): p. 1858-65.

117. Takehara N, N.M., Ogata T, Nakamura T, Matoba S, Gojo S, Sawada T, Yaku H, Matsubara H, *AutoLogous Human CArdiac-Derived Stem Cell to Treat Ischemic cArdiomyopathy (ALCADIA).* American Heart Association Scientific Sessions 2012.

118. Yee, K., et al., *Allogeneic Cardiospheres Delivered via Percutaneous Transendocardial Injection Increase Viable Myocardium, Decrease Scar Size, and Attenuate Cardiac Dilatation in Porcine Ischemic Cardiomyopathy.* PLoS ONE, 2014. **9**(12): p. e113805.

119. Doetschman TC, E.H., Katz M, Schmidt W, Kemler R, *The in vitro development of blastocyst-derived embryonic stem cell lines: formation of visceral yolk sac, blood islands and myocardium.* J Embryol Exp Morphol, 1985. **87**: p. 27-45.

120. Burridge, P.W., et al., *Production of de novo cardiomyocytes: human pluripotent stem cell differentiation and direct reprogramming.* Cell Stem Cell, 2012. **10**(1): p. 16-28.

121. Fernandes, S., et al., *Human embryonic stem cell-derived cardiomyocytes engraft but do not alter cardiac remodeling after chronic infarction in rats.* J Mol Cell Cardiol, 2010. **49**(6): p. 941-9.

122. Tian, L., et al., *Imaging neural activity in worms, flies and mice with improved GCaMP calcium indicators.* Nat Methods, 2009. **6**(12): p. 875-81.

123. Shiba, Y., et al., *Allogeneic transplantation of iPS cell-derived cardiomyocytes regenerates primate hearts.* Nature, 2016. **538**(7625): p. 388-391.

124. Laflamme, M.A., et al., *Cardiomyocytes derived from human embryonic stem cells in pro-survival factors enhance function of infarcted rat hearts.* Nat Biotechnol, 2007. **25**(9): p. 1015-24.

125. Caspi, O., et al., *Transplantation of human embryonic stem cell-derived cardiomyocytes improves myocardial performance in infarcted rat hearts.* J Am Coll Cardiol, 2007. **50**(19): p. 1884-93.

126. van Laake, L.W., et al., *Human embryonic stem cell-derived cardiomyocytes survive and mature in the mouse heart and transiently improve function after myocardial infarction.* Stem Cell Research, 2008. **1**(1): p. 9-24.

127. Ye, L., et al., *Patching the heart: cardiac repair from within and outside.* Circ Res, 2013. **113**(7): p. 922-32.

128. Reinecke, H., et al., *Survival, integration, and differentiation of cardiomyocyte grafts: a study in normal and injured rat hearts.* Circulation, 1999. **100**(2): p. 193-202.

129. Fernandes, S., et al., *Comparison of Human Embryonic Stem Cell-Derived Cardiomyocytes, Cardiovascular Progenitors, and Bone Marrow Mononuclear Cells for Cardiac Repair.* Stem Cell Reports, 2015. **5**(5): p. 753-62.

130. Yang, X., L. Pabon, and C.E. Murry, *Engineering adolescence: maturation of human pluripotent stem cell-derived cardiomyocytes.* Circ Res, 2014. **114**(3): p. 511-23.

131. Nussbaum, J., et al., *Transplantation of undifferentiated murine embryonic stem cells in the heart: teratoma formation and immune response.* FASEB J, 2007. **21**(7): p. 1345-57.

132. Buja, L.M. and D. Vela, *Immunologic and inflammatory reactions to exogenous stem cells implications for experimental studies and clinical trials for myocardial repair.* J Am Coll Cardiol, 2010. **56**(21): p. 1693-700.

133. Riolobos, L., et al., *HLA engineering of human pluripotent stem cells.* Mol Ther, 2013. **21**(6): p. 1232-41.

134. Zimmermann, W.H., et al., *Engineered heart tissue grafts improve systolic and diastolic function in infarcted rat hearts.* Nat Med, 2006. **12**(4): p. 452-8.
135. Lesman, A., et al., *Transplantation of a tissue-engineered human vascularized cardiac muscle.* Tissue Eng Part A, 2010. **16**(1): p. 115-25.
136. Stevens, K.R., et al., *Physiological function and transplantation of scaffold-free and vascularized human cardiac muscle tissue.* Proc Natl Acad Sci U S A, 2009. **106**(39): p. 16568-73.
137. Xu, C., et al., *Efficient generation and cryopreservation of cardiomyocytes derived from human embryonic stem cells.* Regen Med, 2011. **6**(1): p. 53-66.
138. Nunes, S.S., et al., *Biowire: a platform for maturation of human pluripotent stem cell-derived cardiomyocytes.* Nat Methods, 2013. **10**(8): p. 781-7.
139. Zwi-Dantsis, L., et al., *Derivation and cardiomyocyte differentiation of induced pluripotent stem cells from heart failure patients.* Eur Heart J, 2013. **34**(21): p. 1575-86.
140. Rohr, S., *Role of gap junctions in the propagation of the cardiac action potential.* Cardiovascular Research, 2004. **62**(2): p. 309-322.
141. Janse, M.J., T. Opthof, and A.G. Kleber, *Animal models of cardiac arrhythmias.* Cardiovasc Res, 1998. **39**(1): p. 165-77.
142. Song, H., et al., *Interrogating functional integration between injected pluripotent stem cell-derived cells and surrogate cardiac tissue.* Proc Natl Acad Sci U S A, 2010. **107**(8): p. 3329-34.
143. Fernandes, S., et al., *Cardiac cell therapy: overexpression of connexin43 in skeletal myoblasts and prevention of ventricular arrhythmias.* J Cell Mol Med, 2009. **13**(9B): p. 3703-12.
144. Lal, H., et al., *The GSK-3 Family as Therapeutic Target for Myocardial Diseases.* Circ Res, 2015. **116**(1): p. 138-149.
145. Weinberger, F., et al., *Cardiac repair in guinea pigs with human engineered heart tissue from induced pluripotent stem cells.* Science Translational Medicine, 2016. **8**(363): p. 363ra148.
146. Robey, T.E., et al., *Systems approaches to preventing transplanted cell death in cardiac repair.* J Mol Cell Cardiol, 2008. **45**(4): p. 567-81.
147. Sekine, H., et al., *Cardiac cell sheet transplantation improves damaged heart function via superior cell survival in comparison with dissociated cell injection.* Tissue Eng Part A, 2011. **17**(23-24): p. 2973-80.
148. Moon, S.H., et al., *The use of aggregates of purified cardiomyocytes derived from human ESCs for functional engraftment after myocardial infarction.* Biomaterials, 2013. **34**(16): p. 4013-26.
149. Stevens, K.R., et al., *Scaffold-free human cardiac tissue patch created from embryonic stem cells.* Tissue Eng Part A, 2009. **15**(6): p. 1211-22.
150. Schaaf, S., et al., *Human engineered heart tissue as a versatile tool in basic research and preclinical toxicology.* PLoS One, 2011. **6**(10): p. e26397.
151. Zhang, D., et al., *Tissue-engineered cardiac patch for advanced functional maturation of human ESC-derived cardiomyocytes.* Biomaterials, 2013. **34**(23): p. 5813-20.
152. Thavandiran, N., et al., *Design and formulation of functional pluripotent stem cell-derived cardiac microtissues.* Proc Natl Acad Sci U S A, 2013. **110**(49): p. E4698-707.
153. Kreutziger, K.L., et al., *Developing vasculature and stroma in engineered human myocardium.* Tissue Eng Part A, 2011. **17**(9-10): p. 1219-28.

154. Sekine, H., et al., *Cardiac Cell Sheet Transplantation Improves Damaged Heart Function via Superior Cell Survival in Comparison with Dissociated Cell Injection.* Tissue Engineering Part A, 2011. **17**(23-24): p. 2973-2980.

155. Finney, V. and I. Bernstein, *Immobilization of Notch Ligand is required for induction of Notch signaling.* 2000.

156. Beckstead, B.L., et al., *Methods to promote Notch signaling at the biomaterial interface and evaluation in a rafted organ culture model.* J Biomed Mater Res A, 2009. **91**(2): p. 436-46.

157. Shen, Y.H., M.S. Shoichet, and M. Radisic, *Vascular endothelial growth factor immobilized in collagen scaffold promotes penetration and proliferation of endothelial cells.* Acta Biomater, 2008. **4**(3): p. 477-89.

158. Osathanon, T., C.M. Giachelli, and M.J. Somerman, *Immobilization of alkaline phosphatase on microporous nanofibrous fibrin scaffolds for bone tissue engineering.* Biomaterials, 2009. **30**(27): p. 4513-21.

159. Yannas, I., *Materials for skin and nerve regeneration: Biological analogues of the extracellular matrix.* . Mat Sci Tech, 1992(14): p. 179-208.

160. L.H.H. Olde Damink, P.J.D., M.J.A. van Luyn, P.B. van Wachem, P. Nieuwenhuis, J. Feijen, *Cross-linking of dermal sheep collagen using a water-soluble carbodiimide* Biomaterials 1996. **17**: p. 765-773.

161. Tulloch, N.L., et al., *Growth of Engineered Human Myocardium With Mechanical Loading and Vascular Coculture.* Circulation Research, 2011. **109**(1): p. 47-59.

162. Ruan, J.L., et al., *Mechanical stress promotes maturation of human myocardium from pluripotent stem cell-derived progenitors.* Stem Cells, 2015.

163. Bhandari, S., *Engineering a Novel Device to Implement Afterload on Human Stem Cell-Derived Cardiac Tissues* Masters Thesis, University of Washington, Seattle. , 2015.

164. Hansen, A., et al., *Development of a Drug Screening Platform Based on Engineered Heart Tissue.* Circulation Research, 2010. **107**(1): p. 35.

165. Walsh, S., et al., *Cardiomyocyte cell cycle control and growth estimation in vivo—an analysis based on cardiomyocyte nuclei.* Cardiovascular Research, 2010. **86**(3): p. 365-373.

166. Tong, W., et al., *Hypoxia inhibits cardiomyocyte proliferation in fetal rat hearts via upregulating TIMP-4.* Am J Physiol Regul Integr Comp Physiol, 2013. **304**(8): p. R613-20.

167. Liu, Z., et al., *Regulation of cardiomyocyte polyploidy and multinucleation by CyclinG1.* Circ Res, 2010. **106**(9): p. 1498-506.

168. Thomson, K.S., et al., *Prevascularized Microtemplated Fibrin Scaffolds for Cardiac Tissue Engineering Applications.* Tissue Engineering. Part A, 2013. **19**(7-8): p. 967-977.

169. Crapo, P.M., T.W. Gilbert, and S.F. Badylak, *An overview of tissue and whole organ decellularization processes.* Biomaterials, 2011. **32**(12): p. 3233-43.

170. Gilbert, T.W., T.L. Sellaro, and S.F. Badylak, *Decellularization of tissues and organs.* Biomaterials, 2006. **27**(19): p. 3675-83.

171. Cornwell, K.G., A. Landsman, and K.S. James, *Extracellular matrix biomaterials for soft tissue repair.* Clin Podiatr Med Surg, 2009. **26**(4): p. 507-23.

172. Singelyn, J.M., et al., *Catheter-deliverable hydrogel derived from decellularized ventricular extracellular matrix increases endogenous cardiomyocytes and preserves cardiac function post-myocardial infarction.* J Am Coll Cardiol, 2012. **59**(8): p. 751-63.

173.   Singelyn, J.M., et al., *Naturally derived myocardial matrix as an injectable scaffold for cardiac tissue engineering.* Biomaterials, 2009. **30**(29): p. 5409-16.

174.   DeForest, C.A. and D.A. Tirrell, *A photoreversible protein-patterning approach for guiding stem cell fate in three-dimensional gels.* Nat Mater, 2015. **14**(5): p. 523-531.

175.   Singelyn, J.M. and K.L. Christman, *Injectable materials for the treatment of myocardial infarction and heart failure: the promise of decellularized matrices.* J Cardiovasc Transl Res, 2010. **3**(5): p. 478-86.

176.   Burdick, J.A., *Injectable gels for tissue/organ repair.* Biomed Mater, 2012. **7**(2): p. 020201.

177.   Dai, W., et al., *Thickening of the infarcted wall by collagen injection improves left ventricular function in rats: a novel approach to preserve cardiac function after myocardial infarction.* J Am Coll Cardiol, 2005. **46**(4): p. 714-9.

178.   Lee, H.B. and M.D. Blaufox, *Blood volume in the rat.* J Nucl Med, 1985. **26**(1): p. 72-6.

179.   Pandey, R., et al., *Cyclosporin A Disrupts Notch Signaling and Vascular Lumen Maintenance.* PLoS ONE, 2015. **10**(3): p. e0119279.

180.   Laflamme, M.A., et al., *Formation of human myocardium in the rat heart from human embryonic stem cells.* Am J Pathol, 2005. **167**(3): p. 663-71.

181.   Shi, C. and E.G. Pamer, *Monocyte recruitment during infection and inflammation.* Nat Rev Immunol, 2011. **11**(11): p. 762-774.

182.   Xu, H., et al., *Notch-RBP-J signaling regulates the transcription factor IRF8 to promote inflammatory macrophage polarization.* Nat Immunol, 2012. **13**(7): p. 642-650.

183.   Kadota, S.P., Lil; Reinecke, Hans; Murry, Charles E, *In Vivo Maturation of Human Induced Pluripotent Stem Cell Derived Cardiomyocytes in Neonatal and Adult Rat Hearts.* Stem Cell Reports, 2016.